Investigation of Anodic Dissolution Process to Overcome the Challenges during Micro-Manufacturing

A thesis submitted

in partial fulfillment of the requirements

for the degree of

Doctor of Philosophy

By

Abhinav Kumar

Roll No.-176103020

Department of Mechanical Engineering

Indian Institute of Technology Guwahati

Guwahati, India

May, 2023

Department of Mechanical Engineering
Indian Institute of Technology Guwahati
Guwahati-781039
INDIA

CERTIFICATE

It is certified that the work contained in the thesis entitled "**Investigation of anodic dissolution process to overcome the challenges during micro-manufacturing**", submitted by **Abhinav Kumar**, Roll No. 176103020 to the Indian Institute of Technology Guwahati for the degree of Doctor of Philosophy has been carried out under my supervision in the Department of Mechanical Engineering, Indian Institute of Technology Guwahati. This work has not been submitted elsewhere for the award of any other degree or diploma.

Dr. Manas Das
Department of Mechanical Engineering
Indian Institute of Technology Guwahati
Guwahati-781039, Assam, India

Date: 22.05.2023

Declaration

I declare that this written submission represents my idea in my own words and where others' ideas or words have been included, I have adequately cited and referenced the original sources. I also declare that I have adhered to all principles of academic honesty and integrity and have not misrepresented or fabricated or falsified any idea/data/fact/source in my submission. I understand that any violation of the above will be cause for disciplinary action by the institute can also evoke penal action from the sources which have thus not been properly cited or from whom proper permission has not been taken when needed.

Date: 22/05/2023

Abhinav Kumar
Roll No.: 176103020

Dedicated to

My Grand Parents

ACKNOWLEDGEMENT

I would like to take this opportunity to pay my deep sense of respect and sincere gratitude to my supervisor, Dr. Manas Das, Department of Mechanical Engineering, Indian Institute of Technology Guwahati, Assam-781039 for his invaluable advice, resourceful guidance, inspiring instructions, active supervision and constant encouragement without which it would not have been possible for me to reach to this point.

I also wish to thank to my doctoral committee members, Dr. S. Senthilvelan, Dr. Sajan Kapil and Dr. Subrata Majumder for their guidance, moral support and encouragement to my ideas in the subject as well as other areas of innovations. I must not miss the opportunity to thank all the Professors of Mechanical Engineering Department, Indian Institute of Technology Guwahati, whose motivation and timely help molded me in all possible forms.

I would also like to thank Mr. Jiten Basumatary for his support in carrying out my work in advanced manufacturing lab. I am very much thankful to workshop superintendent Mr. N. K. Das and workshop technicians Mr. Upen Gohain and Mr. Santosh Gogoi for their help to fabricate my experimental setup and workpieces. I would like to acknowledge Central instrument facility (CIF) of IIT Guwahati for kind assistance to carry out my research work.

Last, but not least, I am deeply indebted to my parents for the sacrifices they have borne to ensure the fulfillment of my dreams. I would like to thank my family for their support and motivation during my PhD.

The time I spent with all my friends and seniors at IIT Guwahati, Dr. Manjesh Kumar, Niranjan Kumar Chaudhary, Mukesh Kumar, Mukesh Sharma, Ambrish Singh, Hari Narayan Singh Yadav, Ranajit Mahanti, Anand Mohan Pandey, Atul Singh Rajput, Akash Tyagi, Dr. Kaustubh Khaire, Keili Durgaprasad, Dr. Anupam Alok, Dr. Chandan Kumar, Dr. Anwesa Barman, who made my life enjoyable and memorable on the campus.

ABHINAV KUMAR

Abstract

Micro-manufacturing plays a vital role in manufacturing components due to the increasing demand for micro-electromechanical systems (MEMS) such as actuators, sensors, etc. It can be performed with conventional and non-conventional processes. The major challenge with traditional micromachining is the forces and vibration due to direct contact between the tool and workpiece, poor surface integrity, low dimensional accuracy, and frequent breakage of microtools. However, among non-conventional micromachining processes, mainly the thermal-induced processes such as laser beam machining (LBM) and electrical discharge machining (EDM) are widely used, which induces residual stress on the workpiece surface, producing crack-prone areas, high energy consumption, poor dimensional tolerance, and low surface integrity. Micro-manufacturing faces two significant challenges: the microtool's non-availability and the requirement of excellent surface integrity of fabricated micro-components.

The present thesis focuses on solving the two major challenges of micro-manufacturing via the electrochemical-based method. The significant advantage of this method is high dimensional accuracy and better surface integrity. The thesis is divided into two sections. The first section includes the development of electrochemical micromachining (EMM) setup and the fabrication of microtools. The second section consists of developing an electropolishing (EP) setup and improving the surface integrity of electrical discharge machined components.

In the first section, an experimental setup of EMM has been designed and developed for the fabrication of micro-features. The developed setup consists of subsystems: the power supply unit, tool and workpiece holding unit, electrolyte and filtration unit, and the CNC controller for precise movement. EMM is also termed an anodic dissolution process, i.e., the terminal which acts as an anode (connected to the positive terminal of the power supply) will undergo atom-by-atom dissolution. The electrolyte container is made of Perspex material, a non-conductive and non-reactive material, so there is no charge loss during the process. One major hurdle in developing the EMM setup is to provide a power supply to the rotating tool. It is solved with the help of a carbon brush arrangement. A fixture is also developed for holding and supplying power to the workpiece. With the developed EMM setup, microholes are fabricated with the help of a microtool diameter of 500 µm. The fabricated microholes have an entry and exit diameter of 654 µm and 538 µm, respectively.

The developed EMM setup is used to fabricate microtools as it produces the least damage to the tool surface during fabrication. The commercially available tungsten microtool

having an initial diameter of 500 µm is further reduced using two different techniques. In the first technique, the tool is placed inside the pre-fabricated hole of diameter 2 mm on stainless steel (SS) plate, and the effect of tool rotation is analyzed. Comsol® Multiphysics software is used to create a 2D model to study the variation of current density distribution in the interelectrode gap (IEG).

The tool is kept adjacent to the SS plate in the second technique, and the analysis is based on the IEG during machining. Here, two arrangements are made: the fixed tool and the fixed IEG. In the fixed tool system, the electrodes (tool and workpiece) are held stationary, i.e., no tool feed is given to the workpiece. As the machining progresses, the IEG increases, and the current density value decreases, which leads to non-uniform distribution of current density. This technique fabricates an average diameter of 105.5 µm microtool. In the fixed IEG, the IEG between the tool and the workpiece remains constant. During machining, as the material dissolves, the electrode is moved toward the workpiece, maintaining IEG fixed. The current density is uniform for fixed IEG, producing a uniform surface finish of the fabricated microtool. This technique manufactures an average diameter of 86.26 µm microtool.

In the second section of the thesis, an experimental setup of electropolishing (EP) has been designed and developed for the surface integrity improvement study of the electrical discharge machined thin-cruciform gimbal flexure of the gyroscope. The material used for the fabrication of the gyroscope is maraging steel. An organic electrolytic combination of acetic acid and perchloric acid in the volume ratio of 3:1 is selected. A polarization curve is drawn to find the voltage-current characteristics of the selected electrolyte on the maraging steel workpiece. Preliminary experiments are performed, and it is found that EP at a temperature of 60 °C, magnetic stirrer rotation of 400 rpm, and polishing time of 6 mins, gives a maximum improvement of 56.25% in surface roughness and 60.3% in surface reflectance. X-ray photoelectron spectroscopy (XPS) analysis suggests the formation of oxide layer after EP. The corrosion test with 3.5 wt.% NaCl solution is performed, and it is observed that the corrosion resistance of the electropolished surface increases. The preliminary experimental study suggests the suitability of the selected electrolyte combination while electropolishing of maraging steel components.

Now, the next step is to find the feasibility of EP for the electrical discharge machined component. A cavity is formed via EDM, and its surface integrity is analyzed after EP. The surface integrity includes residual stress, surface morphology, microstructure, tribological properties, etc. The generated surface residual stress after EDM is measured using "$\sin^2\psi$

method" of *X-ray Diffraction* (XRD). It is found that a tensile residual stress of 407.17 MPa is generated after EDM, which is successfully reduced to 35.27 MPa after EP. A non-uniform recast layer (between 3.93 µm–7.55 µm) is formed over the surface after EDM, which is successfully removed after EP. The EDM machined surface's morphology generates many surface defects like micro-cracks, globules, voids, craters, and pockmarks, which are successfully removed after EP, and a highly polished surface is obtained. Energy-dispersive X-ray spectroscopy (EDS) analysis suggests the inclusion of components of tool material and carbide formation after EDM. However, EP removes the recast layer; thus, the surface regains its elemental composition similar to the base material. Hence, EP can enhance the surface integrity of the electrical discharge machined components.

Finally, the thin-cruciform gimbal flexure of the gyroscope is fabricated via EDM. The parameters are optimized by response surface methodology, and ANOVA analysis is performed for surface roughness to find the percentage contribution of each parameter. The optimized parameters that provide the best electropolishing effect are 50 °C temperature, 650 rpm of magnetic bid rotation, and 350 sec of polishing time, which reduces the surface roughness value from 1.18 µm to 0.112 µm. The nanoindentation study is performed, and the maximum indentation values for the base material, EDM machined (i.e., on the recast layer), and electropolished surfaces are 300 nm, 250 nm, and 310 nm, respectively. The harder the surface, the lesser indentation is observed. The hardness and Young's modulus values of electropolished surfaces are slightly reduced compared to the base material as the oxide layer is formed after EP.

Table of Contents

List of Figures

List of Tables

NOMENCLATURES

ψ	Tilt angle (radian)
θ	Diffraction angle (radian)
$\emptyset$	Diameter of copper tool (mm)
η	Current efficiency
ν	Poisson's ratio
φ	Potential across electrodes (V)
J_n	Normalized current density (A/m^2)
d	Crystallographic plane distance (Å)
R_a	Average surface roughness
AFF	Abrasive flow finishing
Al_2O_3	Aluminium oxide
ANOVA	Analysis of variance
CH_3COOH	Acetic acid
CMG	Chemo-mechanical grinding
CNC	Computer numerical control
DI	Deionized water
DOE	Design of experiment
E	Young's modulus (GPa)
ECM	Electrochemical Machining
EDM	Electrical Discharge Machining
EDS	Energy-Dispersive X-Ray Spectroscopy
EMM	Electrochemical Micromachining
EP	Electropolishing
F	Faraday's constant of electrolysis (C/mol)
FEA	Finite element analysis
FESEM	Field emission scanning electron microscope
IEG	Interelectrode gap
$HClO_3$	Perchloric acid
HNO_3	Nitric acid
IEG	Interelectrode Gap
LSV	Linear sweep voltammetry

MAAFM	Magnetically assisted abrasive flow machining
MAF	Magnetic abrasive finishing
MFAF	Magnetic field assisted finishing
MRAFF	Magnetorheological abrasive flow finishing
MRF	Magnetorheological finishing
MRR	Material Removal Rate
NaCl	Sodium Chloride
$NaNO_3$	Sodium Nitrate
R-MRAFF	Rotational magnetorheological abrasive flow finishing
RSM	Response surface methodology
SiC	Silicon carbide
XPS	X-Ray Photoelectron Spectroscopy
XRD	X-ray Diffraction

Chapter 1 Introduction and Literature Survey

1.1 Introduction

Modern manufacturing industries require miniature components/features in various areas like automotive, aerospace, electronics, medical devices, and optics to enhance the product's functionality. The increasing demand revolutionizes the manufacturing industries. The fabrication of micro-features such as micro-channels attains a lot of attention which helps in drug delivery, fluid flow study, and mixing of fluids. The fluid flow is considered laminar, which enhances micro-channels' heat transfer [1]. Micro-hole in the fuel injector nozzles, printers nozzles, etc., improves the functionality as well as precision of the work. Micro-texturing enhances tribological and wettability properties by increasing the surface area [2]. The addition of fins on the external surface of the micro-components enhances heat transfer; However, it changes the dimensional stability. Surface texturing may be a better solution to this problem, which increases the overall surface area and further enhances heat transfer. Most of us fear inserting hypodermic needles, as suggested by the doctor, into the body while taking medicine due to the high insertion force. A possible way to reduce this insertion force is to create a micro-texture over the surface of the hypodermic needle as it decreases the overall contact area [3]. Fabrication of micro-mold while manufacturing micro-injection requires a specially designed micro-manufacturing technique. Surface roughness plays a crucial role during the post-processing of the component’s fabrication. The micro-components require an ultra-high surface finish, reducing wear and tear and enhancing their working performance. The micro-components fabricated from additive manufacturing have high surface roughness, and the produced components fail for direct use. Therefore, a post-processing technique is necessary to reduce the surface roughness of the micro-components.

Researchers all around the globe find this attractive and try to contribute in an innovative way to fulfill the demands. For the last several decades, researchers have been working continuously to transform the macro-manufacturing process for the fabrication of micro-features and its post-processing on any hard-to-machine materials. Micro-manufacturing processes can be divided into two major sub-divisions, i.e., micromachining and finishing/polishing (i.e., post-processing).

1.2 Micro-Manufacturing Processes and Challenges

Micro-manufacturing processes include the machining and finishing micro-components; hence, they can be broadly classified into these two categories. It is further divided into conventional and non-conventional processes, as discussed in the following sub-sections. A flow chart of the micro-manufacturing processes is summarized in Fig. 1.1.

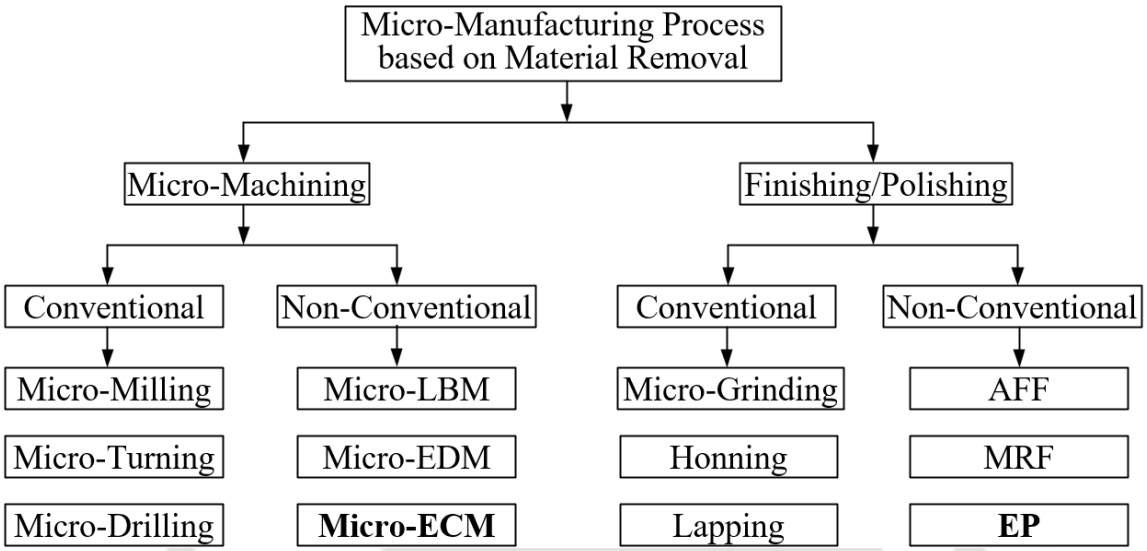

Fig. 1.1 Flow chart of micro-manufacturing process based on material removal

1.2.1 Micromachining

Micromachining is defined as the removal of material from a component in the micron range. The tolerance limit required in micromachining is also very high. Microtools are needed to remove such small materials with precise machining. Micromachining can be performed by conventional and non-conventional processes.

1.2.1.1 Conventional Processes

The conventional machining process involves direct contact between the tool and the workpiece. Due to direct contact, a large amount of force is applied during machining. Due to this, the machining rate is high, and the tolerance and surface roughness of the machined components is high. A few conventional micromachining processes are discussed below.

Micro-Milling

In micro-milling, the machining scale, namely the depth of cut, is at the micron level, and the machined feature size is smaller than 1 mm. The uncut chip thickness constantly changes as

the cutter rotates. The milling operations can be performed in three ways; side milling, face milling, and end milling. It finds its application in the fabrication of precision molding dies, micro-features such as micro-dimples, micro-channels, etc. Micro-milling cutters are made of very hard materials, as there is direct contact between the tool and the workpiece. The hard tools can be fabricated by conventional methods such as grinding and polishing or non-conventional processes such as focused ion beam (FIB) and electrical discharge machining (EDM). The formation of burr is a critical issue limiting the product quality of micro-milled components.

Micro-Turning

Micro-turning is one type of micromachining process that uses a solid tool, and its material removal mechanism is almost similar to conventional turning operations. Cutting speed, feed, and depth of cut are the primary process parameters for micro-turning. The typical process responses are surface roughness, flank wear, material removal rate (MRR), and machining time. Due to the vibration generated during micro-turning in the lathe, the produced components have burrs and high surface roughness. Micro-turning is performed at high spindle speed due to the fabrication of micro-parts from a small diameter workpiece.

Micro-Drilling

Micro-drilling is the process of fabricating a hole in the workpiece whose diameter equals or below 1 mm. Micro-drills frequently break down before they wear out. This is mainly because of the relatively significant load on the drill bit compared to its strength. Even a slight change in process parameters or an increase in forces can cause catastrophic destruction of these fragile tools. Hence, selecting appropriate parameters, including tool material, shape and geometry, and lubrication, is very important to obtain satisfactory micro-drill performance.

Micro-drills rotate at a tremendously high speed; consequently, the friction causes high temperatures. In addition, the chips formed during machining increase stress on the cutting edges of the drill. These eventually lead to fatigue and subsequent breakage of the micro drill. For this reason, selecting a suitable material for the micro drill is crucial. Tool materials generally used are tungsten carbides (WC), high-speed steel (HSS), cemented carbide, and polycrystalline diamond (PCD), etc. Various steps of grinding manufacture these micro-drills.

Challenges

The major challenge with the conventional micromachining processes is the direct contact between the tool and the workpiece, which involves higher forces and produces vibration during machining. These vibration leads to the formation of burrs and degrades the surface finish of the components. In micromachining, micro tools tend to break down faster than wear out. Hence, frequent breakage of micro tools takes place. Fabrication of complex micro-components is cumbersome via conventional micromachining processes.

1.2.1.2 Non-Conventional Processes

Non-conventional machining process does not involve direct contact between the tool and the workpiece. Due to this, negligible forces are involved during machining. Hence, the machining rate is low; however, the tolerance and surface finish of the machined components are very high. A few major non-conventional micromachining processes are discussed below.

Micro-Laser Beam Machining

In laser beam micromachining (LBMM), material removal occurs through the ablation process, where the target material under laser irradiation absorbs the laser energy and transforms it into liquid or vapor. The material in the focal region is heated to the melting temperature and subsequently to vaporization temperature depending on laser intensity, work material properties, and pulse duration. The recoil action expels the melted liquid from the interaction region (laser focus), and the vapor removes itself directly from the focus area.

Heat diffusion also reduces the micromachining operation's accuracy because boiling results in material removal not limited to the beam's spot size. Hence, in many materials, it is impossible to create features with dimensions smaller than 10 μm even though the minimum laser spot size might be in the range of one micron. Heat diffusion also results in a larger heat-affected zone (HAZ). The alternate heating and subsequent cooling waves propagate through the HAZ, which may result in mechanical stress leading to micro-cracks (or macro cracks) in the surrounding material, which causes premature device failure.

Micro-Electrical Discharge Machining

In electrical discharge micromachining (EDMM), material removal occurs due to the thermal erosive action of the electrical discharges (i.e., sparks) between the electrodes generated from a pulse DC power supply. The tool (i.e., cathode) and the workpiece (i.e., anode) are

connected to the positive and negative terminals of the DC power supply. The electrodes are immersed in the dielectric fluid (kerosene, paraffin oil, deionized water, etc.). Due to a very high electric field gradient across the two electrodes, a plasma channel is formed, and a discharge occurs through the dielectric. Every discharge (or spark) melts and /or vaporizes a small amount of material from both electrodes; a part of the molten material is removed from the interelectrode gap (IEG) by the flowing/flushing dielectric fluid, and the remaining re-solidifies on the machined surface. The resolidified material is known as the recast layer. The net result is that each discharge leaves a small crater on both electrodes.

EDM has become an indispensable process in modern manufacturing industries because of its ability to produce complex shapes with high accuracy in difficult-to-cut but electrically conducting materials. The spark size can be substantially reduced by selecting the machining parameters; also, the sparking frequency can be considerably increased to create micro-features with high accuracy and better surface finish on components. Then, the process is called "electrical discharge micromachining." Thus, the key is to limit the energy in each discharge to make micro-featured products with high accuracy and good surface finish. To achieve this, the energy required in a single discharge should be approximately 10^{-7} J.

Micro-Electro Chemical Machining

Electrochemical micromachining (EMM) consists of an electrolytic cell, and machining occurs following Faraday's laws of electrolysis. Here, the workpiece is connected to the positive terminal (i.e., anode), and the tool is connected to the DC power supply's negative terminal (i.e., cathode). A non-toxic salt solution is used as an electrolyte, and controlled metal removal occurs from the anode when the current flows through the electrolytic cell from a constant/pulse DC power supply. This process is widely practiced in aerospace, automobile, and other heavy industries for shaping, sizing, deburring, and finishing operations. Many metals and alloys, including conducting ceramics and highly corrosion-resistant alloys, can be machined by EMM. Most thin films of metals and alloys used in microelectronic industries can be anodically dissolved (or machined) in neutral electrolyte salts (such as sodium nitrate, sulfate, or chloride) commonly used in EMM. The dissolved metal ions form hydroxides that precipitate, which remain suspended in solution and can be easily filtered, thus significantly minimizing safety and waste disposal problems.

Accumulating reaction products in solution and electrolyte depletion is a minor concern in EMM. The metal removal rate, micro-feature profile, surface finish, and uniformity of metal removal are some of the performance evaluation criteria in EMM. The material

removal rate in EMM depends on the specific electrochemical behavior of the metal-electrolyte system and is determined by the current density in IEG.

Challenges

The significant challenges with the non-conventional micromachining processes are the slow material removal rate and high energy consumption, which increases production costs. The thermal-induced processes such as LBMM and EDMM induce residual stress on the workpiece surface, producing crack-prone areas. However, EMM does not create any residual stress. Precise control of the process parameters gives a better surface finish to the fabricated micro-components.

1.2.2 Finishing

Finishing is generally termed as the reducing surface roughness of the components. The surface roughness should be as low as possible for better performance of the parts. The products with high surface roughness will have a little life span because of corrosion and wear. Proper finishing of the products is necessary to achieve a better life span of products, whether large or miniature. Machining provides the desired component shape; finishing processes remove the irregularities from the machined component's surface. Finishing processes do not change any geometry, only reduce the surface roughness. Finishing can be performed by conventional and non-conventional approaches.

1.2.2.1 Conventional Process

In the conventional finishing processes, friction between the abrasive/abrasive-tool and the workpiece is responsible for material removal and producing a good surface finish with close tolerances. This process is simple and does not require immense machine knowledge. The primary conventional finishing processes are discussed below.

Grinding

Grinding, an abrasive finishing process, is widely used to reduce the surface roughness of the machined components. In this process, a grinding wheel bonded with abrasive particles is used to finish the surface of the workpiece. The workpiece is pressed against the grinding wheel such that contact is always developed between them for proper finishing. The abrasive particles act as a single-point cutting tool to remove the material from the surface. This

process gives more material removal rate compared to other traditional finishing processes. Here, abrasion is the reason for material removal. Due to the random orientation of abrasive particles, it requires the highest specific cutting energy.

Honing

Honing is performed by a honing tool or stone, which is an abrasive stick or abrasive stone. The honing tool moves up and down and rotates inside the component to be finished. The honing tool abrades the workpiece surface along a predefined path with the help of cutting pressure and cutting velocity. It leaves a cross-hatched surface which is also helpful for fuel retention in an internal combustion cylinder. This process is generally employed to finish inner cylinder surfaces.

Lapping

The lapping process provides a high degree of surface flatness by pressing a lapping plate over the workpiece with abrasive media in between them. It ensures proper match of surfaces. A conditional ring or retaining ring maintains uniform slurry distribution. The workpiece is rotated while in contact with the abrasives particles. Because of the shearing action of abrasive particles, the irregularities from the surface are removed, and an ultra-polished surface is obtained. The size and type of abrasives used for valve lapping depend upon the finishing requirements. Generally, used to polish small components like slip gauges, gears, valves, etc.

Challenges

Conventional finishing methods are very efficient for finishing the workpiece which is simple in geometry. However, these finishing techniques cannot finish complex geometry in miniature dimensions. Grinding wheels are rigid and cannot finish intricate shapes of miniature components. Honing is generally employed for internal surfaces but finds it challenging to finish the intricate shapes. Lapping requires the workpiece to rotate for finishing. i.e., the component must be axis-symmetry to get uniform finishing. The conventional finishing process can reduce surface roughness to a very low value but not be suitable for finishing intricate shapes or any customized shape of micro-components.

1.2.2.2 Non-conventional Process

Non-conventional finishing processes are in great demand due to their capability to finish any complex shapes of miniature dimensions. The final surface roughness of the finished component is very low, even in a nanoscale. A few important non-conventional micro-finishing processes are discussed below.

Abrasive Flow Finishing

Abrasive flow finishing (AFF) is a process in which a small quantity of material is removed by flowing a semisolid abrasive-laden putty over the surface to be finished. The media has a high viscosity such that it can be held between fingers like a rubber ball which deforms by applying a little pressure. Two vertically opposed cylinders extrude abrasive media back and forth through passage(s) formed either by the workpiece and tooling or by the workpiece alone. This process is suitable for deburring, radiusing, polishing, removing recast layers, producing compressive residual stresses, etc. The process can machine tens of parts simultaneously to enhance productivity. This process has high flexibility, i.e., the same machine can be used to do various jobs by changing toolings, machining parameters, media, and abrasives.

Magnetorheological Finishing

Magnetorheological Finishing (MRF) is a non-conventional finishing technique that utilizes a smart fluid that stiffs as it comes in the vicinity of the magnetic field. Like AFF, it consists of abrasive and carbonyl iron particles (CIPs) mixed with additives. This MRF fluid and the workpiece to be polished are kept in a fixture such that magnetic lines stiffens the MRF fluid. This stiff fluid passes through the miniature component, and depending upon the magnetic strength, the stiff MR fluid removes the irregularities from the surface and provides a polished surface. The final surface roughness depends on the concentration of abrasive particles, CIPs, magnetic strength, and polishing time.

Electrochemical Polishing

Electrochemical Polishing (EP) is a non-conventional finishing process in which an electrolytic cell is developed. The workpiece to be polished is made as the anode, and the tool is made as the cathode. A polarization curve is drawn to find the polishing region. Generally, the acidic electrolyte is used for EP. The hardness of the workpiece does not have any effect

on EP. Any complex shape or intricate location can be effectively electropolished. When a potential is applied, the anode undergoes anodic dissolution with the release of hydrogen gas at the cathode. The cathode is generally made from chemically inert materials. Researchers are utilizing EP to polish the complex components fabricated from additive manufacturing.

Challenges

The major challenge with the non-conventional finishing processes is the slow material removal rate and high energy consumption, increasing the production cost. These processes can finish any complicated or intricate shape but require a dedicated setup for finishing. Most of the finishing processes need abrasives to remove surface irregularities. Abrasives are very costly and cannot be reused due to the mixing of debris from the workpiece. However, EP utilizes only chemicals, which can be reused as the debris from the workpiece acts as a residue. However, only conductive workpieces can be electropolished. Precise control of process parameters gives a better surface finish to the fabricated micro-components.

1.3 Anodic Dissolution Based Processes

Anodic dissolution-based processes involve an electrolytic cell in which the workpiece is made as an anode, and the tool acts as the cathode. As the workpiece material undergoes dissolution upon supply of potential difference between the electrodes, it is termed an anodic dissolution process, which can be employed for machining and polishing. In machining, the shape on the tool is the negative replica of the shape to be produced on the workpiece. The controlled anodic dissolution takes place, and finally, the shape exactly negative of the tool is formed on the workpiece. However, in EP, only the surface connected to the anode and surface irregularities are removed to reduce the surface roughness to nano-scale. It also enhances corrosion resistance by forming an oxide layer.

1.3.1 Electrochemical Micromachining (EMM): An Overview

Electrochemical micromachining (EMM) is one of the non-conventional micromachining techniques. In EMM, material removal follows Faraday's laws of electrolysis. EMM appears to be a promising micromachining technology due to its advantages, which include high MRR, better precision and control, rapid machining, and environmentally friendly electrolyte. It also permits the machining of chemically resistant materials like titanium, copper alloys, super alloys, and stainless steel [4].

EMM is an anodic dissolution process where the workpiece acts as an anode and the tool as a cathode, separated by a minimal inter-electrode gap (IEG). Both tool and workpiece are dipped inside the electrolyte, and an electrolytic cell is formed. A separate workpiece and tool fixtures are also arranged for holding them. The tool is connected to the negative terminal, and the workpiece is connected to the positive terminal of the DC power supply. Upon applying the potential difference between the electrodes, an electric current passes through it. The schematic diagram of the EMM experimental setup is shown in Fig. 1.2. The workpiece dissolves locally in shape, which is approximately the negative replica of the tool. Thus, in EMM, the desired final form of the workpiece depends on the tool shape.

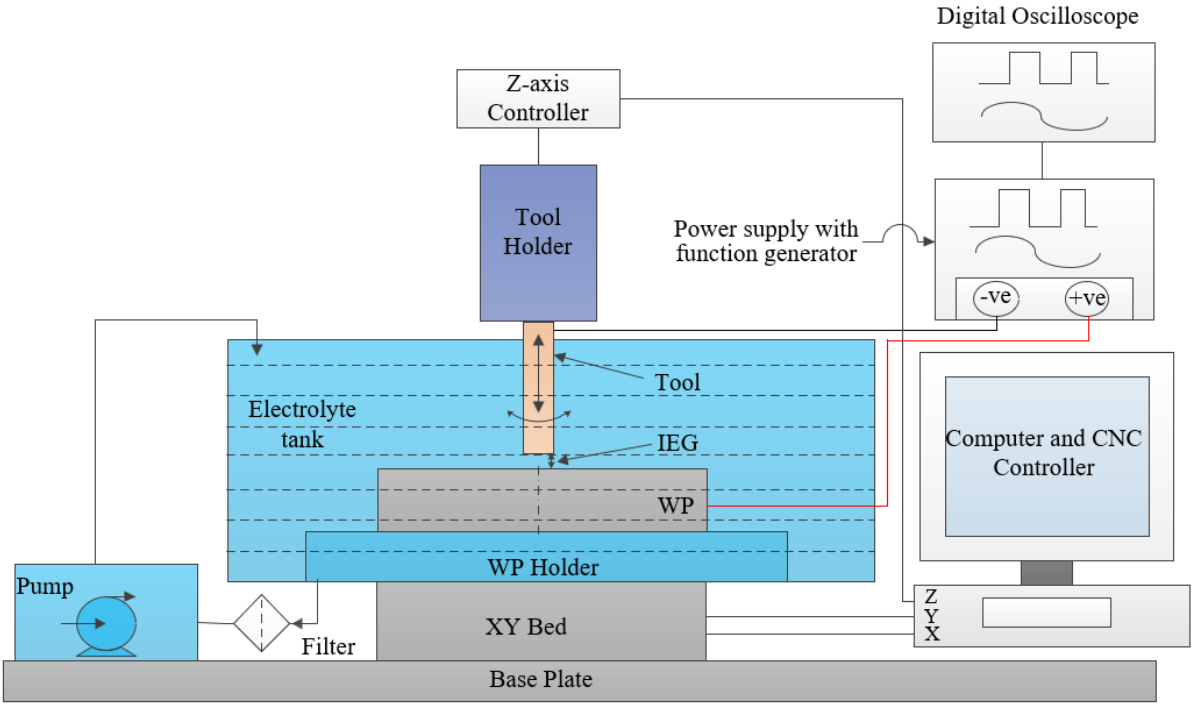

Fig. 1.2 Schematic diagram of EMM experimental setup

In EMM, the workpiece dissolves, which is connected to the anode, so it is also called anodic dissolution. The metal dissolution takes place atom by atom from the workpiece and forms precipitates in the electrolyte. Hydrogen gas evolves at the cathode, and the metal is removed as ions from the anode. The reactions that take at the anode and cathode are

At cathode: $$2H_2O + 2e^- \rightarrow H_2 \uparrow + 2OH^- \quad (1.1)$$

At anode: $$M \rightarrow M^+ + e^- \quad (1.2)$$

$$M^+ + (OH)^- \rightarrow M(OH)$$

The EMM setup consists of an electrolyte purification system to filter electrolytes mixed with debris particles for reuse. A computer numerical control (CNC) controller is connected to the XYZ axes via a computer for precise axes movement.

Material removal in EMM is governed by Faraday's laws of electrolysis [5]. In EMM, the material is removed from the workpiece atom by atom. So, the workpiece is made as the anode and the tool as the cathode in the electrolytic cell. Faraday's laws of electrolysis are described below:

- The amount of substance dissolved or deposited is proportional to the amount of electricity passed.
- The amount of different substances deposited or dissolved by the same quantity of electricity is proportional to their chemical equivalent weights.

The mathematical expression of Faraday's laws is expressed in Eq. (1.3)

$$m = ItA / zF \tag{1.3}$$

where m is mass in grams, I is current strength (Amp), t is the time (seconds), A is atomic weight, and z is the valency of dissolution, F is Faraday's constant (96500 As). From Ohm's law

$$V = IR \tag{1.4}$$

where V is the potential difference, I is the machining current, and R is the resistance. Further, m can be written as

$$m = \frac{EVt}{RF} = \frac{EVta}{F\rho l} \tag{1.5}$$

where $R = \rho l / a, \rho$ is the resistivity of the electrolyte, l is the IEG, a is the cross-sectional area of the machining zone, and E is the gram equivalent weight of material (A/z). Thus, the material removal rate (MRR) can be expressed as

$$MRR_{ther} = \frac{EV}{RF} \tag{1.6}$$

EMM finds its application in the fabrication of various micro-features like micro-holes, micro-channels, etc., as well as for microtools fabrication.

1.3.2 Electrochemical Polishing: An Overview

Electrochemical Polishing (EP) is a particular case of electrolysis in which the workpiece, which is to be polished, serves as an anode & the tool as the cathode. On applying the potential difference between these electrodes, an electric current flows through the electrolyte. Electrons are carried away from the anode surface to the cathode. At the anode, the metal electrode gets oxidized to metal ions by losing electrons & then dissolving into the electrolyte, causing material removal. At the cathode, the electrode gains electrons & gets reduced, liberating hydrogen gas. Material removal rate depends on various factors like workpiece material, EP time, temperature, etc. However, current density and EP time generally control the surface roughness of the workpiece.

(a) (b)

Fig. 1.3 Surface conditions (a) before and (b) after EP [6], [7]

The benefit of electropolishing is that it delivers a smoother, reflective surface and improves surface hydrophilicity. Perhaps more important, electropolishing preferentially dissolves free ions, inclusions, and embedded particles from the surface of the workpiece.

This process improves the near-surface chemistry of the material and promotes the formation of a corrosion-resistant surface layer. It is also very cost-effective compared to other polishing methods. The surface condition of the workpiece before and after EP is shown in Fig. 1.3. All the surface irregularities and scratches on the workpiece surface have been removed after EP.

In EP, Jacquet's theory is used to analyze the anodic dissolution process. The current density-voltage curve for EP contains four regions, i.e., etching, passivation, limited current plateau & gas evolution region, as shown in Fig. 1.4. In the etching region, the workpiece is directly dissolved. In the passivation region, the slight decrease in current density with an increase in applied voltage typically indicates the generation of the passive layer on the anodic surface. In the polishing region, the passivation layer is stabilized, and anions dissolved from the metal surface diffuse through the passivated layer. In the gas evolution region, the passive oxide film's breakage leads to the pitting on the anodic surface. EP occurs in the polishing region (limiting plateau region) at constant current density.

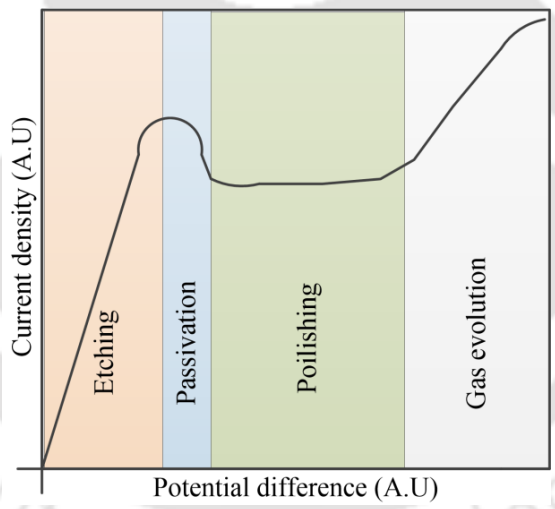

Fig. 1.4 Current density-voltage curve of electropolishing [8]

The theory best explains the mechanism of EP is Jacquet's viscous layer theory. According to this theory, a thin viscous layer is formed between the metal surface & electrolyte during anodic dissolution. The high electrical resistance of the viscous layer limits the material dissolution. The viscous layer formed is thick in the valley region and thin in the protruding regions of the surface profile, as shown in Fig. 1.5. Hence, the electrical resistance also varied in these regions due to which material dissolution is slower at valleys & faster at protruding regions. This difference in the dissolution rates creates a polishing effect on the

workpiece surface. The movement of metal ions from the workpiece surface to the bulk electrolyte is limited by the thickness of the viscous layer [9].

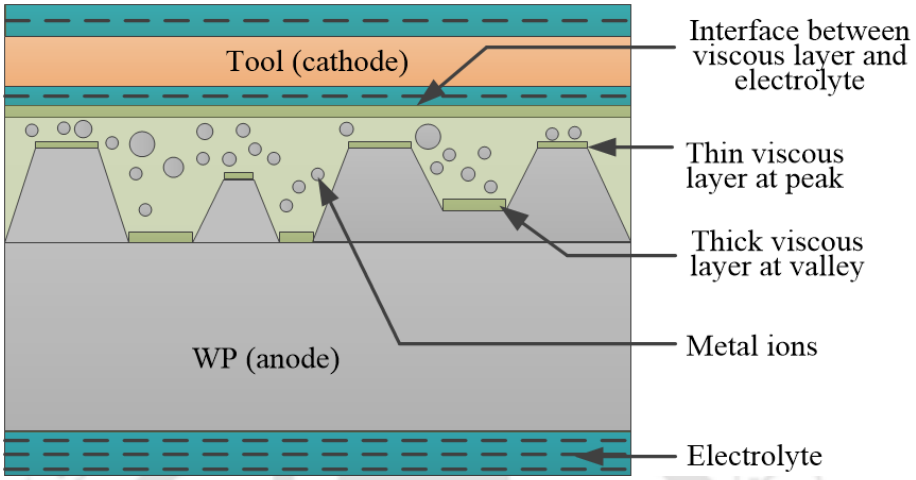

Fig. 1.5 Mechanism of anodic dissolution in EP

1.4 Literature Survey

In this section, an extensive literature survey has been performed for the electrochemical-based processes, mainly machining and polishing, to overcome micro-manufacturing challenges. This section is further divided into sub-sections. In subsection 1.4.1, a detailed study is performed to develop the experimental setup of EMM. The components and their resolution suitable for micromachining have been presented. Subsection 1.4.2 includes thorough research about the influential process parameters to achieve the required precision. In subsection 1.4.3, a detailed study of the various processes for microtool fabrication is presented. In subsection 1.4.4, a summary of the literature on EMM is presented.

In subsection 1.4.5, a detailed study is performed for the development of the experimental setup of EP. In subsection 1.4.6, thorough research about the influential process parameters for achieving a high surface finish is discussed. In subsection 1.4.7, a detailed study about the surface integrity analysis of the electropolished component is performed. In subsections 1.4.8 and 1.4.9, applications and literature summary of EP have been presented.

1.4.1 Development of Experimental Setup of EMM

Considering the importance of EMM, researchers from various research laboratories, research institutes, and universities have attempted to develop the EMM setup. However, a developed experimental machining setup must fulfill individuals' requirements while performing

experiments for a better understanding of the process. With the wide application of this process in various fields in recent years, there is an urgent need for a commercial EMM setup suitable for machining microfeatures. Progress in the development of experimental setups has been reviewed in detail in this section.

Bhattacharyya et al. [10] developed an experimental setup of EMM to conduct micromachining to understand its fundamental process. The developed EMM setup mainly consisted of several sub-components: mechanical machining unit, micro tooling system, electrical power & control system, and electrolyte flow system. All these sub-components were integrated so that the developed experimental setup could perform fundamental research in EMM, fulfilling the requirements of micromachining objectives like the precise movement of axes, power supply, etc. Several experiments were also performed at different process parameters to understand the capabilities of the developed setup.

Kurita et al. [11] developed an EMM experimental setup that consists of a current sensor between the electrodes (i.e., tool and workpiece) to monitor the IEG. The authors performed preliminary experiments to ensure the feasibility of the developed setup and investigated the influence of machining parameters on machining accuracy. The optimum process parameters were obtained to machine 3D shape with high accuracy from the developed experimental setup. A square electrode of 200 μm was selected to fabricate 3D microfeatures.

Mithu et al. [12] developed an electrolytic cell for in-process monitoring based on waveforms generated during EMM to reduce the detrimental effects associated with the process. The developed setup consists of a function generator to generate pulses at different parameters, a digital storage oscilloscope to record the generated pulses, computer-controlled guide system for feeding the tool and the workpiece. Pulse waveforms generated during machining were correlated with material removal rate, machining time, and the dimensions of the machined micro-holes. From the experimental results, the authors concluded that the waveform generated during machining bears significant information about the MRR, machining time, and the dimension of the fabricated micro-holes.

Zhang et al. [13] developed an experimental setup for EMM to fabricate the microtool and microfeatures on the workpiece. The developed experimental setup consisted of mechanical movement equipment, an ultra-short pulse power supply, an electrolyte circulation system, and a hall current sensor for detecting the machining status. They machined the precise microgrooves with sharp edges on a nickel sheet by EMM using an in-situ fabricated tungsten microtool and ultra-short voltage pulses. However, the flow

characteristics and no tool rotation produce a rough surface on the manufactured tool, which generates burrs on the fabricated workpiece.

Mishra et al. [14] developed an experimental setup for electrochemical milling, which consists of three axis stage for the precise movement of the tool and workpiece with a resolution of 0.1 µm. The DC power supply was provided with a frequency of 20 kHz. An electrolyte tank with the filtration unit was also attached. For flushing, an external nozzle was used. It was observed that the depth of the machining profile was restricted to 0.6 mm, and flushing was inefficient. The authors suggested tool rotation and internal flushing for efficient flushing.

Mishra et al. [15] utilized an inner spray rotating tool for the electrochemical milling of Nimonic-263 alloy. A rotary union was designed and developed indigenously to facilitate the electrolyte supply through the tool and the current supply to the rotating tool. It was concluded that tool rotation is preferred as it provides a more accurate and higher surface finish of the machined profiles.

Kunar et al. [16] developed an experimental setup for EMM, which can fabricate micro-features over a large area. An arrangement was made to fix the cylindrical tool of 19.8 mm diameter and 11 mm thickness with micro-holes of 800 µm. The fixture was made such that constant IEG was maintained and ports connected for the electrolyte flow. An arrangement was also made to provide a power supply to the electrodes. With the help of a developed setup, the same tool can be reused, thus minimizing the overall cost.

1.4.2 Influence of Major Process Parameters in EMM

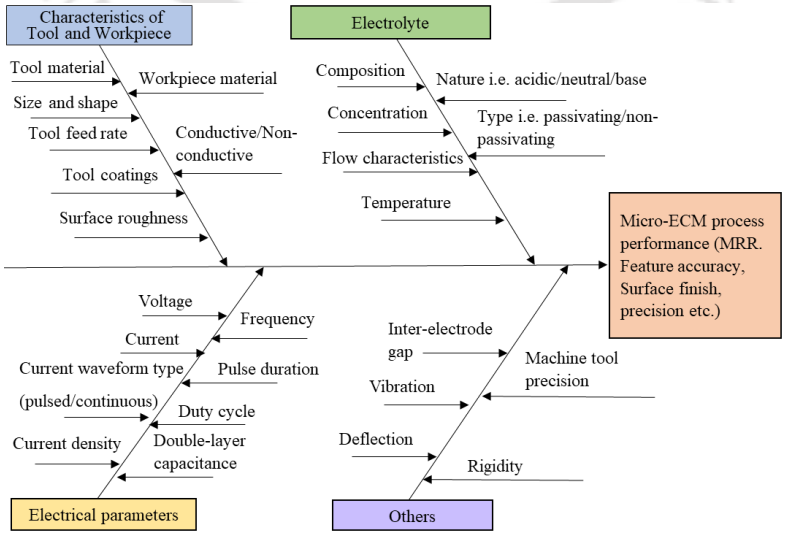

Fig. 1.6 Fish-bone diagram of EMM process parameters

A fishbone diagram for process parameters of EMM is shown in Fig. 1.6. Also known as the Ishikawa diagram (or) cause and effect diagram, indicating the influential EMM process parameters. The following process parameters must be optimally controlled to achieve effective and high-precision machining in the micron range.

- Tool and workpieces like shape, size, surface quality, tool coatings, tool feed rate, surface finish, etc., play a significant role in the surface finish of final machined components.
- Electrolyte parameters such as type of electrolyte, its concentration, temperature, flow rate, etc., ensure the electrical circuit's continuation and proper flushing of the debris from the machining zone.
- Electrical parameters such as power supply (continuous or pulse), duty cycle, and frequency provide the sufficient potential for anodic dissolution. It also helps to increase the machining accuracy.
- Mechanical capabilities of machining setup such as resolution, rigidity, and the interelectrode gap between the tool and workpiece help in machining at micron dimension. The CNC machine bed, with a resolution of 0.1 µm in all three axes, provides precise movement of the electrodes.

Li et al. [17] considered the current density distribution at the workpiece surface, which is determined solely by the Ohmic effects, and the electrodes are defined as equipotential surfaces. This signifies that as the interelectrode gap between the electrodes increases, ohmic resistance increases, thus decreasing current density.

Rathod et al. [18] studied the influence of EMM process parameters during the fabrication of micro-grooves in stainless steel with pulsed power. For achieving higher machining accuracy, lower voltage, lower electrolyte concentration, higher pulse frequency, lower duty ratio, and higher tool feed rate are recommended. However, to achieve higher MRR, higher voltage, lower frequency, higher duty ratio, higher electrolyte concentration, and higher tool feed rate are recommended. Therefore, an optimum condition with an applied voltage of 2.8 V, pulse frequency of 8 MHz, a duty ratio of 35%, electrolyte concentration of 0.15 M, and tool feed rate of 0.25 µm/s provides a minimum depth overcut of 10 µm and width overcut of 55 µm, having an aspect ratio of 2.31.

Ayyappan and Sivakumar [19] experimentally investigated to improve the material removal rate of the EMM process using an oxygen-enriched electrolyte. It was observed that

MRR increases as the electrolyte concentration increases. With the addition of oxygen, the oxidation of metal oxides enhances the machined surface to improve the MRR. With the oxygenated NaCl environment, an MRR of 7.33 g/min with R_a of 1.90 μm is obtained compared to an MRR of 1.98 g/min and R_a of 3.13 μm in an aqueous NaCl environment.

Rathod et al. [20] investigated the machining accuracy and surface roughness of microgrooves fabricated by EMM. It was observed that electric field localization plays a vital role in generating accurate microgrooves. The microgroove's linearity improves with an increase in pulse frequency and microtool scanning speed with decreased applied voltage, duty ratio, and electrolyte concentration. The minimum average surface roughness (R_a) of 0.104 μm was obtained with an optimized parameter.

Patel et al. [21] performed micro-texturing on flat and curved surfaces by EMM. A 2D numerical model was developed in Comsol multiphysics software. It was observed that the current density becomes highest when IEG is 50 μm because of low path resistance compared to the IEG of 200 μm. A proper indexing mechanism was proposed to maintain the constant IEG during EMM on curved surfaces.

1.4.3 Microtool Fabrication

For the fabrication of micro-components, the tool must be in micron dimension. The specification required for microtool is micro-dimension, good accuracy, and better surface finish. The surface finish should be good because the microtool cannot be further machined. Conventional machining processes can fabricate microtools; however, chances of tool breakage and poor dimensional accuracy limit its use in microtool fabrication.

Oliaei et al. [22] reviewed different microtool designs and their fabrication techniques (conventional as well as non-conventional manufacturing techniques). John and Fengzhou [23] studied various tool designs, materials, and fabrication techniques. They also discussed minimizing tool wear and suggested microtool manufacturing at the industrial level.

1.4.3.1 Fabrication of Microtool by EDM

Electrical discharge machining (EDM) is very popular in non-conventional micromachining as it is commercially available. It is very user-friendly, and the material removal rate is also high. It is a non-contact machining process; thus, hard materials can be easily machined. In EDM, the electrodes are immersed in the dielectric fluid, mainly kerosene. The repetitive

amount of controlled energy produces sparks between the electrodes, and these sparks remove material from the workpiece surface by melting and vaporization.

For the fabrication of the microtool via EDM, the tool to be produced in the micron shape is switched to the positive terminal, and the workpiece is connected to the negative terminal. Researchers have found three different techniques for fabricating the micro tool: sacrificial stationary block, sacrificial rotating disk, and guided running wire, as shown in Fig. 1.7.

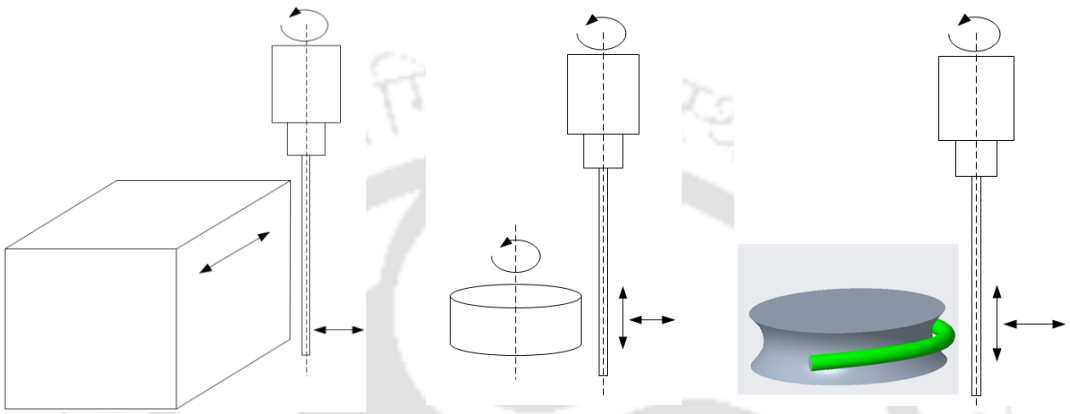

Fig. 1.7 Schematic diagram of (a) sacrificial stationary block, (b) sacrificial rotating disk, and (c) guided running wire [24]

In the sacrificial stationary block, the tool is connected to the positive terminal, and the stationary block is fixed to the negative terminal of the EDM power supply. The electrically neutral fluid, the dielectric, flows between the electrodes, and repetitive sparks take place between them to remove materials from the tool surface. The block is held stationary while the tool has rotary and linear motions. A taper microtool is formed as the lower portion of the tool interacts more with the block and produces more wear. A good surface finish of the fabricated tool can be achieved using this technique.

In a rotating sacrificial disk, the sacrificial electrode rotates about its axis along with the rotary and linear motion of the tool. The block and the tool are immersed in the dielectric fluid, and continuous sparks occur between them. Due to the uniformly distributed spark, the surface finish of the microtool is becomes good.

In guided running wire, the wire fitted in a spool continuously rotates around the tool to remove the material. The area over which the spark is generated is significantly less; thus, the spark is concentrated. As the wire rotates, fresh wire is available for the tool surface. The dielectric fluid is filled between the tool and the wire. Good dimensional uniformity is

achieved due to the availability of fresh wire. However, the achieved surface finishing is not good.

Acharya et al. [24] performed a comparative study on three different systems for fabricating micro-dimension tools, as shown in Fig. 1.7. Tungsten microtools were fabricated using micro-EDM. All the microtools manufactured from three techniques were analyzed to find the process capabilities like diameter, length, and taper angle. For the same input parameters, it was found that the tool has different wear rates for three techniques. The stationary sacrificial block gives the least diameter, whereas the rotating sacrificial disk gives minimum length and taper angle. The microtool fabricated by three different techniques is shown in Fig. 1.8.

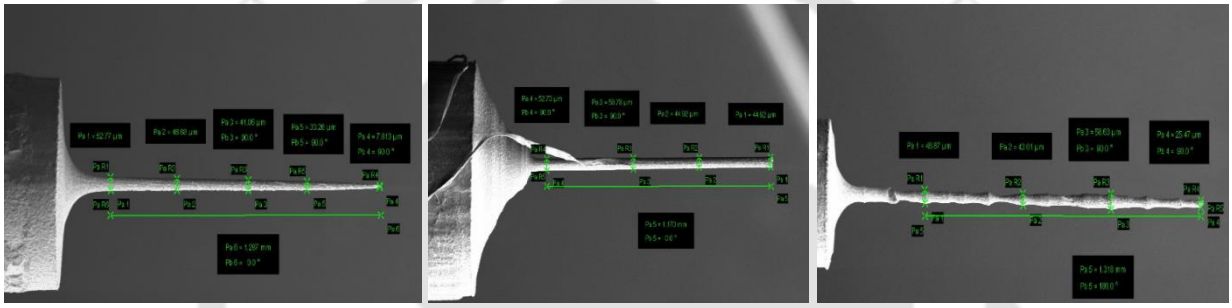

(a) (b) (c)

Fig. 1.8 Final microtool fabricated by (a) sacrificial stationary block, (b) sacrificial rotating disk, and (c) guided running wire [24]

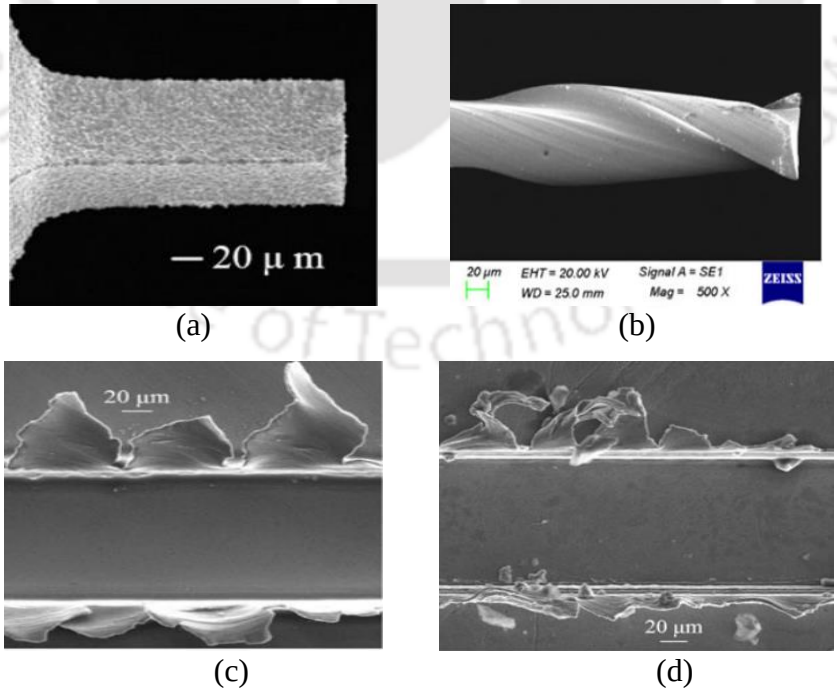

(a) (b)

(c) (d)

Fig. 1.9 (a) Fabricated tool (b) commercial tool, and fabricated micro-channel with (c) fabricated tool (d) commercial tool [25]

Malayath et al. [25] fabricated a 100 µm diameter micro-end mill tool of tungsten carbide using electric discharge machining (EDM). For the fabrication of the microtool, a replica of the tool is created on the block. Micro-channel of width 110 µm and depth 40 µm having a surface roughness of 70 nm was fabricated using this micro-end mill tool on aluminum. On the ground of machining performance, the machined microtool is matched with the commercial end mill tool of 100 µm diameter, as shown in Fig. 1.9. Fabricated micro-end mill provides a better surface finish on a fabricated micro-channel of SS304L.

Sankha and Promod [26] fabricated microtools from copper. Different profiles of microtools are generated, such as square, circular, and zigzag, with the help of wire-cut electrical discharge machining (WEDM), as shown in Fig. 1.10. The optimal tool design was achieved using the Taguchi design of experiments technique. Fabricated microtools were utilized to fabricate micro-channels on glass surfaces using ultrasonic machining (USM).

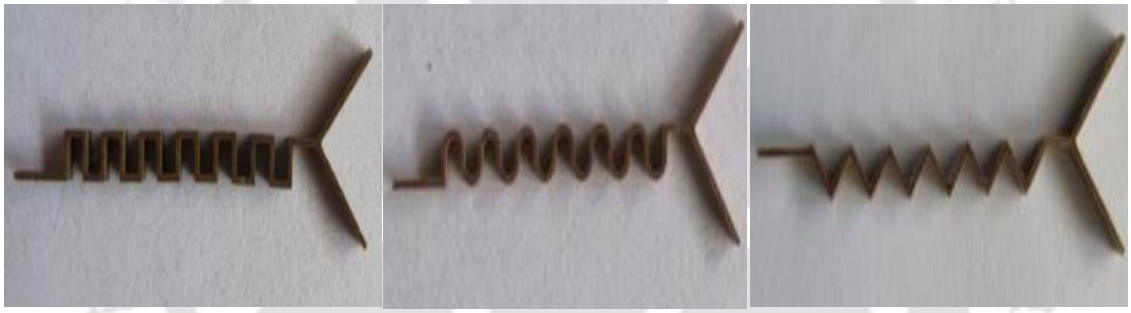

(a) (b) (c)

Fig. 1.10 Fabricated copper microtool (a) square, (b) circular, and (c) zigzag [26]

Wang et al. [27] fabricated a disk-type microtool by wire-EDM, as shown in Fig. 1.11. A graphite sheet of thickness 500 µm is cut into circular form with a 3 mm center hole. The disk electrode is made with a minimum edge width of 50 µm. The micro-ECM milling module is assembled over the wire-EDM setup, thus avoiding the re-clamping of the fabricated disk tool, which increases precision. Finally, the disk electrode (Fig. 1.11(a)) of 90 µm edge width is used to manufacture the microgroove of 146 µm width (Fig. 1.11(b)) with a surface roughness of 0.26 µm. The array of disks electrode is shown in Fig. 1.11(c).

From the above literature survey, it is found that EDM and WEDM are very effective in fabricating different shapes and sizes of microtools for micromachining. It can produce microtools below 100 µm with reasonable accuracy. As it is a commercially available process, fabrication is straightforward. But it has some limitations, such as sparks produced during machining deteriorate the surface finish and the strength of the fabricated microtool. Spark causes localized heating, which changes the grain structure also.

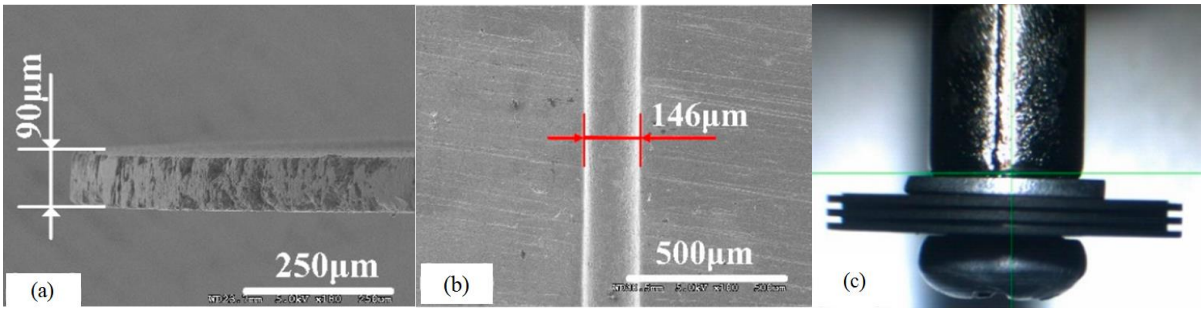

Fig. 1.11 (a) Single disk tool, (b) fabricated microgroove, and (c) array of disks tool [27]

1.4.3.2 Fabrication of Microtool by FIB

Focused ion beam machining (FIB) can mill any material precisely to fabricate microfeatures. In FIB, an ion beam focuses directly on the workpiece for material removal. Depending upon the intensity and diameter, the dimensions of the microfeatures are fabricated. The FIB consists of various parts like a liquid metal ion source, vacuum system, precise stages, detectors, ion column, and a gas inlet with a computerized control system, as shown in Fig. 1.12. The most used liquid metal ion is gallium (Ga) in FIB [28].

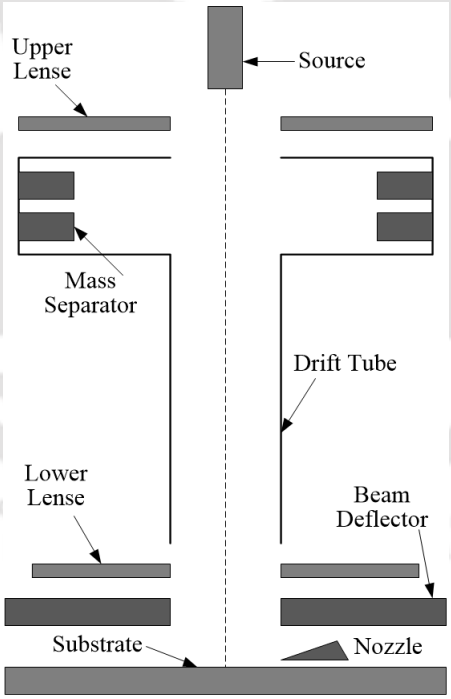

Fig. 1.12 Schematic of FIB setup [28]

As ions are larger and heavier than electrons, their movement is slow and easy to control. When the workpiece is bombarded with accelerated Ga ions, the material is removed from the workpiece atom by atom. This process of removal of atoms is called a physical sputtering process. By controlling the accelerated ions, a final micro-shape component can be

fabricated. This principle is utilized to fabricate microtools made of harder materials like high-speed tool steel, tungsten carbide, and single-crystal diamond [28].

Bhavsar et al. [28] critically reviewed the focused ion beam technology to fabricate the microtool. The step-by-step procedure has been described for the fabrication of microtools for the materials like tungsten carbide, single-crystal diamond, and high-speed tool steel.

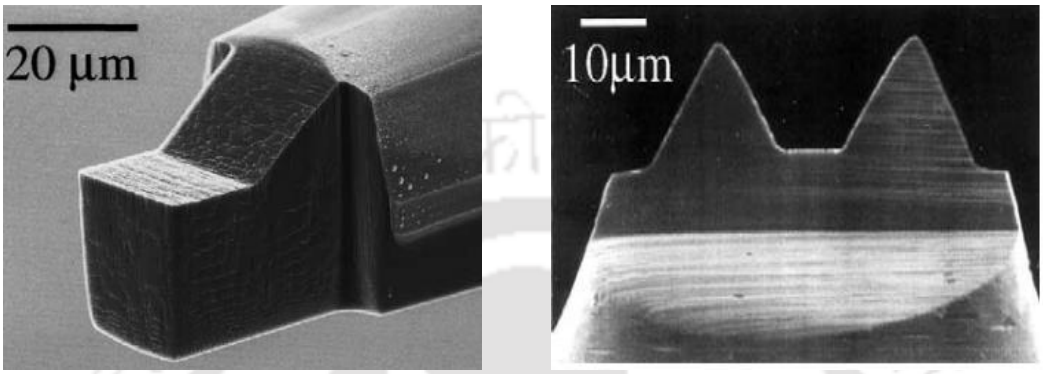

(a) (b)

Fig. 1.13 Fabricated microtool by FIB (a) rectangular tip (b) double-triangle tip [29]

Picard et al. [29] utilized FIB sputtering to shape cutting tools in the micron range with a radius of curvature in nano-meter. Tools with rectangular, triangular, and other complex-shaped face designs were fabricated on materials like high-speed tool steel, tungsten carbide, and single-crystal diamond. The cutting-edge roughness of the tool produced was less than 0.05 µm. The beam of 20 nA will result in 30 min or less time to fabricate. Tools with rectangular and double-triangle tips are shown in Fig. 1.13 (a & b). The fabricated microtool was used for manufacturing cylindrical components with ultra-precision.

Adams et al. [30] fabricated tungsten carbide microtools of 18 µm width using focused ion beam technology, as shown in Fig. 1.14. A 20 keV gallium beam has been directed on tungsten carbide to produce different facets. An edge radius of 0.1 µm with sharp cutting edges was obtained. The fabricated sharp cutting edges can machine single-crystal diamond; however, it can be blunt while machining cemented carbide. A different facet of the fabricated tool is shown in Fig. 1.14. The fabricated microtool was used to manufacture curvilinear features.

The main benefits of this process are high resolution and accuracy; however, the low material removal rate is a challenging issue for FIB, which bounds this process for fabricating micro-cutting tools with 100 µm diameter or lesser [30]. It also allows us to observe the tool while fabrication; thus, sub-micron precision was reproducible. Bombardment of Ga^+ ions on the tool surface creates a point defect, which reduces the strength of the microtool.

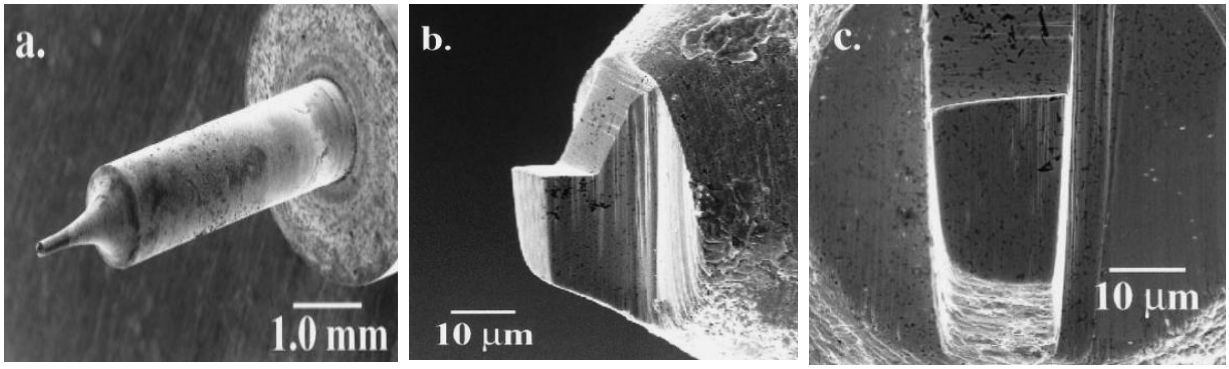

Fig. 1.14 Fabricated microtool by FIB (a) top view, (b) back rake facet, and (c) side rake facet [30]

1.4.3.3 Fabrication of Microtool by ECM

Electrochemical machining (ECM) is a non-conventional machining process. This process follows the laws of electrolysis established by Faraday. Material is removed from the workpiece surface atom by atom [31]. An electrolytic cell is developed in which anodic dissolution occurs from the anode on the supply of potential difference. In general, material removal takes place from the workpiece, which is made as an anode and connected to the positive terminal of the power supply. The tool is the negative replica of the shape to be generated on the workpiece. The tool is connected to the z-axis and fed toward the machining workpiece. For fabrication of microtool from ECM, the tool should be connected to the anode, as material removal in ECM is by an anodic dissolution process, i.e., connected to the positive terminal of the power supply. Depending on the cathode shape, the material is removed from the anode. Hence, the cathode is made the replica of the tool dimension to be fabricated [32], [33].

Jain et al. [34] fabricated a microtool of diameter 80 μm from 1000 μm steel wire. A copper wire of diameter 1300 μm is made as the cathode and the steel wire of diameter 1000 μm as an anode. Applying the pulsed DC of 6V, the anodic dissolution starts, and the final dimension of the microtool is achieved, as shown in Fig. 1.15. Sulphuric acid of concentration 0.1 M was used as an electrolyte. Both electrodes of length 30 mm were dipped in the electrolyte. The variation of the tool diameter and MRR with respect to time was analyzed. Due to the oxide layer and dust particles on the surface, initial MRR is slow and then increases with time. The total machining time was 65 min. The fabricated microtool was used for machining in micron dimensions.

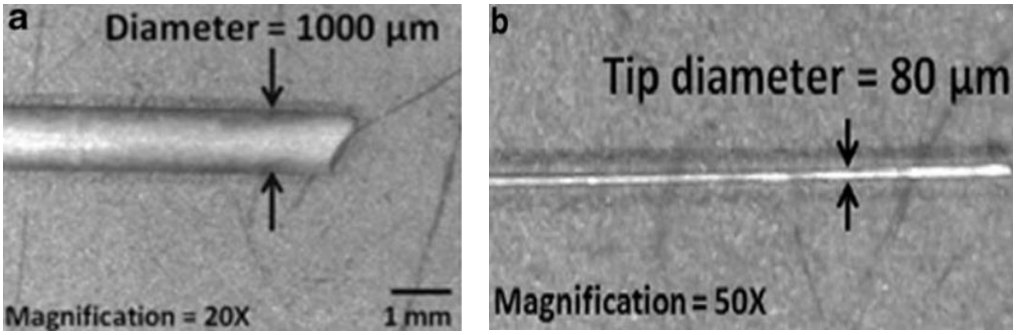

Fig. 1.15 Fabrication of microtool (a) initial and (b) final diameters [34]

Sethi et al. [35] fabricated a tungsten carbide alloy (WC–Co) microtool. With an initial diameter of 510 µm, the microtool of 111.2 µm diameter was manufactured using micro-wire-electro chemical machining (WECM). An environment-friendly electrolyte, i.e., citric acid, was used during experiments. The final shape and size of the fabricated microtool can be seen in Fig. 1.16.

Fig. 1.16 SEM image of fabricated microtool [35]

Rathod et al. [36] fabricated disk microelectrodes using electrochemical machining. The cylindrical tool was placed inside a hole, and its diameter was reduced. An arrangement was made to manufacture a disk-type tool with a larger diameter at the base and a smaller diameter at the other part. While machining, the tool with a larger diameter faces towards the workpiece having a smaller IEG. For smaller diameter, the IEG becomes bigger. This will lead to a circular hole instead of a tapered hole. The fabricated micro-hole is compared with the cylindrical and disk-type tool in Fig. 1.17. A tapered hole forms from the cylindrical tool as the whole tool's surface takes part in the microhole fabrication. The area near notation 1 is continuously under the influence of the tool, while the area under notation 2 has the least IEG during machining. However, for the disk-type tool, the area near notation 3 has a larger IEG than the area near notation 4. Thus, IEG increases in other parts of the workpiece than the

actual machining area with a disk-type tool. This tool is used to fabricate a taperless microhole.

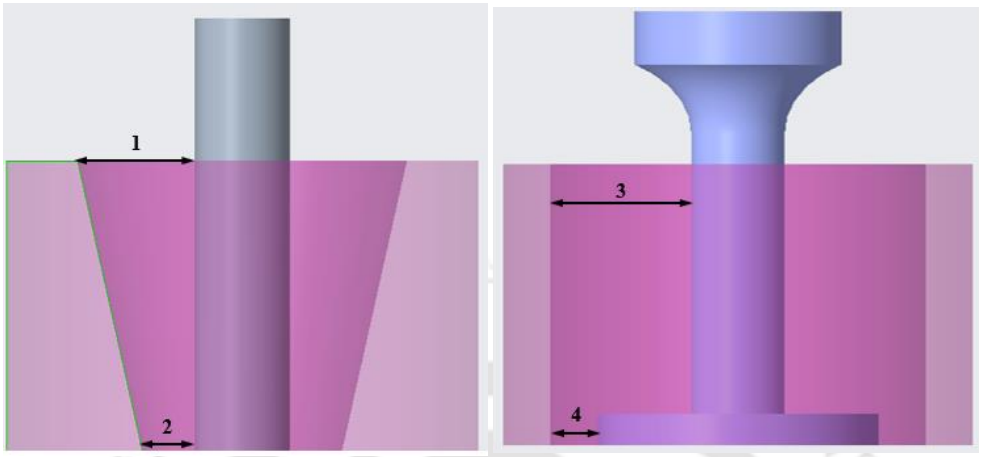

(a) (b)

Fig. 1.17 Comparison of micro-holes between (a) cylindrical and (b) disk-type tools

Sangeethakrishnan et al. [37] utilized EMM for the fabrication of microtools. The polarity of the tool and the workpiece are interchanged, i.e., the tool is connected to a positive terminal, and the workpiece is fixed to the negative terminal of the DC power supply. The hollow copper tool with an initial diameter of 800 µm was fabricated to 300 µm diameter using reverse EMM, and its SEM image is shown in Fig. 1.18. The fabricated microtool is in a conical shape. The influence of electrolyte concentration was studied with and without reciprocating feed. MRR and overcut were analyzed with the hollow microtool, and it was found that MRR increases and overcut decreases. The conical tip is used to fabricate the printed circuit board (PCB).

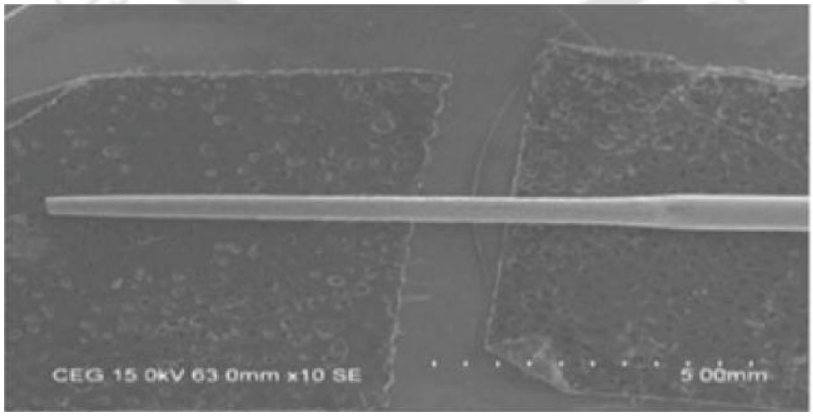

Fig. 1.18 SEM image of fabricated hollow conical tool [37]

Subrat et al. [38] numerically and experimentally analyzed the fabrication of a microtool with a high aspect ratio made from high carbon steel, as shown in Fig. 1.19(a). The microtool was fabricated by controlled electrochemical machining (ECM) at 5% sodium chloride solution in deionized water. At optimum machining conditions, the average diameter of the fabricated tool is 60 µm with an aspect ratio of 75. Multiple tool electrodes were also fabricated with a tip diameter of 130 µm. A black film surface was formed on the surface of the fabricated microtool. These provide a smooth surface finish to the microtool. This fabricated microtool creates a hole on a 400-µm-thick glass substrate by electrochemical discharge machining. The Comsol® Multiphysics package was used for the simulation to find the variation of current density during tool fabrication. With an increase in machining time, current density decreases, as shown in Fig. 1.19(b)

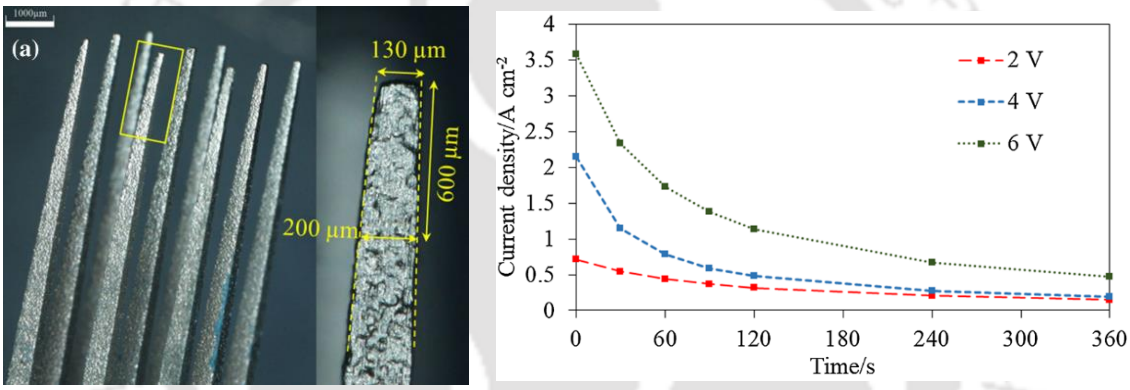

(a) (b)

Fig. 1.19 (a) Fabricated microtool and (b) current density profile [38]

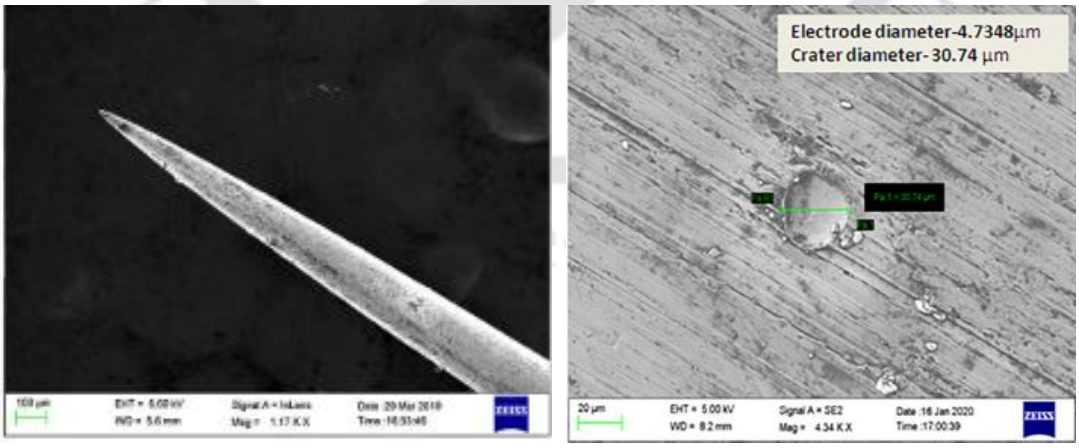

(a) (b)

Fig. 1.20 (a) Fabricated microtool and (b) crater on Ti-6-Al-4V workpiece [39]

Saha et al. [39] fabricated a tungsten carbide microtool of diameter below 10 µm by electrochemical etching, as shown in Fig. 1.20(a). An AC power supply was utilized to avoid

contamination of the tool surface. Taguchi methodology was adopted to optimize the input parameters such that minimum diameter with maximum material removal rate is achieved. The fabricated microtool was used to create a crater on the Ti-6-Al-4V workpiece with the help of micro-EDM, as shown in Fig. 1.20(b).

From the above literature, it can be seen that ECM is very effective in fabricating different shapes and sizes of microtools for micromachining. It can produce a microtool below 10 µm with reasonable accuracy. Unlike EDM, there is no spark produced during microtool fabrication. It offers several advantages over EDM, such as a good surface finish, the least damage to the tool surface, and low machining cost.

1.4.3.4 Fabrication of Microtool by Composite Material

Nowadays, the composite material has become very popular and can be used as a microtool if the reinforcement material is metal. Due to its lightweight and less corrosive nature, it is durable. The advantage of composite material is that it can be molded according to the desired shape and size. For the ECM process, the tool is the negative replica of the feature to be produced on the workpiece. So, it is favored as the microtool while machining micro-features.

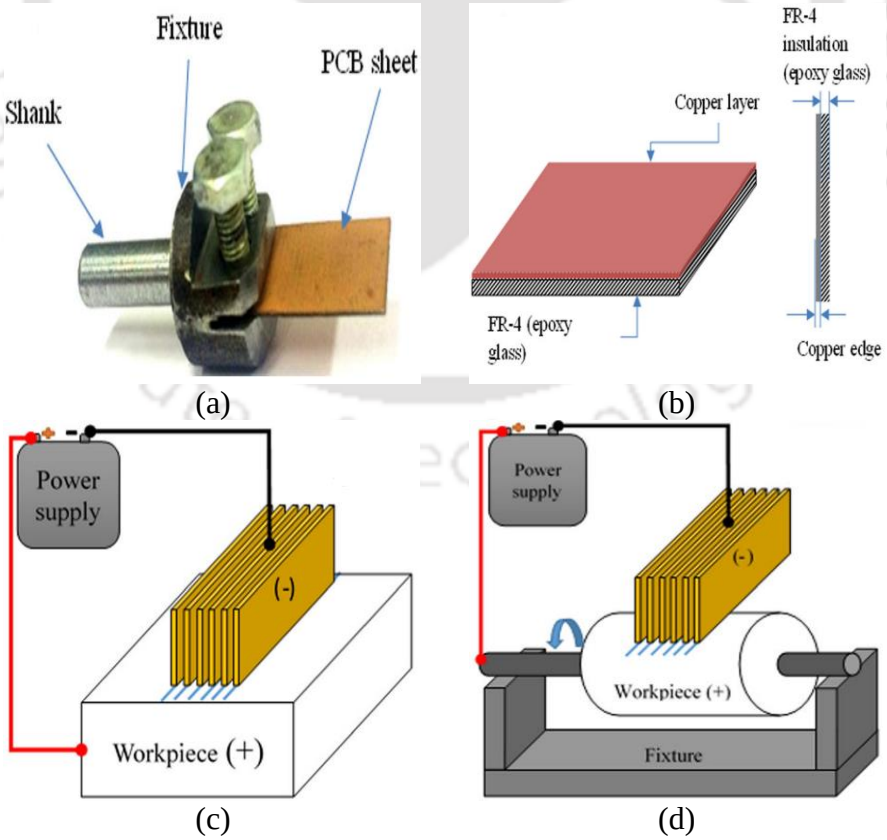

Fig. 1.21 (a) PCB tool with fixture and (b) PCB sheet and its cross-section; Micro-channel on (c) flat and (d) curve surfaces [21]

Patel et al. [21] fabricated a composite microtool made of the printed circuit board (PCB) with a thin layer of copper of 30 µm. The thin layers of copper act as a microtool to fabricate micro-channels and micro-pillars. A series of PCB were connected in series. The assembled microtool used for the fabrication of micro-channel over flat and curved surfaces is shown in Fig. 1.21. The electrolyte used was 5% wt. of sodium nitrate ($NaNO_3$). It was found that peripheral micro-grooves fabricated on curved surfaces using composite tools are wider and shallower when matched to the micro-channels fabricated on flat surfaces. For the curve surface, proper indexing has to be performed to get accurate and suitable dimensions of micro-features.

1.4.4 Literature Summary for EMM

For the fabrication of micro-features, several conventional, as well as non-conventional micromachining processes are available. In conventional micromachining processes, there is always a chance of tool failure, and forces are also induced during machining as there is always a direct contact between the tool and the workpiece. However, in non-conventional micromachining processes, there is no contact between the tool and the workpiece. Some non-conventional micromachining processes are EDM, LBM, ECM, etc. For the fabrication of microtools, thermoelectric-based machining processes such as EDM and LBM are utilized; however, it induces recast layer, burrs, and heat-affected zone. EMM, an anodic dissolution-based process, utilizes electrical and chemical energy and does not produce defects as produced by thermoelectric-based machining processes. EMM has a lot of potential for the fabrication of microtools. Several EMM setups have been designed and developed for the fabrication of micro-features; however, setup for the fabrication of microtools has not been developed.

1.4.5 Development of Experimental Setup of EP

The experimental setup of electropolishing is similar to the electrochemical micromachining setup with certain modifications. As, it is also an anodic dissolution process, it also requires a power supply. The electrolyte used in EP is generally acidic. Thus, a glass beaker is preferred as an electrolytic tank as it is non-reactive to acids and also non-conductive. Several researchers have developed an EP setup for the polishing of complex components.

Brent et al. [40] optimized the electrochemical polishing process parameters using the Taguchi design of experiment for the components manufactured by additive manufacturing.

An electropolishing setup was developed utilizing a glass beaker in which electrodes were dipped in an acidic electrolyte. The glass beaker was kept over the hot plate, which had the provision of a magnetic stirrer. The hot plate provides sufficient heat to raise the temperature of the electrolyte, and a magnetic stirrer was used to stir the electrolyte to remove bubbles.

The selection of cathode material for EP also plays an important role. The cathode material should be relatively inert in the electrolyte and, for best results, should be nobler than the metal or alloy being electropolished. The functional cathode materials include copper, nickel, graphite, and platinum. The surface area of the cathode should be much greater than that of the anode [41].

Tyagi et al. [42] reduced the roughness of the internal surface of an additive manufactured 316 steel component by chempolishing and electropolishing. Initially, chempolishing was more efficient than EP for the internal surface. However, with the introduction of a counter electrode, EP became more efficient compared to chempolishing for the internal surface polishing.

1.4.6 Influence of Major Process Parameters in EP

EP is assumed to be carried out in two processes, i.e., anodic leveling or macro-smoothening & anodic brightening or micro-smoothening. Anodic leveling aims to reduce the surface roughness of greater than 1 μm by increasing the material dissolution rate. This is achieved by increasing current density through applied voltage in protruding and valley portions. Anodic brightening aims to reduce surface roughness to less than 1 μm. Some of the influencing EP factors are discussed below.

1.4.6.1 Effect of Temperature on EP

Temperature plays a significant effect in electropolishing as the change in temperature alters the conductivity and viscosity of the electrolyte. At lower temperatures, the diffusion of metal ions is reduced, leading to a decreased current density [43]. As temperature increases, the viscosity of the electrolyte decreases, and the fresh electrolyte is continuously supplied. Generally, an increased temperature leads to faster mass dissolution. It was assumed that an increase in temperature reduces viscous film thickness & increased diffusion rate. EP of porous austenitic stainless-steel in phosphoric-sulphuric acid at higher temperatures resulted in a better surface finish due to increased current density [44]. However, EP of aluminium in 1:8 perchloric acid to ethanol at an elevated temperature of 40°C created etching pits on the

aluminum cavity. This was due to the absence of a limiting plateau region in the current density-voltage curve at higher temperatures. So, EP of aluminum at more elevated temperatures should be avoided to prevent the formation of etching pits in its cavity [45]. Tyagi et al. [46] electropolished additive manufactured steel to reduce the surface roughness. It was concluded that the percentage contribution of temperature, agitation, and electrochemical bath composition is 40%, 32%, and 24%, respectively. At 104 ºC, a maximum reduction in surface roughness is observed. Thus, the temperature range to reach an optimum electropolishing result for a specific system should be carefully selected.

1.4.6.2 Effect of Electrolyte Composition on EP

The primary function of an electrolyte is to act as a medium for current, heat, and reaction products. EP uses various organic and inorganic electrolytes. For EP of stainless steel, electrolytes mainly contain phosphoric and sulphuric acid in the ratio of 1:1 or 2:1, along with de-ionized water [47]. EP of different metals requires different electrolytes. The other metals may need different types of electrolytes, and the properties of electrolytes directly influence the final EP effect [48]. The volume ratio is a crucial factor in the EP for various materials. In EP of copper, surface roughness decreases with an increase in acid concentration [49]. An EP of 30 Nb-Ti alloys in methanolic sulphuric acid with three different acid concentrations, i.e., 1M, 2M, and 5M, current density decreases on increasing acid concentration; however, the limiting current density broadens, thus increasing the polishing effect. EP of the same alloy in a mixture of phosphoric acid and sulphuric acid electrolyte also showed the same results on increasing the volume ratio of sulphuric acid [44], [50] as the thicker viscous layer is formed. As current density reduces, anodic dissolution also decreases.

Table 1.1 shows the trend of electrolyte composition utilized for EP. In general, the sulfuric acid-based electrolyte was used as it gives a high surface finish with high reflectance. However, its fumes are harmful to the operator as well as the equipment nearby. Thus, the researchers are finding an alternative electrolyte combination for EP. It can be seen from Table 1.1 that over the years, the trend of organic or aqueous-based electrolytes has increased. These electrolytes are easy to handle and less harmful to the operator than sulfuric acid.

Table 1.1 Trend of electrolyte composition for EP

SL. No.	Year	Material	Electrolyte composition
1.	2003	AISI 316L [51]	Sulfuric acid (H_2SO_4): Ortho-phosphoric acid (H_3PO_4)=2:3
2.	2006	AISI 304, 316 [52]	Ortho-phosphoric acid (V) 85% (35% vol.), glycerine 99% (50% vol.), distilled water (15% vol.)
3.	2009	AISI 304 [53]	Aqueous 2.4 M H_2SO_4, 5.9 M H_2SO_4
4.	2012	AISI 304, 316 [54]	Sulfuric acid (VI) 96% (50% vol.), ortho-phosphoric acid (V) 85%, (50% vol.)
5.	2013	AISI 316L [55]	H_3PO_4 (60% v/v), H_2SO_4 (40% v/v).
6.	2014	AISI 316L [56]	H_3PO_4 85% (60% v/v), H_2SO_4 95–97% (20% v/v), glycerine 99.5 % (10% v/v), H_2O (10% v/v).
7.	2016	Fe-Ni-Co Alloy [57]	Mixture of acetic acid and perchloric acid
8.	2016	AISI 304 [58]	H_3PO_4 (51 wt.%), H_2SO_4 (35 wt.%), triethanolamine (3 wt.%), H_2O (11 wt.%)
9.	2016	SS316L [59]	$HClO_4$ 70% (20% v/v), CH_3COOH 98% (80% v/v).
10.	2017	SS316L [60]	100 ml methanol (CH_3OH) containing 300 ml of 93% sulfuric acid solution
11.	2019	SS316L [61]	H_3PO_4 (35% v/v), H_2SO_4 (60.5% v/v), triethanolamine (4.5% v/v)
12.	2019	Steel AISI 304 [62]	H_3PO_4, H_2SO_4, triethanolamine (3 wt.%)
13.	2020	SS316L [63]	Electrolyte consisting of phosphoric acid, glycerol and distilled water
14.	2020	Co–Cr dental alloy [64]	The electrolyte consisted of H_3PO_4 solution (in volume concentration of 81%) and pure ethylene glycerol with the volume ratio of 3:1.
15.	2020	Nickel-titanium shape memory alloy [65]	Methanol-perchloric acid
16.	2020	Tungsten [66]	H_3PO_4 (81% v:v) : Glycerol = 3:1, and NaOH aqueous solution (0.27 mol/L, 0.5 mol/L)
17.	2021	Inconel 718 [67]	The polishing electrolyte is composed of analytical grade sulfuric acid (H_2SO_4-97%) and methanol (CH_3OH-99.5%)
18.	2021	Maraging steel [68]	60 vol.% phosphoric acid, 30 vol.% sulfuric acid, 9.7 vol.% DI water with glycerol (0.3 vol.%).

1.4.6.3 Effect of Polishing Time on EP

The time the electrodes are dipped into the electrolyte with the current flowing through it is termed polishing time. The higher the polishing time, the higher will be the anodic dissolution. However, the surface roughness of the workpiece tends to improve as the polishing time increases with a faster rate at the beginning of polishing, and the rate decreases very low with an increase in the polishing time [52]. Surface roughness decreases with increased polishing time, but after attaining an optimum roughness, it starts to increase due to pitting on the surface [69]. Wang et al. [70] electropolished nickel-titanium alloy to optimize

the process parameters. It was observed that up to 100 sec of polishing time, surface roughness decreases; however, after 100 sec, the surface roughness increases. Lee [71] electropolished the stainless steel 316L to determine the influence of process parameters. The rate of decrease in surface roughness is not uniform during the polishing time. Up to 120 sec of polishing time, the reduction rate in surface roughness is high; however, it was almost constant afterward.

1.4.6.4 Effect of Initial Surface Roughness of Workpiece

The initial surface roughness of the workpiece should be considered carefully for a fast and effective EP process because the EP has a limitation in polishing quality. The polishing effect needs a difference in the potential distribution at the protruding and valley positions on the workpiece surface. When the viscous layer is even with the smoothed workpiece surface, the material removal rate would be significantly low because of the slight difference in potential distribution [8]. Lee and Shin [72] considered two nitinol shape memory alloy samples with an initial surface roughness of 2 µm and 1 µm. The samples were electropolished, keeping other parameters constant. It was observed that the surface roughness achieved after EP was 0.98 µm and 0.31 µm, respectively. A similar observation was found when the initial surface roughness of the workpiece was mechanically polished with different grit paper of 600, 1800 & 3000, and electropolishing was performed on all the components. Minimum surface roughness was observed for the mechanically polished workpiece with 3000-grit paper [71].

1.4.6.5 Effect of Electrolyte Rotation on EP

Electrolyte rotation plays a vital role in the formation of the viscous layer. It reduces the viscous layer's thickness, thereby reducing the resistance and increasing the current density in the passive region. It helps in faster anodic dissolution [50]. However, there should be an optimum rotation speed to obtain minimum surface roughness, as high rotational speed decreases the surface finish [73]. At higher rotation speed, the surface roughness may start to increase after a certain point by removing too much of the viscous film, which prevents the valley position of the surface. Tyagi et al. [46] optimized the process parameters to electropolish the additive-manufactured components. It was observed that EP for 300 seconds at 104 °C temperature and agitation at 200 rpm yielded the most significant improvement in surface smoothening. The viscous layer is unstable at higher agitation, leading to surface pitting.

1.4.6.6 Effect of IEG on EP

EP performs at constant current density. The current density between the electrodes varies by changing the IEG as the resistance between the electrodes changes. However, an optimum gap should be maintained such that uniform anodic dissolution takes place by forming a stable passive layer, and the gap bubbles should escape easily.

Ramasawmy and Blunt [74] observed the current density variation as IEG changes. A very high current density was observed when the gap between the electrodes lies between 0.5 to 1 mm. However, with this high current density, severe pitting starts on the surface, degrading the surface roughness. Tailor et al. [75] established a numerical model for forming a passive layer and its stabilization in electrochemical polishing. It is observed that the stabilization of the passive layer is crucial for effective electropolishing. The interelectrode gap (IEG) was varied between 2 and 10 mm. It was observed from the numerical model that an IEG of 6 mm gives the best electropolishing effect. During the EP process, hydrogen gas evolves at the cathode in bubble form. These bubbles continuously grow and burst out. However, this bursting of bubbles at minimal electrode gaps affects the closely placed EP nitinol surface. So an appropriate IEG should be carefully chosen for EP.

1.4.7 Influence of EP on surface integrity

1.4.7.1 Surface Elemental Composition

The base material has specific properties for a particular application. However, most of the machining/finishing process changes the elemental composition after processing, which is not desirable. The changes in the elemental composition of the base material after EP is negligible.

Lappin et al. [76] electropolished the micro-electro-discharge-machined stainless-steel stents to achieve a smooth and uniform surface. High-energy discharge pulses caused rough surface layers and shape edges during EDM. It was observed that after EP, the surface roughness is reduced to 28 nm from 400 nm. EDS analysis suggests that carbon was deposited on the surface after EDM, which was successfully removed after EP.

Tyagi et al. [77] electropolished additively manufactured 316 steel components. The major EP parameters were electropolishing time, temperature, agitation, and electrolyte composition. It was observed that after EP, the surface roughness of the component was reduced from 2 µm to 0.07 µm, and a mirror-like surface was obtained. However, the surface elemental composition remains unchanged.

1.4.7.2 Residual Stress

Most thermal-induced machining processes like EDM and LBM leave a recast layer and residual stress on the surface, which is undesirable. A post-processing technique must be adopted to remove these defects. EP removes the recast layer and the residual stress from the top surface. Das et al. [78] calculated the deformation, microstructure, and residual stress via the finite element-based technique. It was observed that EDM being a thermoelectrical process, produces a recast layer up to some micron depth. Alternatively, heating and cooling generate the residual stress and form the martensite phase due to rapid cooling. Boban and Ahmed [79] utilized the wire electrical discharge polishing to improve the additive-manufactured stainless steel's surface integrity and mechanical properties. The stainless steel was manufactured by selective laser melting, producing a recast layer and generating residual stress. A post-processing technique was utilized to remove these stresses and make the component free from stresses.

1.4.7.3 Surface Morphology

Surface defects such as micro-cracks and micro-voids are present on the surface after the machining due to rapid heating and cooling in the thermo-electric-based machining process. Wang and Han [80] performed single-step and multi-step sequential machining in electric discharge machining. It was observed that surface defects such as cracks, craters, porosity, and debris were present after EDM. These defects deteriorate the performance as well as the surface finish of the components. Thus, post-processing is required to remove these surface defects.

Tyagi et al. [42] performed the contact angle analysis on the additive-manufactured components polished by chempolishing and electropolishing. A contact angle of 90º on the sandblasted and chempolished surfaces was observed, signifying hydrophobic surfaces. However, a contact angle of 45º was observed for the electropolished surface, signifying a hydrophilic surface, which can be used in applications such as antifogging, biomedical, filtration, heat pipes, etc. Ahmadkhaniha et al. [68] studied the microstructural effect of selective laser melting (SLM) and electropolishing on the performance of maraging steel. It was observed that the microstructure of the fabricated samples after SLM consists of several defects, which were successfully removed after EP. A reduction of 65% in surface roughness was observed after EP.

1.4.7.4 Tribological Improvement

EP enhances the surface finish, which increases the wear resistance and decreases the friction coefficient. Boban and Ahmed [79] used wire electrical discharge polishing to remove the surface irregularities on the additive-manufactured steel. It was observed that a reduction of 18.6 % in friction coefficient was measured using pin-on-disk.

GUO et al. [81] investigated the surface integrity of electron beam melted Ti-6Al-4V by precision grinding and electropolishing. It was observed that the surface roughness of the fabricated part was very high. The post-processing technique was utilized to reduce the surface roughness, and a comparative analysis was performed between electropolishing and precision grinding. EP gave good results; however, precision grinding coupled with EP gave better results.

1.4.7.5 Mechanical Property

Mechanical property mainly includes the hardness of the surface. During EDM, a recast layer is formed on the surface due to changes in the phases of the material. This recast layer is very hard and prone to initiate cracks, leading to the component's premature failure. Srinath et al. [82] characterized the EDM machined maraging steel using nano-indentation. It was observed that the indentation depth of the base material is higher than the recast layer. As harder the surface, the lesser will be the indentation depth. Due to this, the recast layer's hardness and elastic modulus are higher than the base material.

Han and Fang [63] electropolished 316L stainless steel in the sulfuric acid-free electrolyte to analyze the hardness of the surface. Nano-indentation tests were performed on the base material and the electropolished surface. Due to the formation of a passive oxide layer on the surface, the hardness of the electropolished surface is slightly reduced. However, an electropolished surface enhances the surface finish and corrosion resistance.

1.4.7.6 Corrosion Resistance

Electropolishing creates a passive layer that increases surface resistance against corrosion. This will be useful for metals like copper, brass, aluminum, and carbon steel to enhance their corrosion resistance. Hryniewicz et al. [83] electropolished Co-Cr alloy to improve its corrosion resistance. It was found that the corrosion current density had been reduced from $1.9\times10{-}8$ Acm^{-2} to 6.0×10^{-9} Acm^{-2} after EP signifying an increase in corrosion resistance. Kityk et al. [84] electropolished medical-grade stainless steel Mn AISI, AISI 316Ti, and AISI

304 to enhance corrosion resistance. EP also affects biofilm formation and microbial activity. The salt spray tests indicate that the electropolished pieces experience greater corrosion resistance than the passivated and raw parts.

Ajmal et al. [67] performed isotropic etching on nickel-based superalloy Inconel 718. Various polishing characteristics like potentiodynamic behaviour, corrosion resistance, surface roughness, and material removal rate were studied. The electrolyte selected was sulfuric acid in methanol. It was concluded that corrosion resistance is increased by increasing sulfuric acid concentration. Initially, the surface roughness of 0.86 nm was achieved from 62.7 nm with an MRR of 2.73 mm^3/min at 3A for 300 s.

Electropolishing can enhance the metal's natural shine by eliminating or minimising stains, heat discolouration and minor scratches, improving the workpiece's appearance [85].

1.4.8 Applications of EP

1.4.8.1 Deburring

Burrs on the components are usually generated after mechanical machining, which leads to shape deviation of the components and deteriorates their designed function. Several techniques have been described to remove burrs on components fabricated from bulk materials, mainly conventional and non-conventional finishing processes. Schaller et al. [86] reduced surface damage from mechanical techniques with electrochemical methods. The generated burrs after the mechanical cutting of brass and stainless steel were eliminated completely by the EP process. EP is a common technique for deburring macro parts made of bulk material that was applied on RF MEMS microstructures made of electroplated nickel [87]. In EP, the valley part of the surface roughness in the workpiece is covered with oxygen or a thicker viscous film than the protruding part; all the burrs present on the surface will be easily removed. EP also protects the surface from hydrogen embrittlement.

1.4.8.2 Surface Roughness Improvement

The primary application of EP is to improve the surface roughness of the component, which is generally inaccessible by conventional methods. EP is widely used for the final surface treatment, especially for the coronary stent, because of the smooth surface and improved corrosion resistance by a passive oxide layer on the polished surface [8].

Sojitra et al. [54] characterized the laser-cut cardiovascular stent for its smooth surface and corrosion resistance after electropolishing. A reduction of 78.1 % in surface roughness

was observed, and the corrosion rate was reduced from 2 mpy to 0.5 mpy after EP. The electrolytic solution used was H_2SO_4 and H_3PO_4, each at 50% (v/v). Tyagi et al. [46] had electropolished additive manufactured (AM) stainless steel to reduce the surface roughness. EP parameters like electrolyte composition, temperature (most dominating), agitation, EP time & fixed-parameter current density of 80 A/dm^2 were considered. Three electrolyte solutions named X, Y & Z of different compositions were prepared. By Taguchi Analysis, optimum parameters were EP time of 300 sec, the temperature at 104 °C, composition X (41 g phosphoric acid +45 g sulfuric acid +14 g water = 100 ml) & agitation at 200 rpm. The EP sample's roughness measurement results showed that surface roughness was below 0.1 µm R_a, and a minimum of 200 µm material removal was achieved to attain the optimum surface finish. The unpolished surface has a flaky texture, while the EP surface has hexagonal microstructure regions.

1.4.9 Literature Summary for EP

EP is the most efficient and economical post-processing technique with numerous advantages. Most of the thermal-induced machining process, like EDM, LBM, etc., induces surface defects, recast layer, residual stress and changes in surface morphology of the components in the macro and micron domain. Thus, a post-processing technique is always recommended to remove these defects from the surface to improve its performance. From the literature survey, it is observed that EP can remove these surface defects from intricate shapes inaccessible by conventional polishing techniques. It is very economical and does not change the original base material composition. It also forms an oxide layer over the surface, enhancing corrosion resistance. In general, sulfuric acid-based electrolytes were utilized for EP, which are harmful to the operator and the equipment attached to it.

1.5 Motivation Behind Present Research Work

An essential requirement for the fabrication of micro-features is the microtools. These tools are not readily available in the market. These micro tools must be fabricated per the requirement, and the dimension needed. Several micromachining processes manufacture the microtool, such as EDM, FIB, etc. These processes are thermoelectric machining processes, which induce recast layer, heat affect zone, and residual stress. Due to these defects, high aspect ratio microtools are not recommended to be fabricated by these processes. These defects also damage the dimensional accuracy of the microtool. The cylindrical shape of the

microtool is required for better accuracy of the micro-features to be fabricated. Thus, another process must be developed to manufacture the microtool to avoid surface defects and be capable of producing a cylindrical shape.

EMM, being a non-conventional machining process, can fabricate microtools without any surface defects. This micromachining process is still under investigation, and several researchers are working to utilize this process to fabricate the microtool. Faraday's laws of electrolysis govern EMM. It uses electrical as well as chemical energy for the removal of material. Thus, it does not induce any surface defects on the microtool surface. The microtool, without any surface defects, provides good dimensional accuracy and lasts longer.

Several micro-components specially fabricated by additive manufacturing or any components having intricate shapes require finishing/polishing to remove all the defects produced from initial machining processes. Most machining processes, like EDM, LBM, etc., are suitable for fabricating micro-components, leaves recast layer, surface defects, and heat-affected zone. The recast layer is hard, brittle, and prone to damage during operation. The surface roughness after machining/fabrication from additive manufacturing is also very high. These defects degrade the performance of the component fabricated from it. Thus, a post-processing technique is a must that removes these surface defects and, at the same time, does not alter the base material composition.

Electropolishing is a non-conventional polishing technique that can remove all the surface defects produced from the prior machining processes. It is economical and removes a layer of material from the top surface so that all the surface defects are anodically dissolved. As the electrolyte is used in EP, it can easily move to intricate shapes to remove the surface defects from these areas. EP also forms an oxide layer over the surface, increasing the component's corrosion resistance. The material is removed in the micron dimension to reduce surface roughness. EP also does not change the base material's composition.

1.6 Objectives of the Present Thesis

The proposed research plans to utilize the electrochemical micromachining (EMM) process to fabricate microtools to manufacture microfeatures on surfaces. Electrochemical polishing (EP), similar to EMM, reduces the surface roughness along with surface brightening while removing the heat-affected layer and overcoming the problem associated with other processes. The following objectives are proposed for the current research work:

- To design and develop an experimental setup for electrochemical micromachining (EMM), which includes subcomponents like mechanical controller, power supply, tool positioning unit, and machining chamber.
- To fabricate microtools using EMM for generating different microfeatures over the workpiece.
- To develop a simulation-based model of the EMM process to analyze the current density variation at the interelectrode gap.
- To design and develop an experimental setup for electropolishing (EP) to finish Maraging steel 300 components.
- To investigate the EP performance on residual stress on EDM machined Maraging steel surface.
- Surface integrity analysis such as surface roughness, surface reflectance, wettability, and tribological properties on electrical discharged (EDM) machined maraging steel followed by electropolishing while observing the improvement.
- To study the effect of various process parameters of EP to enhance the surface finish of thin-cruciform gimbal flexure of the gyroscope.

1.7 Organization of the Thesis

The thesis is organized into eight chapters with references. The introduction to the various micromachining and finishing/polishing processes in conventional and non-conventional domains and the related literature review are discussed in **Chapter 1**. The literature review is divided mainly into Electrochemical Micromachining (EMM) and Electrochemical Polishing (EP). For EMM, a literature review is carried out to build an experimental setup of EMM. This setup will be suitable for the fabrication of the micro-features. An extensive literature review is carried out to fabricate microtools through different micromachining processes, and their related advantages and disadvantages are discussed. In EP, a literature review is carried out to build an experimental setup of EP. This fabricated setup will be suitable for polishing maraging steel. An extensive literature review is carried out to analyze the electropolishing characteristics of maraging steel for different electrolyte compositions.

The design and development of the electrochemical micromachining (EMM) setup for the fabrication of micro-features are discussed in **Chapter 2**. The setup consists of computer numerical control (CNC), which helps precise movement in all three axes. An electrolytic container is made of Perspex material containing electrolytes and a fixture arrangement for

holding the workpiece and the tool. An electrolyte flow system with a filtration unit is attached such that the electrolyte is mixed with debris particles after EMM is filtered and can be reused again. The initial set of experiments is performed to fabricate microfeatures.

In **Chapter 3**, design modification has been performed in the electrochemical micromachining (EMM) setup to fabricate microtools. Two methods have been employed to fabricate the microtool. In the 1st method, the tool is placed inside a pre-installed hole, and in the 2nd method, the tool is placed adjacent to the workpiece. In the 1st setup, the conical microtool has been fabricated, and in the 2nd setup, the cylindrical microtool has been fabricated. In both cases, a tungsten tool of diameter 500 μm is utilized for the microtool fabrication.

In **Chapter 4**, a setup has been designed and developed for the electropolishing of maraging steel 300. An electrolytic cell is developed with the electrolyte combination of acetic acid and perchloric acid. A preliminary set of experiments has been performed to determine the feasibility of the process parameters like electrolyte temperature, agitation, and polishing time on surface characteristics of maraging steel while electropolishing.

In **Chapter 5** investigates electropolishing performance on surface residual stress and morphology of electrical discharge machined maraging steel. As EDM is a thermoelectric-based machining process, it induces surface residual stress and changes the morphology. A cavity is machined with the help of EDM, and its residual stress is calculated using the ' $\sin^2\psi$ method' of X-ray Diffraction (XRD). The capabilities of EP are investigated to remove the residual stress successfully.

In **Chapter 6**, surface integrity analysis of electrical discharged machined maraging steel followed by electropolishing has been performed. The surface integrity analysis includes surface residual stress, wear analysis, surface roughness, surface reflectance, and wettability of maraging steel after EDM and EP. A comparative study of all these surface integrity parameters has been performed, and it is observed that after EDM, the surface contains several defects, which degrades the surface integrity. However, surface defects are removed after EP, and surface integrity is improved.

In **Chapter 7**, electropolishing of the thin-cruciform gimbal flexure of the gyroscope is performed. EDM fabricates the thin-cruciform gimbal flexure of the gyroscope; however, it creates surface defects such as micro-cracks, craters, voids, etc. A statistical model is developed considering all the significant EP process parameters to minimize surface

roughness. It is observed that after EP, surface defects generated due to EDM has been successfully removed.

Discussion about the conclusions and critical findings of the present study with the future scope is presented in **Chapter 8**.

Chapter 2 Design and Development of EMM Setup

2.1 Introduction

Electrochemical micromachining (EMM) is a non-conventional technique that is of great interest in the area of micromachining due to its various advantages. During EMM, no sparks are generated, and no thermal damage to the tool and the workpiece. The microtool plays a vital role in micromachining, and fabrication is challenging. The microtools have very small dimensions and, thus, have low strength. As EMM provides significantly less damage to the microtool, frequent change of the microtool is avoided. This leads to the efficient and low cost of micromachining, unlike traditional machining. As EMM is very important in micromachining, researchers are taking more interest in it. More research is going on in the development of EMM setup and its performance. The following sections will discuss the design and development of the EMM setup.

2.2 EMM Setup

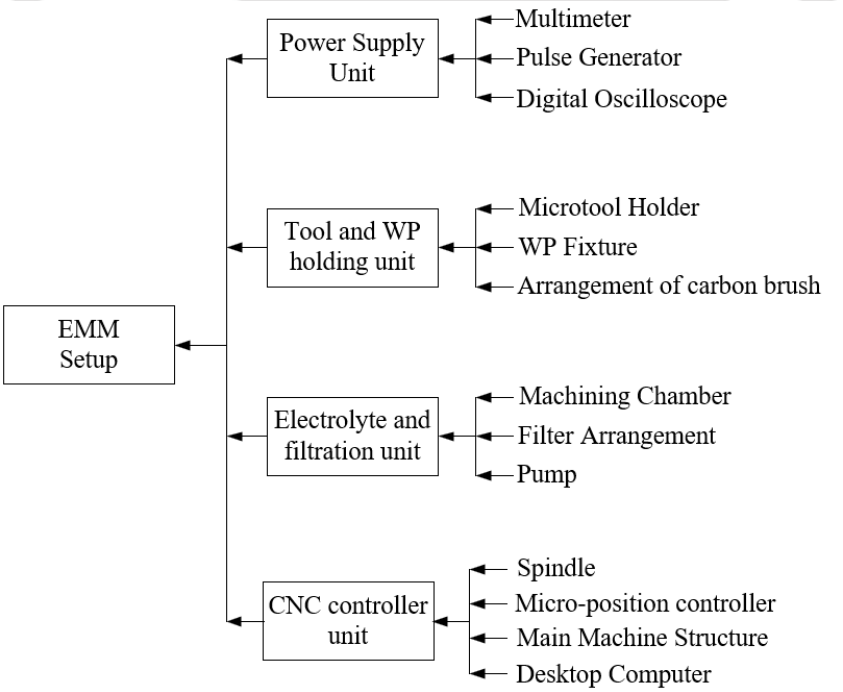

Fig. 2.1 Different subsystems of developed EMM setup

The increasing demand for miniature components leads to the development of the Electrochemical micromachining (EMM) setup. The setup consists of sub-systems: power supply unit, tool and workpiece holding unit, electrolyte and filtration unit, and the CNC

controller for precise movement. The various subsystems of the developed EMM setup are shown in Fig. 2.1. EMM includes electrolyte and power supply to the electrodes; selecting electrolyte container and other accessories is critical. In the following section, each subsystem will be explained in detail.

2.2.1 Power Supply Unit

Anodic dissolution starts in EMM as potential is applied between the tool and the workpiece via the power supply unit. The power supply unit generally uses direct current (DC) power. During EMM, for anodic dissolution, the tool is connected to the negative terminal (cathode), and the workpiece is connected to the power supply's positive terminal (anode). Thus, a redox reaction is taking place, supported by DC power only, and the chemical reactions are shown in Eqs. (1.1) and (1.2). However, due to the continuously changing polarity between the electrodes for the AC power supply, a redox reaction does not occur. Thus, the DC power source is selected for EMM.

DC power also has two options, namely constant DC and pulse DC. In constant DC, the amplitude of the potential applied is fixed throughout the process, whereas in pulse DC, the amplitude varies during the process. In pulse DC, there is an on-time (t_{on}) and off-time (t_{off}) during a cycle, which repeats continuously during the process. During the t_{on}, actual machining takes place, and anodic dissolution takes place as the amplitude of potential is maximum; however, during t_{off}, the amplitude of potential is minimum or almost zero, and there is no anodic dissolution during this period. This is provided to ensure the removal of debris particles from the small IEG and supply of fresh electrolytes.

The power supply unit mainly consists of the DC power source, function generator, and digital oscilloscope. The DC power source is the instrument used to supply the potential difference between the electrodes. The present study uses the DC power source (DOA 75 V–4A DC power supply made by Matsusada Inc.). In this power source, the function generator is not built-in. Thus, an external function generator (Make-Rigol, Model-DG4062) is utilized to generate pulse frequency. It has the provision to change the different pulses like sine, square, triangle waves, etc., duty cycle, and frequency. In the present study, a square wave is utilized for EMM, as the amplitude of the potential will be constant. A digital oscilloscope (Make-Scientech, Model-402) having a bandwidth of 70 MHz and a sampling rate of 1GSa/s is attached in parallel between the electrodes to visualize the pulses and their variation between the electrodes. A sample of pulse images in an oscilloscope are shown in Fig. 2.2.

As the frequency of the pulse power increases from 100 kHz to 500 kHz, a distortion in the pulse is observed.

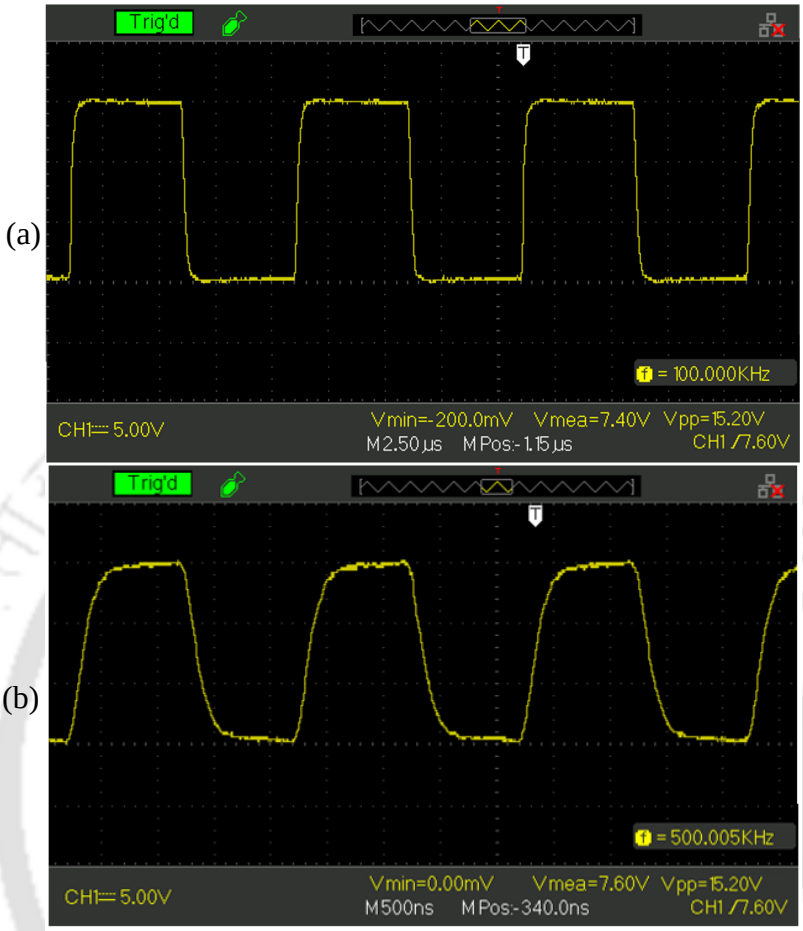

Fig. 2.2 Pulse condition (a) 100 kHz (b) 500 kHz

2.2.2 Tool and Workpiece Holding Unit

In EMM, there is a precise movement of the tool and the workpiece. The tool and the workpiece (electrodes) must be held rigidly to avoid any vibration during motion. In the present case, the tool has an initial diameter of 500 µm, which is very difficult to hold it rigidly. With the help of a mechanical pencil, the gripper is used to hold the lead (0.5 mm) is utilized to hold the microtool, as shown in Fig. 2.3. This arrangement is now fitted to the spindle to rotate the tool. The spindle is fitted to the z-axis of the CNC machine with the help of the aluminum bracket, as shown in Fig. 2.4. An arrangement of carbon brush is made to provide the power supply to the rotating tool. A conducting copper tape is wrapped over the collet of the spindle, and power is supplied to the tool with the help of an electrically conductive wire.

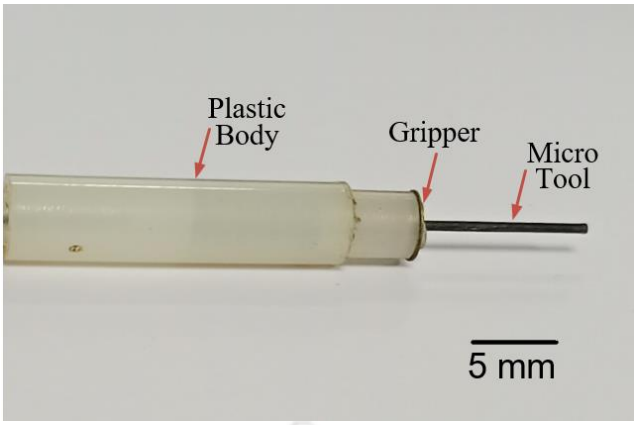

Fig. 2.3 Mechanical pencil to grip the microtool

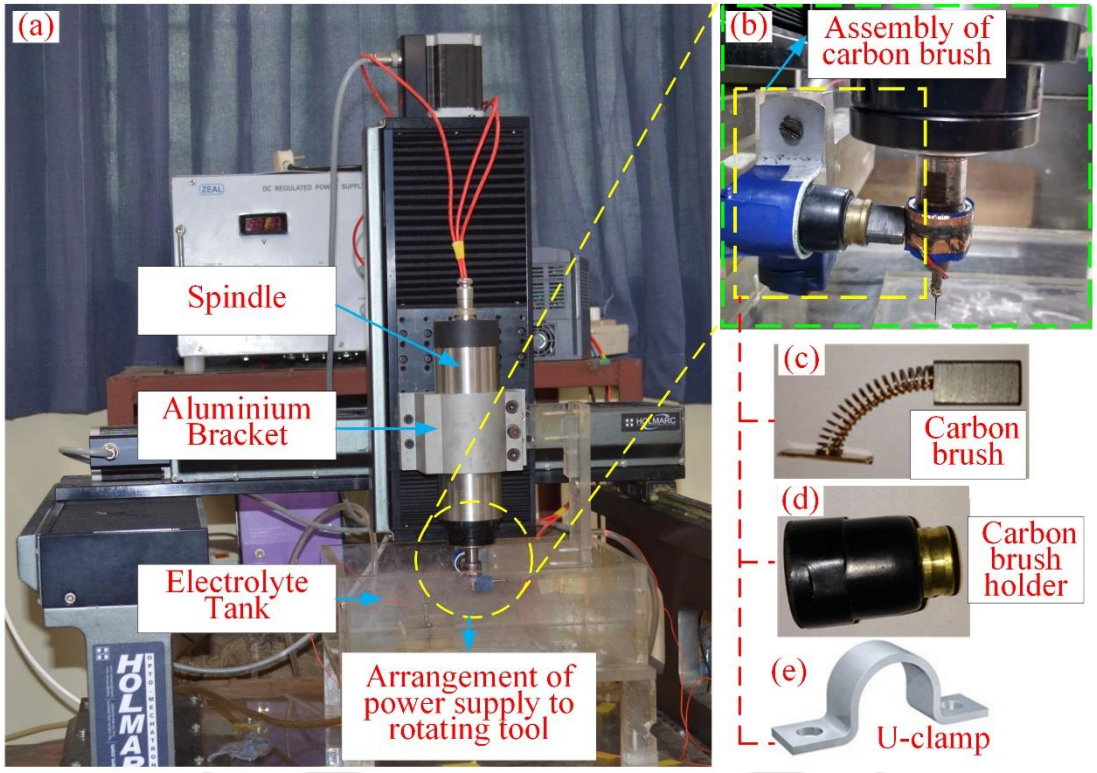

Fig. 2.4 Assembly of spindle with z-axis for tool rotation

The workpiece holding device is made of perspex material as it is dipped inside the electrolyte, so it should not be reactive with the electrolyte and non-conductive. The fixture for the workpiece is made to hold the workpiece and, at the same time, provide a power supply to it, as shown in Fig. 2.5. The complete workpiece fixture is fabricated with the help of perspex, and it is fixed to the electrolyte container. A hole with a tap of 6 mm is made on the perspex sheet to hold and supply power to the workpiece. As these bolts are conductive, to avoid any loss of charge, a gap is maintained between the workpiece and the bolts, as shown in Fig. 2.5(a). The bolts (1 to 4), as marked in Fig. 2.5(b), do not contact the workpiece; only bolt (5) is connected to the workpiece to provide a power supply.

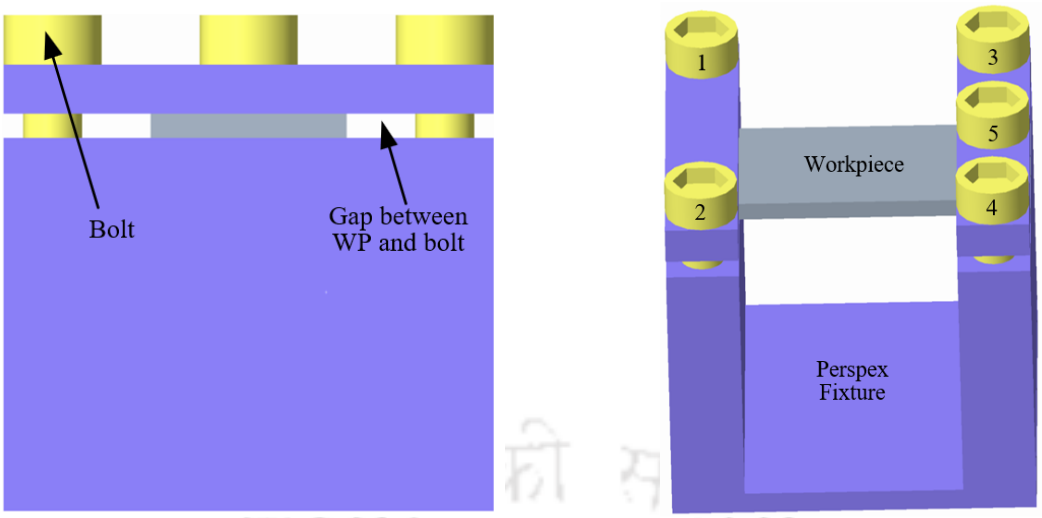

(a) (b)

Fig. 2.5 Workpiece holder (a) Side view (b) Isometric view

2.2.3 Electrolyte and Filtration Unit

An electrolyte acts as a charge carrier to complete the anodic dissolution process, apart from carrying the debris particles from the machining zone. It is supplied with the help of gravity to the IEG, so the microtool does not undergo any vibration. Due to flow, the electrolyte mixed with debris particles moves away from the machining zone, and fresh electrolyte enters the machining zone. It also takes away the heat produces in the IEG.

An electrolyte tank is made of Perspex material as it is non-reactive, transparent, and easy to fabricate. It has the provision to hold the electrolyte and also the workpiece holder. It has an inlet and exit valve for the flow of electrolytes, as shown in Fig. 2.6. A filtration unit removes debris particles from the electrolyte and ensures fresh electrolytes during EMM. The process of electrolyte filtration has been presented in a flow chart, as shown in Fig. 2.6(a). The electrolyte mixed with debris particles is moved from the machining chamber to another tank to settle debris particles. With the help of a pump, the left-over electrolyte is pumped to the top container. With the support of gravity, the electrolyte is passed to the filtration unit for further purification. Afterward, the purified electrolyte is again sent to the machining zone for further machining. This way, the same electrolyte will be reused and ultimately minimizes the machining cost. The complete setup of the filtration unit is shown in Fig. 2.6(b).

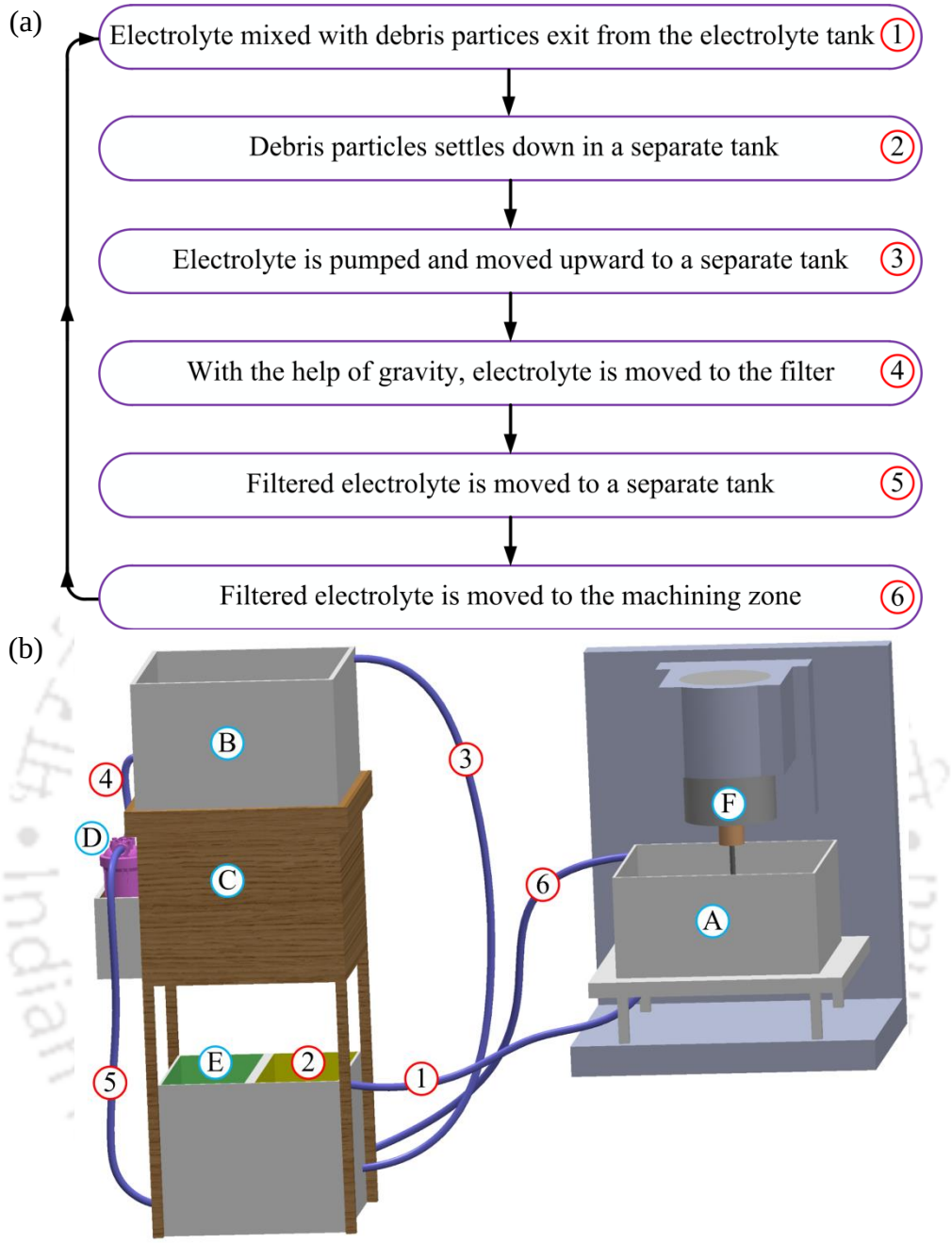

Fig. 2.6 Electrolyte filtration unit (a) Flow chart, (b) schematic of setup, where A- machining chamber, B- electrolytic container with no debris, C- wooden table, D- filter, E- container having filtered electrolyte, and F- spindle & tool assembly

2.2.4 CNC Controller Unit

The precise movement of the tool and workpiece in micromachining is achieved with the help of a CNC machine. In the present study, a CNC machine (make-Holmarc) gantry stage is used, which has three axes in XYZ directions, as shown in Fig. 2.7. The motorized XYZ gantry stage comprises aluminum alloy and steel with black anodized finishing. The configuration of the gantry, the Z-axis, which is fixed to the Y-axis, moves over a fixed

platform. The length and width of this platform covered by Z-movement are limited to traverse in the X and Y axis. The Y-axis is placed over the X-axis, and the guide rail has a recirculating ball bearing. The Maximum load-carrying capacity for the X and Y axis is 20 kg, whereas for Z-axis is 5 kg. The maximum speed for the movement of the X and Y axes is 16 m/sec and for Z-axis is 4 m/sec, with a resolution of 0.1 μm in all three axes. The XYZ axis is placed over three lead screws individually, and the same is shown in Fig. 2.7.

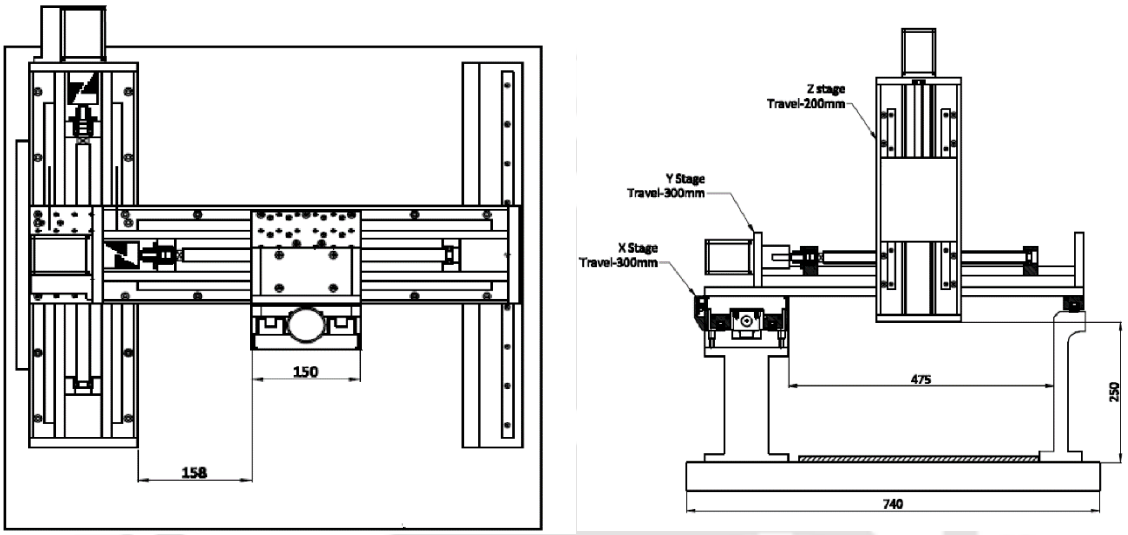

(a) (b)

Fig. 2.7 XYZ Gantry Stage (a) Top and (b) Front View

The precise motion of all three axes is controlled with the help of a microcontroller attached to a computer having Mach3 software. The micro-controller, as shown in Fig. 2.8(a), connects all the stepper motors of all three axes. A dedicated G-code is written on Mach3 software, which is transferred to all these stepper motors for precise movement. A spindle (Fig. 2.8(b)) is also attached to the z-axis, which holds the tool and helps rotate the microtool, and its specification is presented in Table 2.1.

Table 2.1 Specification of spindle

Size	Diameter:65mm Length:200mm
Power	1.5KW
Voltage	220VAC
Speed	10-24000rpm
Frequency	0-400Hz
Run out off	less than 0.05mm
Lubrication	Grease
Cooling	Air Cooled

(a) (b)

Fig. 2.8 (a) Micro position controller and (b) spindle to rotate the microtool

2.3 Microfeature Fabrication by Developed Setup

The developed experimental setup of EMM can be utilized to fabricate microfeatures. The developed setup has the provision of holding microtool as well as providing rotation to it. This helps in the efficient fabrication of microfeatures and the flushing of debris particles. The present study investigates the capabilities of the developed EMM setup. A stainless steel (SS316L) sheet of thickness 3 mm and a tungsten tool of diameter 500 µm (Fig. 2.3) are utilized to fabricate micro-holes.

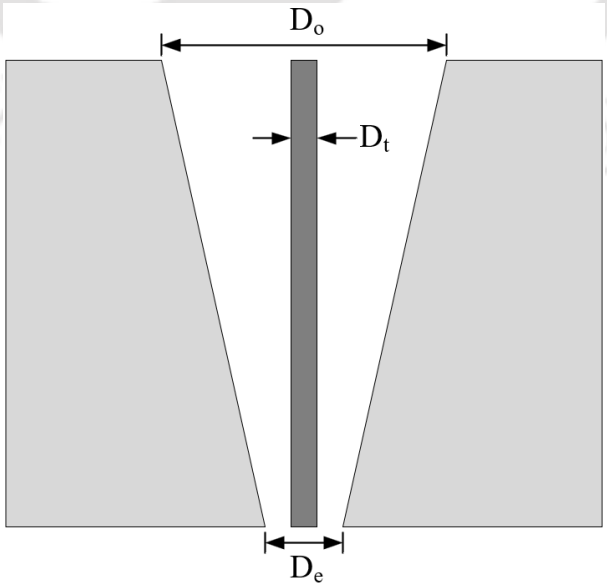

Fig. 2.9 Overcut and conicity during micro-hole fabrication via EMM

The major problem while fabricating micro-holes is the formation of overcut and conicity, as shown in Fig. 2.9. The terms D_o, D_e, and D_t are the entry and exit of the fabricated micro-hole and the diameter of the microtool, respectively. The primary reason for the overcut is the side machining during the EMM. As the tool is not insulated from the sides, during the micro-hole fabrication, the micro-hole's side wall is also machined, leading to overcut. This is undesirable and should be minimized. To quantify it, overcut and conicity are described by Eqs. (2.1) and (2.2).

$$Overcut = (D_o - D_t)/2 \tag{2.1}$$

$$Conicity = (D_o - D_e)/2 \tag{2.2}$$

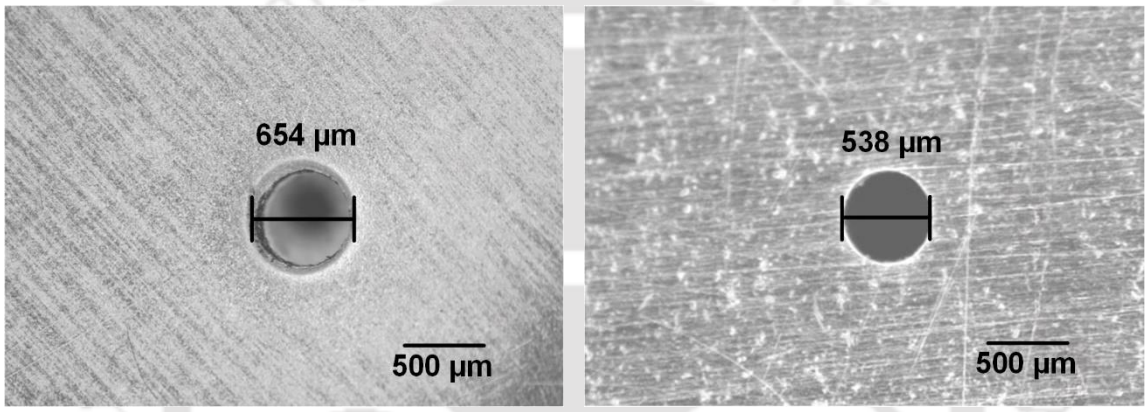

(a) (b)

Fig. 2.10 Microhole at workpiece (a) entry and (b) exit

The machining parameters are obtained from the preliminary study in the present study. The process parameters utilized are a DC voltage of amplitude 10V with a frequency of 200 kHz, a duty cycle of 60%, and sodium nitrate ($NaNO_3$) as an electrolyte with 25 gm/L diluted aqueous solutions used for micromachining. The fabricated microhole is presented in Fig. 2.10. With the microtool of 500 µm, the entry and exit hole diameter of the fabricated micro-hole are 654 µm and 538 µm, respectively. The overcut and conicity calculated using Eqs. (2.1) and (2.2) for the fabricated microhole are 77 µm and 58 µm, respectively.

2.4 Summary

The development of an experimental setup for EMM has been presented in the chapter. The experimental setup consists of sub-systems: the power supply unit, tool and workpiece holding unit, electrolyte and filtration unit, and the CNC controller for precise movement. The pulse DC power supply is attached with a digital oscilloscope to monitor the pulse power. The major problem of supplying power to the rotating tool is solved with the help of

carbon brush arrangement. The workpiece holding device and the electrolyte container are fabricated with the help of Perspex, as it is non-reactive to the electrolytes and also non-conductive. A filtration unit is also attached so the electrolyte mixed with debris particles can be filtered, and the same electrolyte can be reused. It minimizes the overall cost of machining. The precise movement of the tool and workpiece is achieved using a CNC controller. With the developed setup, microholes are fabricated utilizing a microtool of diameter 500 µm.

Chapter 3 EMM Process for Microtool Fabrication

3.1 Introduction

Miniaturization of products has powered micro-manufacturing growth in all sectors, mainly in automobile, biomedical, health care, consumer electronics, and optics. Due to this, a significant increase in the production of micro-dimension parts and several manufacturing methods were implemented to fabricate them on various materials. Microtools are in very much demand due to an increase in the popularity of micromachining. These tools are the one that finally shapes the product. The precise fabrication of miniature products depends on the precision of the microtool. Thus, fabricating precise microtools is a challenge in front of the manufacturing sector. Several traditional and non-traditional manufacturing processes, namely electrical discharge machining (EDM), electrochemical machining (ECM), grinding, turning, ultrasonic machining, and hybrid machining, have been utilized to fulfill the demand for micro-manufacturing on a large variety of materials. Due to the micron size of tools, fabrication and handling of these microtools pose several challenges to the manufacturing industry.

In this chapter, EMM is used to fabricate microtools as it produces the least damage to the tool surface during fabrication. As EMM is an anodic dissolution process, for the fabrication of micro-tool, the tool is made as an anode and the workpiece as the cathode. A tungsten tool of an initial diameter of 500 µm and stainless steel (SS316L) of 2 mm thickness acts as the workpiece. Two different techniques are utilized to fabricate a microtool with sodium nitrate ($NaNO_3$) as an electrolyte. In the first technique, the tool is placed inside the pre-made hole (diameter 2 mm) in stainless steel (SS) plate. For this, the effect of the tool with and without rotation on the surface of the fabricated tool is analyzed. In the second technique, the tool is kept adjacent to the SS plate and rotated. During EMM, the IEG changes as the diameter of the tool reduces. Analysis of the varying IEG during EMM over the fabricated tool surface has been studied. A 2D model of the workpiece zone is analyzed using the Comsol® Multiphysics package to examine the current density distribution in the interelectrode gap for both techniques.

3.2 Materials and Methods

For the experiments, a tungsten rod of diameter 500 µm (Fig. 3.1) and stainless steel (SS) sheet of gauge 2 mm are selected for tool and workpiece material, respectively. Several preliminary experiments were conducted, and according to the feasibility, parameters were chosen for the fabrication of the microtool, and the same is presented in Table 3.1. All the parameters were kept constant as the target was to predict the fabrication of the microtool with the help of Comsol® Multiphysics software.

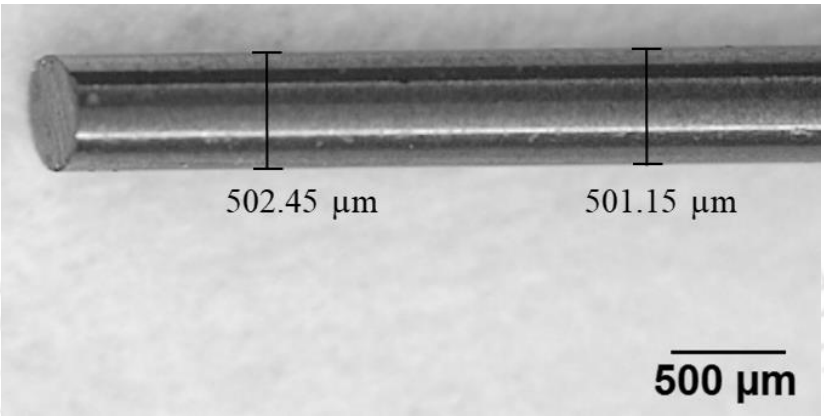

Fig. 3.1 Tungsten tool with an initial diameter of 500 µm

Table 3.1 Parameters for fabrication of microtool

Parameters	Value
Voltage	7 V
Duty cycle	50 %
Frequency	1kHz
Electrolyte	$NaNO_3$
Electrolyte Concentration	3 S/m
Tool rotational speed	600 rpm

Comsol® Multiphysics works on finite element (FE) analysis and is utilized to evaluate the variation of current density during the fabrication of microtool. In the IEG, the distribution of machining voltage is governed by the law of charge conservation [38]. The theory of electric field suggests that the Laplace equation [88] can find potential in the electrolyte domain at any location and is given by

$$\nabla^2\phi = 0 \tag{3.1}$$

where ∇ denotes Laplace's operator and ϕ denotes the metallic conductor's electric potential (V). The electrodes used in EMM are generally metallic conductors, so the current and voltage follow Ohm's law and are used to find the current density (J).

$$J = -\sigma\nabla\phi \tag{3.2}$$

From Ohm's law, resistance (R) in the IEG can be defined as

$$R = \frac{l}{A\sigma} \tag{3.3}$$

where l is IEG, A is the common area between the electrodes, and σ denotes the conductivity of the electrolyte (S/m).

The pictorial representation of the EMM setup utilized to manufacture microtool by keeping the tool inside a pre-install hole is shown in Fig. 3.2. For simplicity, this technique is named setup1. The experimental setup is designed and developed indigenously for the EMM. It consists of various sub-systems: the power supply system, the electrolyte and purification system, and the tool and workpiece handling system (Holmarc XYZ linear stage with the least count of 0.1 µm). The tool is made the anode and switched to the positive terminal of the power supply, and the workpiece is made the cathode and switched to the negative terminal of the power supply. A digital oscilloscope is attached to monitor the pulse power across the power supply. A hole of diameter 2 mm is fabricated on stainless steel. In this setup, the microtool can be manufactured in two possible cases. First, the tool is stationary inside the hole, and second, it is rotated inside the hole about its axis. In both cases, both electrodes (tool and workpiece) are completely dipped into the electrolyte. The electrodes are kept at a potential difference, and anodic dissolution starts.

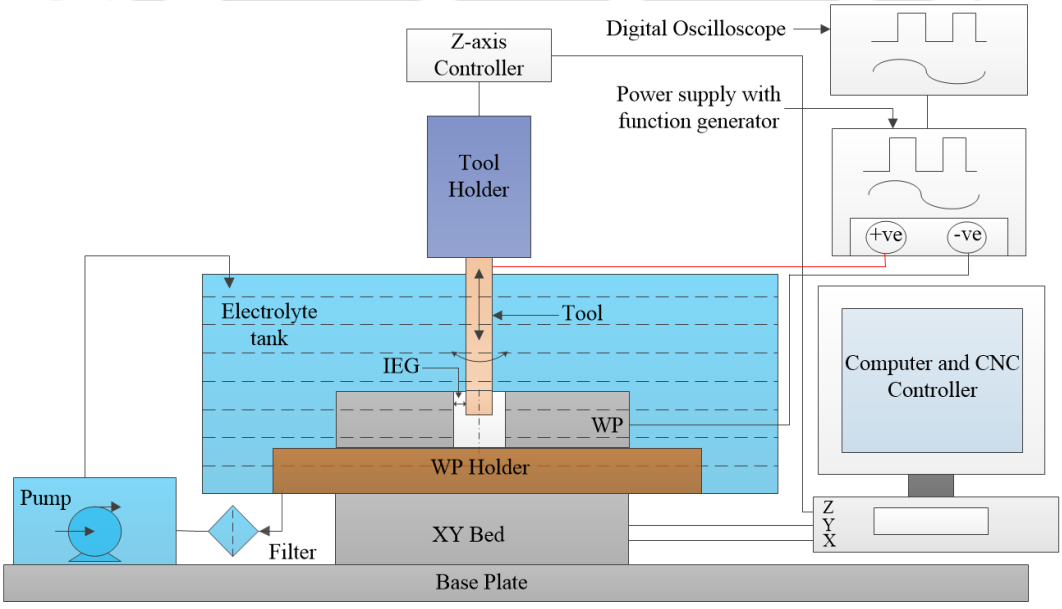

Fig. 3.2 Schematic diagram of EMM for setup1

The schematic setup of the EMM with the tool placed adjacent to the workpiece is shown in Fig. 3.3. For simplicity, this technique is named setup2. The tool is made the anode

and switched to the power supply's positive terminal, and the workpiece is made the cathode and switched to the power supply's negative terminal. The workpiece is stainless steel of thickness 0.5 mm and is placed in front of the tool. In this case, the tool is rotated such that both electrodes are completely dipped into the electrolyte. The electrodes are kept at a potential difference, and anodic dissolution starts. The machining parameters are presented in Table 3.1.

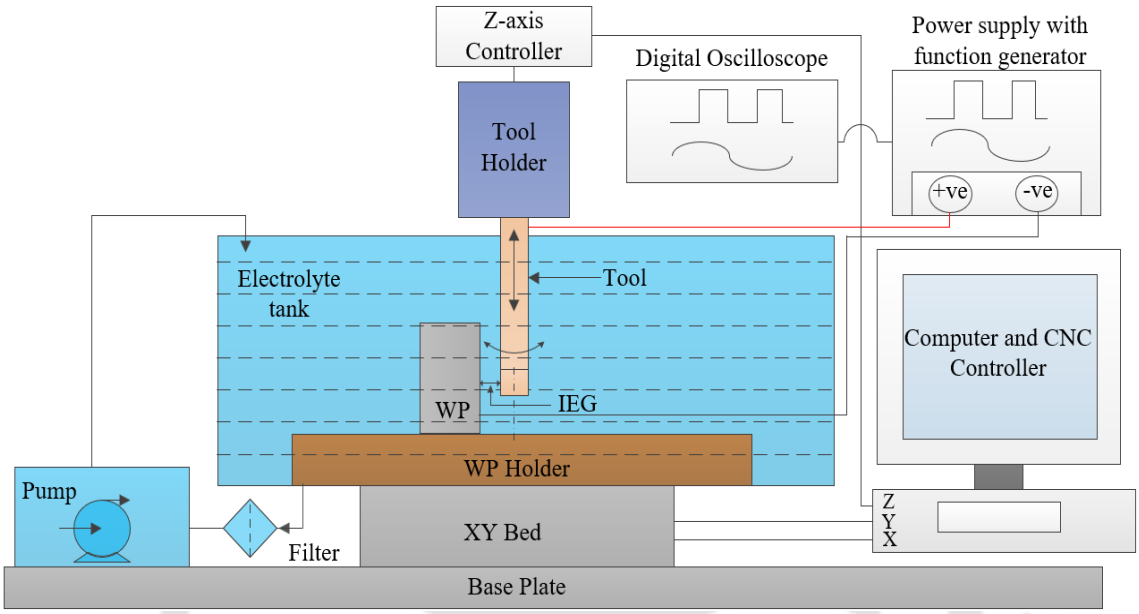

Fig. 3.3 Schematic diagram of EMM for setup2

In the above section, two possible cases of tool fabrication, namely fixed tool and fixed IEG, are utilized. In the first case (as shown in Fig. 3.4(a)), the tool rotates about its axis but is held stationary between the electrodes, i.e., no tool feed is given towards the workpiece. As the machining progresses, anodic dissolution removes the material from the anode. Thus, it increases the IEG as the tool is held stationary. Higher the IEG, the lesser the uniform distribution of current density [89]. Due to this, the current density value decreases during machining and slows the anodic dissolution rate. Thus, it takes more time to fabricate the microtool with this technique. With non-uniform current density, the machining accuracy, like surface finish and material removal rate, also decreases [90].

In the next case (as shown in Fig. 3.4(b)), the IEG between the tool and the workpiece remains constant. During machining, as the material dissolves, the electrode is given the feed with the same rate of linear material removal rate. Thus, it helps in maintaining the IEG fixed. Lesser the IEG, the higher the uniform distribution of current density [89]. Therefore, this technique takes less time to fabricate the microtool than the fixed tool. The fabricated

component's surface finish and material removal rate increase with uniform current density [90].

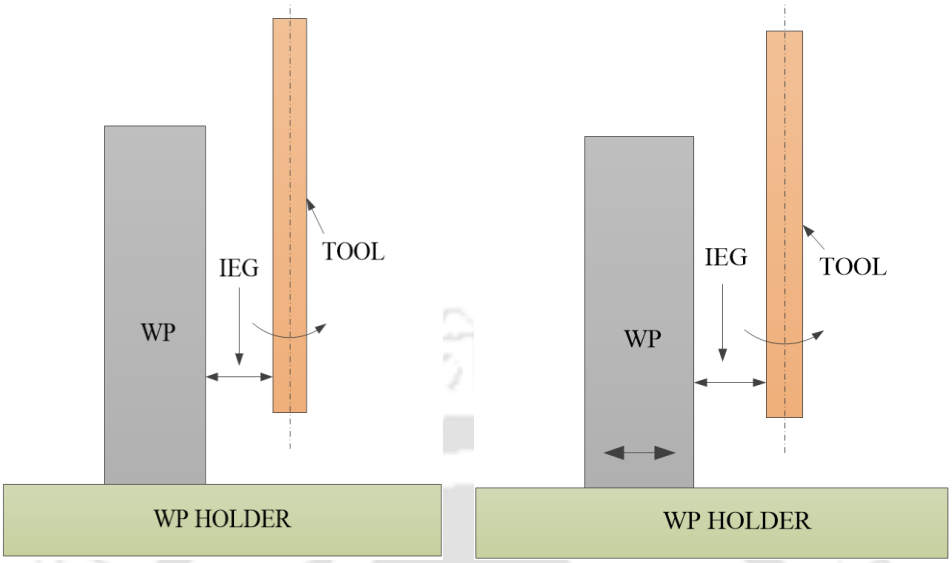

Fig. 3.4 Microtool fabrication using setup2 (a) Fixed Tool and (b) Fixed IEG

The anodic dissolution of the anode in the electrolyte cell during the EMM is determined due to the localized current density [21]. Its distribution along the electrode surface was found using the technique of finite element modeling (FEM) [91]–[94]. For this, electrochemistry and fluid flow are coupled in COMSOL® Multiphysics software. The software helps in analyzing the current density according to our electrochemical cell arrangement. In the present case, two models are framed to fabricate the microtool from EMM. In the first one, the tool is placed inside a pre-install hole in stainless steel (SS) plate; the other one is the tool kept adjacent to the SS plate. Two models have been developed for the second case, namely the fixed tool and the fixed IEG, as shown in Fig. 3.4. The following assumptions have been incorporated into the model:

- The material is isotropic and independent of temperature. Lower machining voltage avoids the Joule's heating.
- The concentration of the electrolyte is homogenous, and its circulation removes the debris particles and gas bubbles from the IEG.
- The electrolyte domain acts as a pure ohmic resistor in the inter-electrode gap (IEG).
- The current efficiency is constant at 100 %.

The linear MRR_l (m/s) in EMM follows Faraday's law of electrolysis [95] which can be described below.

$$MRR_l = \frac{\eta EJ}{F\rho} \tag{3.4}$$

Where, η is the current efficiency, J is the current density (A/m^2), E is the gram equivalent weight of the material (M/z) (M is the atomic mass and z is the dissolution valency), ρ is the anodic material density (kg/m^3), and F is Faraday's constant (96500 As). The linear MRR will help find the linear movement of the tool due to anodic dissolution, increasing the IEG between the electrodes.

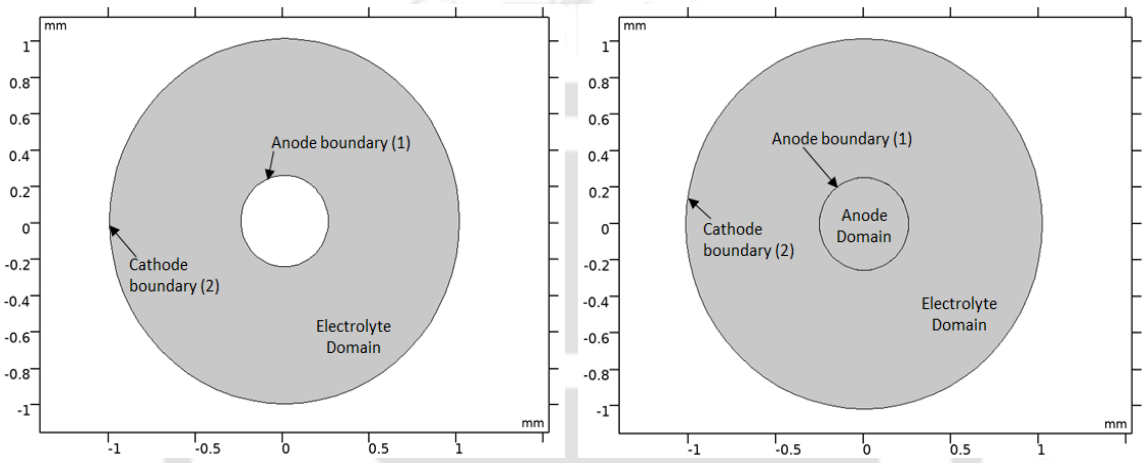

Fig. 3.5 2D geometry model for setup1 (a) without and (b) with tool rotation

The 2D geometry of the arrangement for the tool inside a hole in COMSOL® Multiphysics is shown in Fig. 3.5. Two concentric circles of diameter 500 µm and 2000 µm have been drawn. The top view of tool and workpiece arrangement is shown in Fig. 3.2. Tool is represented by boundary 1 and workpiece is represented by boundary 2. The tool inside a hole without rotation is shown in Fig. 3.5(a). Only the electrolyte domain is created for the primary current distribution. The tool inside a hole with rotation is shown in Fig. 3.5(b). Domains 1 and 2 correspond to anode and electrolyte, respectively. An identical pair has been created by form assembly between the anode and the electrolyte domain. A rotating domain has been assigned to the tool to rotate the electrolyte.

Table 3.2 shows the boundary conditions for both cases of the tool inside the hole. All the boundary conditions are the same for the tool with and without rotation except for the tool's rotational speed. As EMM is an anodic dissolution process, the dissolution properties of the tool are given as the input.

Table 3.2 Boundary conditions for the geometry model of setup1

Boundary condition	Boundary	Mathematical form
Electric potential	Anode (1)	$\phi = V$
Electric potential	Cathode (2)	$\phi = 0$
Non-deforming boundary	Cathode (2)	dx= 0; dy= 0
Deforming electrode surface	Tool boundary (1)	$v = \frac{EJ}{F\rho}$
Rotational speed (only for rotary tool)	Tool domain	f = 600 rpm

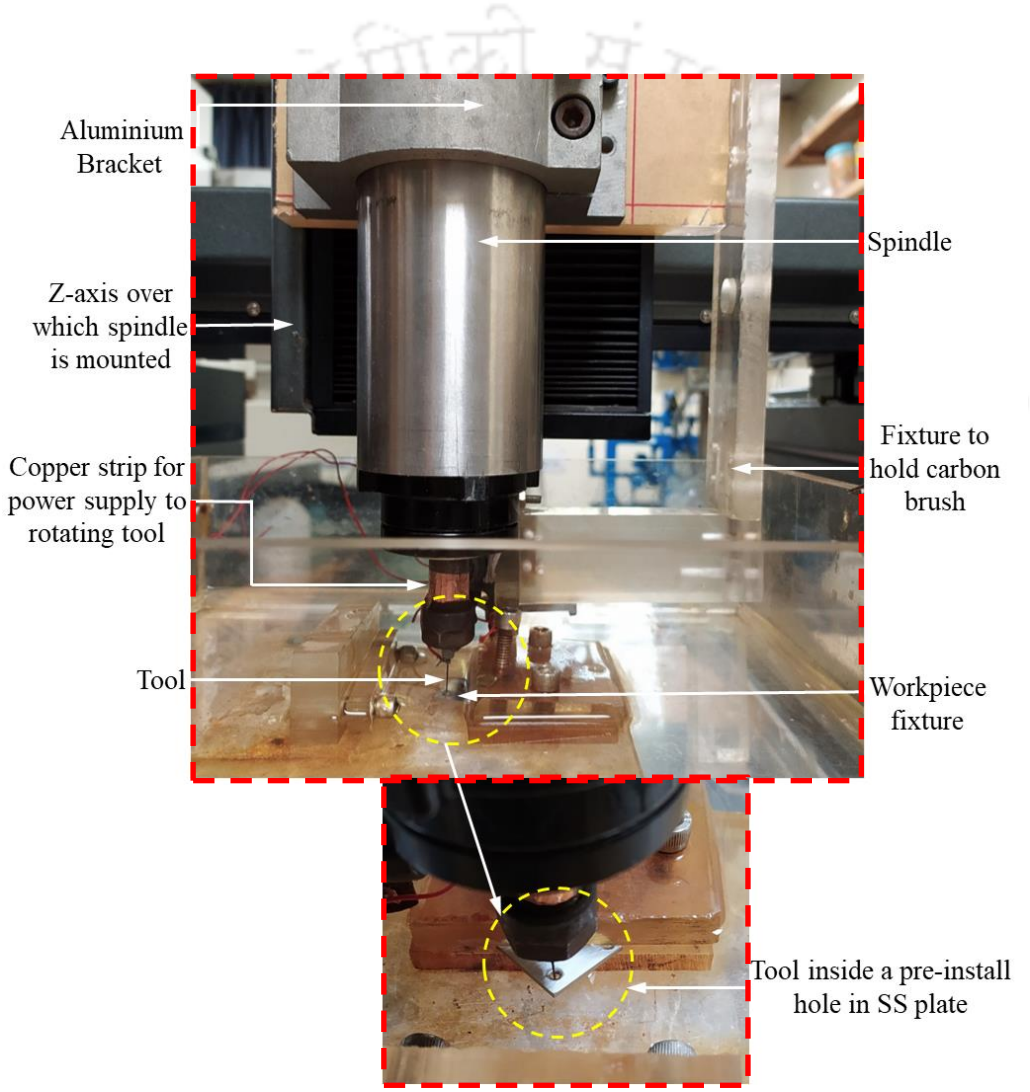

Fig. 3.6 Experimental design for setup1

The experimental design for setup1, i.e., tool inside the pre-install hole, is shown in Fig. 3.6. Tungsten tool of diameter 500 µm is placed inside the hole of diameter 2 mm in the stainless steel (SS316L). The tool is connected to the spindle via the tool holder. The spindle is used to provide the rotary motion to the tool. The workpiece is fixed by the fixture arrangement and switched to the power supply's negative terminal. As the tool diameter has

to reduce by anodic dissolution, it is switched to the power supply's positive terminal. Both electrodes are dipped into the electrolyte. The complete setup is kept in a container made of Perspex. The linear motion of the tool and workpiece is controlled by the CNC controller.

The 2D geometry of the arrangement for the tool adjacent to the workpiece in COMSOL® Multiphysics software (top view of tool and workpiece arrangement as shown in Fig. 3.3) is shown in Fig. 3.7. Domains 1 and 2 correspond to anode and electrolyte, respectively. A circle of diameter 500 µm has been placed adjacent to a 0.5 mm thick rectangular slab for the circular tool. An identical pair has been created by form assembly between the anode and the electrolyte domain. A rotating domain has been assigned to the tool such that it can rotate in the electrolyte about the z-axis. For fixed IEG, a prescribed mesh velocity has been assigned to the cathode (WP) in the x-direction such that it moves to maintain the constant IEG. For the fixed tool, no velocity is assigned to the cathode.

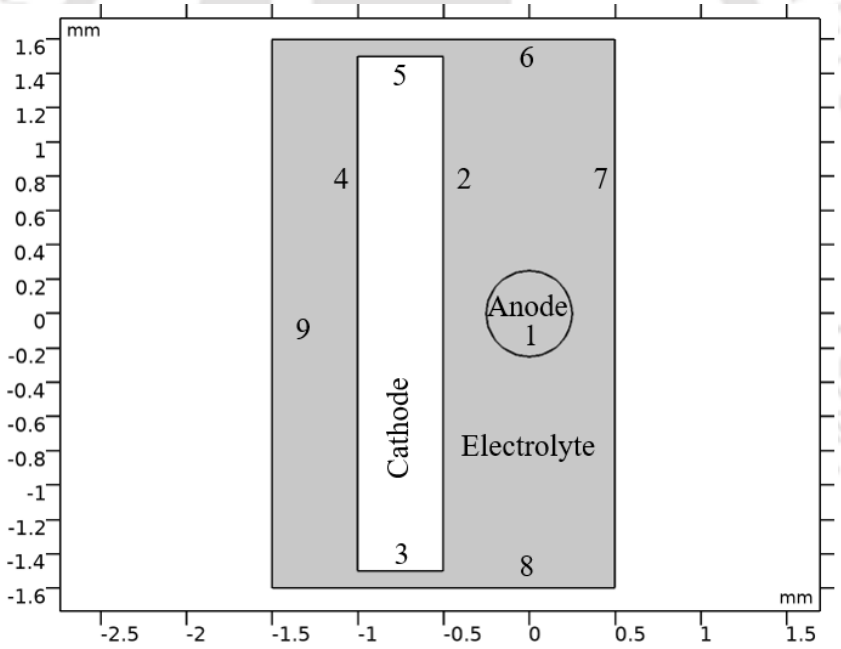

Fig. 3.7 2D geometry model for setup2

Table 3.3 presents the boundary conditions for the tool kept side of the workpiece. Boundary 1 corresponds to the tool (anode) switched to the positive potential and also rotated with 600 rpm. The workpiece (cathode) is a rectangular slab with boundaries (2, 3, 4 & 5) having zero potential. The electrolytic cell walls (6, 7, 8 & 9) have zero displacements in x and y directions and are insulated. All the boundary conditions are the same for the fixed tool and fixed IEG except for the workpiece boundary feed rate towards the tool. For the fixed IEG, the workpiece surface has to move toward the tool. In COMSOL® Multiphysics, as the

tool (anode) undergoes anodic dissolution, it has already been assigned a deforming electrode surface. The workpiece surface is fed towards the tool with the prescribed mesh velocity to keep the fixed IEG. As EMM is an anodic dissolution process, the dissolution properties of the tool are given as the input.

Table 3.3 Boundary conditions for the geometry model for setup2

Boundary condition	Boundary	Mathematical form
Insulation	6,7,8 and 9	$\frac{d\phi}{dn}=0$
Electric potential	Anode (1)	$\phi=V$
Electric potential	Cathode (2,3,4,5)	$\phi=0$
Non-deforming boundary	Electrolyte wall (6,7,8,9)	dx= 0; dy= 0
Deforming electrode surface	Tool boundary (1)	$v=\frac{EJ}{F\rho}$
Prescribed Mesh velocity (only for fixed IEG)	WP boundary (2,3,4,5)	v = 2e-6 m/s
Rotational speed	Tool domain	f = 600 rpm

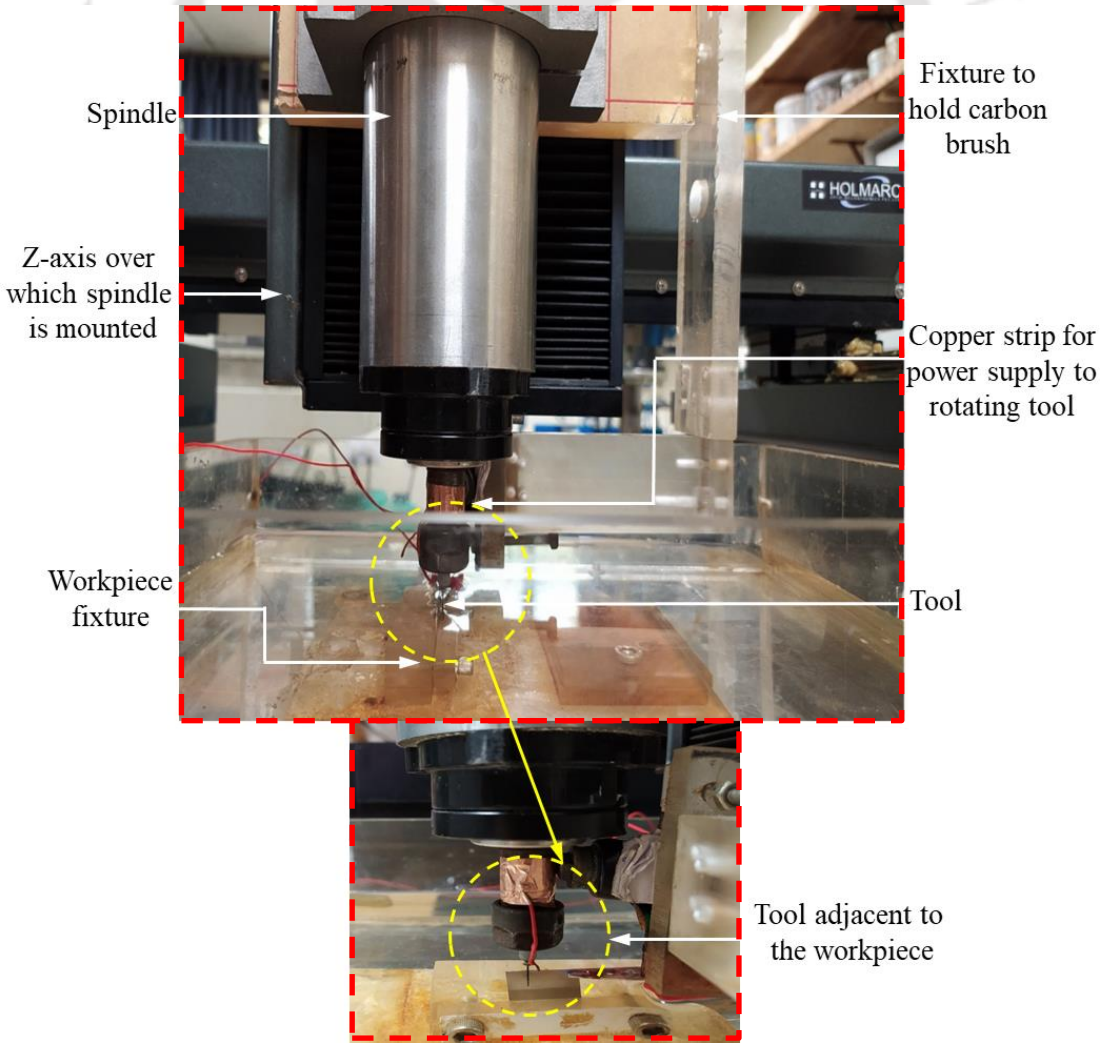

Fig. 3.8 Experimental design for setup2

The experimental design for setup 2, i.e., the tool is placed adjacent to the workpiece, is shown in Fig. 3.8. Tungsten tool of diameter 500 µm is placed adjacent to the flat stainless steel (SS316L) sheet. The tool is connected to the spindle via the tool holder. The spindle is used to provide the rotary motion to the tool. The workpiece is fixed by the fixture arrangement and switched to the power supply's negative terminal. As the tool diameter has to reduce by anodic dissolution, it is switched to the power supply's positive terminal. Both electrodes are dipped into the electrolyte. The complete setup is kept in a container made of Perspex. The CNC controller controls the linear motion of the tool and workpiece.

3.3 Results and Discussion

An EMM setup is designed and developed indigenously to fabricate a microtool. All the experiments were performed in the in-house built setup. The only change done is the reversal of polarity, i.e., the tool acts as the anode, which is switched to the positive terminal, and the workpiece acts as the cathode, which is switched to the negative terminal. As the removal mechanism in EMM is an anodic dissolution process, the tool is connected to the anode. The anodic dissolution of the anode in the electrolyte cell during the EMM is determined due to the localized current density [21]. This section discusses the results of the different fabrication techniques utilized for the tool's fabrication. The machining parameters are presented in Table 3.1. All the experiments are performed three times, and the average is taken. The dimensions of the fabricated microtool are measured using a stereo zoom microscope (Olympus DSX-100). Simulation results, along with the experimental results, are also discussed.

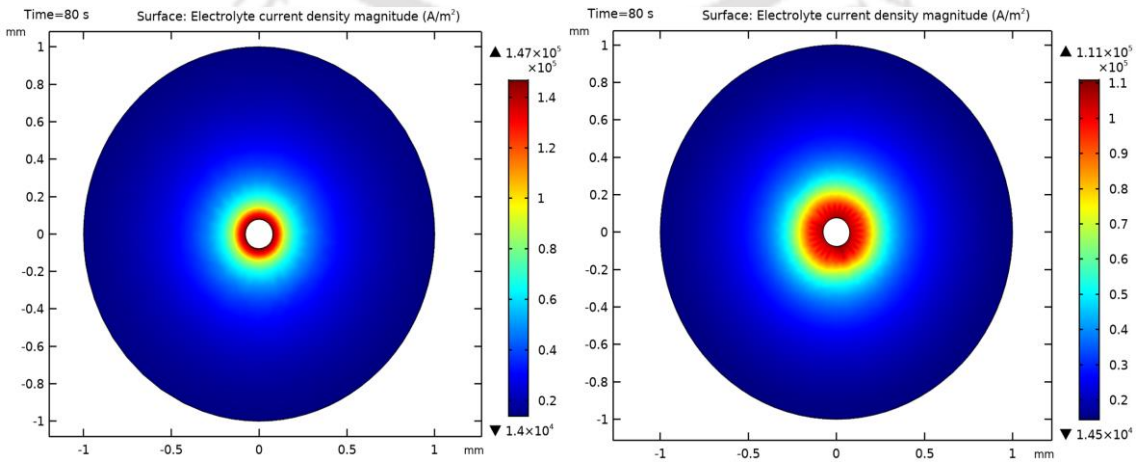

(a) (b)

Fig. 3.9 Current density distribution at 7V and 3 S/m for setup1 (a) without and (b) with tool rotation

The electrolyte current density magnitude for the tool inside the hole without and with rotation is shown in Fig. 3.9. Both techniques have the same input conditions as described in Table 3.1. The simulation ran for 80 seconds, and the current density plots were obtained. It can be inferred that the higher localized current density is observed around the tool surface without rotation due to the sticking of debris particles. However, for the tool with rotation, debris particles are removed from the tool surface due to rotation [96]. Thus, a better surface finish for the tool with rotation is achieved. The same is validated with the experimental results.

As hydrogen gas is electrically non-conductive, it accumulates near the electrodes and reduces the electrolyte conductivity. Thus, a higher current density is required to overcome hydrogen gas, leading to stray machining. The rotation of the tool helps in circulating hydrogen gas and maintains the uniform current density. Thus, the rotation of the tool provides a smooth surface finish.

The tool without rotation and with rotation fabricated at 7 V and 3 S/m experimentally is shown in Fig. 3.10. It can be inferred that the rotary tool circulates the electrolyte in the IEG, which avoids the sticking of debris particles and maintains the uniform current density. Thus, the anodic dissolution from the tool surface is uniform. However, in the case of tool without rotation, the debris particles stick to the tool surface and make the tool surface uneven.

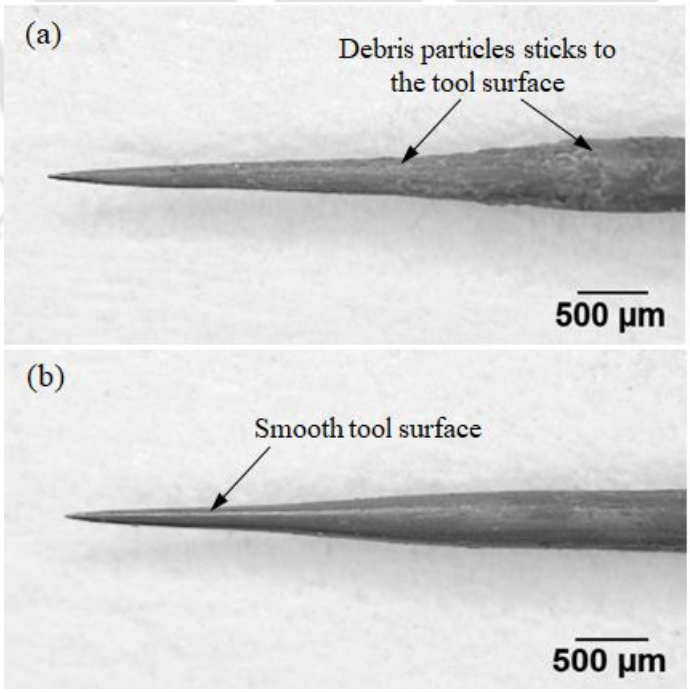

Fig. 3.10 Fabricated microtool at 7V and 3 S/m for setup1 (a) without and (b) with tool rotation

For the fixed IEG, the workpiece surface has to move toward the tool. In COMSOL® Multiphysics software, as the tool (anode) undergoes anodic dissolution, it has already been assigned a deforming electrode surface. To keep the fixed IEG, workpiece surface is fed towards the tool with the prescribed mesh velocity. A set of different feed rates have been selected to find the feed rate for the workpiece surface at 7 V and 3 S/m to maintain constant IEG.

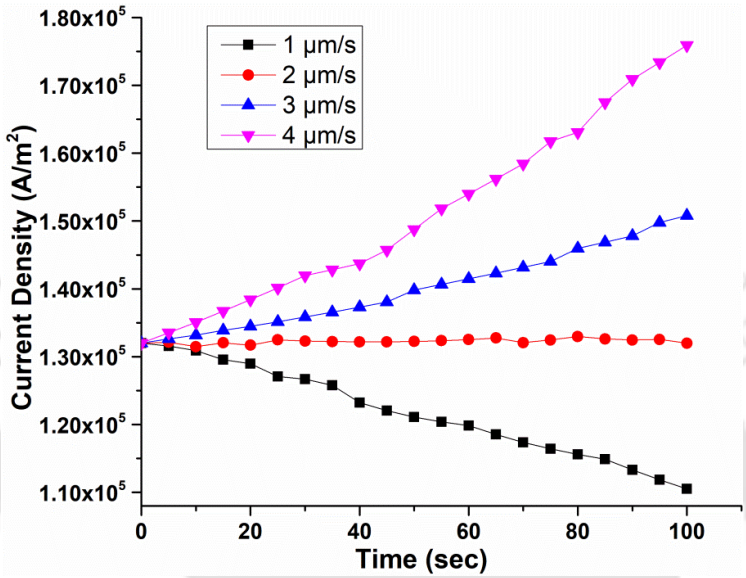

Fig. 3.11 Current density variation at 7V and 3 S/m for setup2 at different cathode feed rates

The current density variation for different workpiece feed rates is shown in Fig. 3.11. It can be inferred that the current density is almost constant for a feed rate of 2 µm/s. As feed rate increases, IEG decreases, current density increases, and vice versa. If the parameters change, the feed rate also changes.

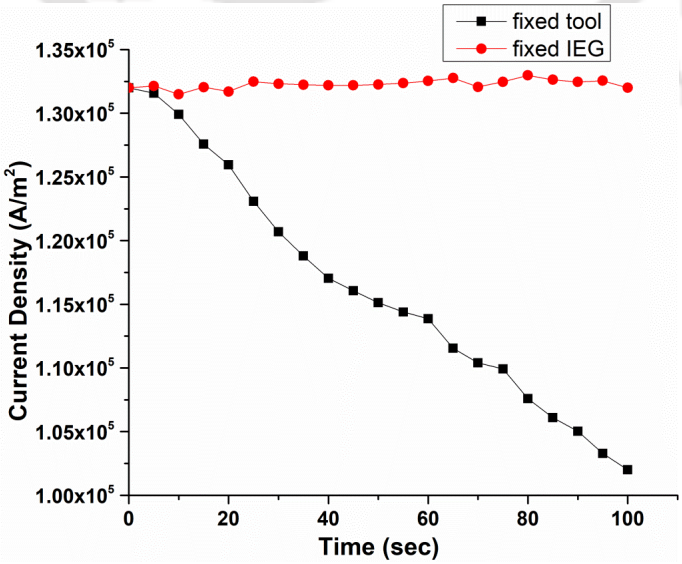

Fig. 3.12 Current density variation for the fixed tool and fixed IEG

For the particular parametric condition, the feed rate is constant. The current density variation for the fixed tool and fixed IEG when the tool is placed adjacent to the workpiece (as shown in Fig. 3.3) is shown in Fig. 3.12. After 2D modeling in COMSOL® Multiphysics, it can be inferred that for fixed tool, current density decreases during machining as IEG increases. However, for the fixed IEG, the current density is maintained constant during machining. The workpiece boundary is moved with a velocity of 2 µm/s toward the tool such that the IEG is kept constant. The constant current density produces uniform material removal from the tool surface and gives a better surface finish.

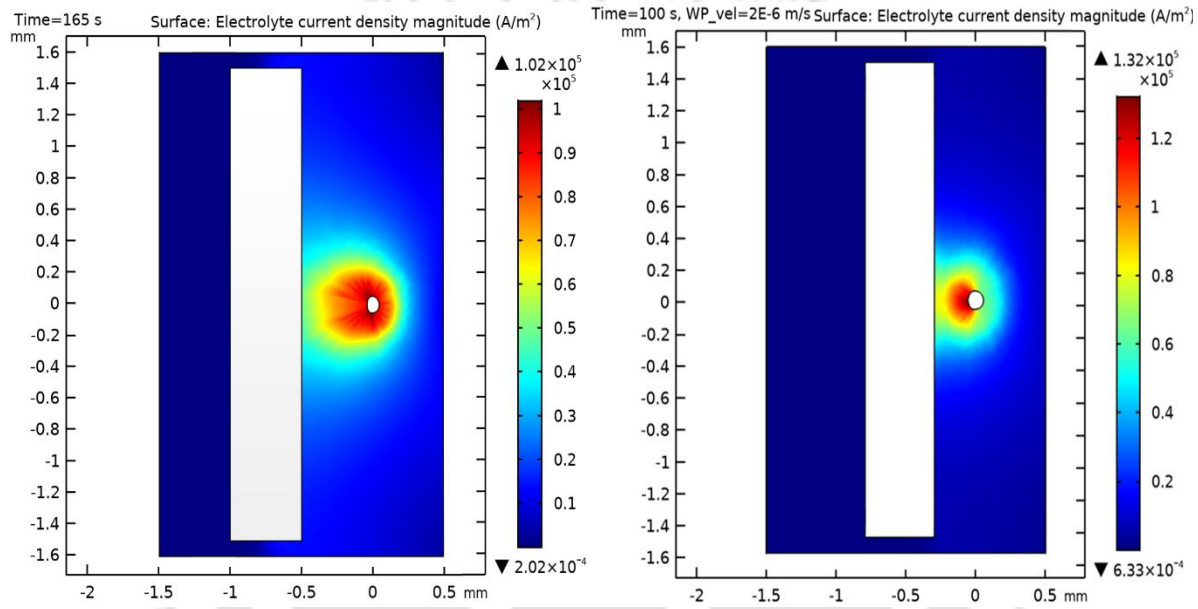

Fig. 3.13 Current density variation at 7V & 3 S/m for setup2 (a) Fixed tool (b) Fixed IEG

The current density variation for the tool arrangement when the tool is kept side of the workpiece is shown in Fig. 3.13. It can be inferred that this technique fabricates cylindrical microtools [97]. The current density and final shape of the tool for fixed tool configuration is shown in Fig. 3.13(a). As the machining progresses, the IEG increases due to anodic dissolution, leading to a decrease in the current density in the IEG. Thus, it produces non-uniform current density and takes longer time to fabricate the microtool. The diameter of fabricated microtool is 92 µm, which takes 165 sec to manufacture. The current density and final shape of the tool for fixed IEG configuration are shown in Fig. 3.13(b). As the machining progresses, anodic dissolution starts; however, with the workpiece feed rate, IEG is maintained constant. Thus, it produces uniform current density and takes a shorter time to fabricate the microtool compared to the fixed tool. The diameter of the fabricated microtool is

74 µm, which takes 100 sec to fabricate. The same is validated with the experimental results also. The fabricated microtools by two different methods, namely fixed tool and fixed IEG experimentally, are shown in Fig. 3.14, keeping the same parameters as described in Table 3.1. With the help of this technique, the cylindrical microtool can be fabricated.

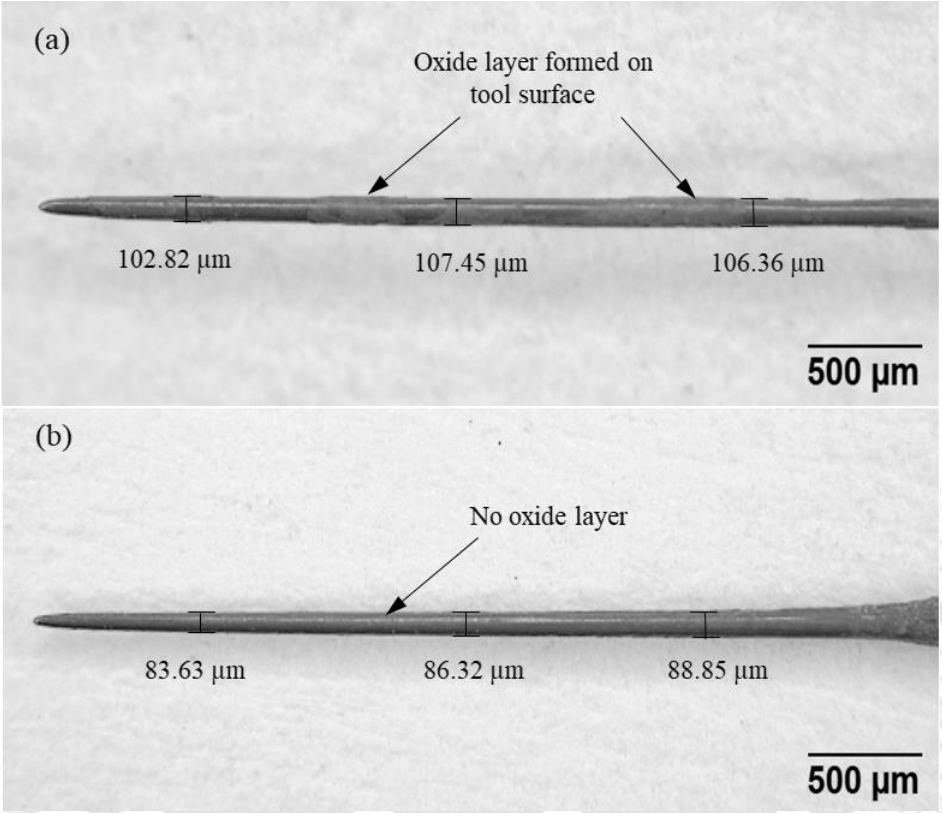

Fig. 3.14 Fabricated microtools by setup 2 (a) fixed tool and (b) fixed IEG technique

The variation of tool diameter when fabricated by keeping the tool fixed is shown in Fig. 3.14(a). It was observed that the oxide layer was formed on the surface due to prolong electrolyte and non-uniform current density distribution [88]. Due to oxide layer formation, the surface of the tool is uneven. The average diameter of the fabricated microtool is 105.5 µm. When compared with the simulation, an error of 12.83% is observed in the diameter. The variation of tool diameter when manufactured by keeping IEG fixed is shown in Fig. 3.14(b). It was observed that the variation in tool diameter is of few microns, and no oxide layer was formed on the surface as the current density distribution is uniform [98]. The average diameter of the fabricated microtool is 86.26 µm. When compared with the simulation, an error of 14.26% is observed in the diameter. The reason for this error is the assumption considered for the simulation. The effect of hydrogen gas bubbles slows down the anodic dissolution rate; thus, the variation in the dimension is observed.

3.4 Summary

The developed experimental setup of EMM can be utilized to fabricate microtools. In the present study, the tungsten tool with an initial diameter of 500 µm is utilized for the fabrication of the microtool. The microtools are fabricated by two techniques: the tool inside the hole (setup 1) and the tool adjacent to a flat workpiece (setup 2). In setup 1, the effect of tool rotation inside the hole during microtool fabrication is analyzed. Due to the sticking of debris particles, non-uniform and high current density develops for the tool inside hole without rotation. However, the tool inside the hole with rotation gives a better surface finish as debris particles are easily removed from the tool surface. In setup 2, two configurations have been utilized fixed tool and fixed IEG. In fixed tool, the electrodes (tool and workpiece) are fixed at their locations; however, in fixed IEG, the electrodes are moved towards each other such that the IEG is maintained constant.

COMSOL® Multiphysics helps to understand the behavior of different tool shapes by visualizing the current density. Fixed tool configuration decreases current density during machining as IEG increases. It results in the formation of an oxide layer over the fabricated tool surface. This technique fabricates an average of 105.5 µm diameter of microtool. Fixed IEG configuration leads to constant current density during machining as IEG is constant. It gives a better surface finish due to the constant machining rate. This technique fabricates an average of 86.26 µm microtool diameter.

Chapter 4 Design and Development of EP Setup

4.1 Introduction

Electropolishing is a nonconventional finishing method that follows anodic dissolution. The polishing setup comprises an anode (sample to be electropolished), a cathode (tool), and an electrolyte. In EP, the electrolyte mainly consists of viscous acidic fluid. EP does not change the crystallographic and grain-boundary structure of the bulk material and never induces any residual stress, which makes it different from other polishing methods. This advantage of EP is utilized as a post-processing method for components fabricated by thermal-induced processes like laser beam machining (LBM), electric discharge machining (EDM), etc. During EP, a layer of material is removed from the surface, reducing the recast layer from the surface. The motivation of the present work is to EP the thin-cruciform gimbal flexure of a gyroscope (made of maraging steel) fabricated by EDM. Initially, an experimental setup is developed, and experiments are performed to determine its capabilities.

In the present chapter, electropolishing of maraging steel is performed. An organic electrolyte solution containing acetic acid with perchloric acid is used for electropolishing. The various parameters, like, polishing time, temperature, and agitation are analyzed. Linear sweep voltammetry (LSV) is performed to generate the polarization curve for maraging steel at a particular solution. Energy-dispersive X-ray spectroscopy (EDS) analysis is performed to investigate the workpiece surface composition before and after EP. The influence of EP parameters on surface roughness and surface reflectance is also presented. The contact angle of the surface is measured with the help of a goniometer to analyze the workpiece surface's wettability before and after EP. The corrosion behavior of the sample before and after EP is also studied.

4.2 Electropolishing Experimental Procedure

In this section, the development of an electropolishing experimental setup has been discussed, along with the steps to be followed for electropolishing. The selection of material and the tool for electropolishing has also been selected. The details about the process parameters for EP and the analysis to be performed for the electropolished surface have been explained.

4.2.1 Experimental Setup

The schematic of the proposed electropolishing setup for maraging steel electropolishing is shown in Fig. 4.1. It is an extended version of the electrochemical machining (ECM) setup. It also contains an electrolyte and cathode and anode holding arrangement. A glass container of 100 ml is used as a chamber for electropolishing. A graphite sheet connected to the power supply's negative terminal is used as a cathode. The cathode is dipped inside the glass electrolyte chamber. A rectangular maraging steel 300 sheet of dimension 25 mm × 10 mm × 3 mm is used as the anode, which connects to the power supply's positive terminal. The complete setup is kept over a hot plate with the magnetic stirrer. The hot plate is used to provide the required amount of heat to increase the electrolyte's temperature. The magnetic bar rotates within the glass chamber with the help of a magnetic stirrer. It agitates the solution during electropolishing. Hence, the dissolved particles are easily cleaned from the workpiece surface [99]. A DC power supply of 60 V and 20 A rating provides a potential difference between the anode and cathode.

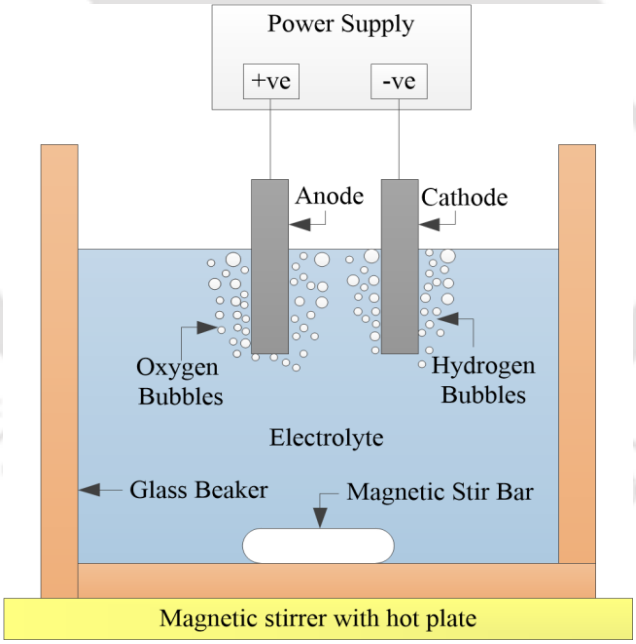

Fig. 4.1 Schematic of electropolishing setup

Table 4.1 Electropolishing process parameters

Parameters	Value
Voltage	6 V
Electrolyte	Vol. ratio of acetic acid and Perchloric acid is 3:1
Polishing time	4–10 min
Agitation	0–600 rpm
Temperature	30–75 ºC

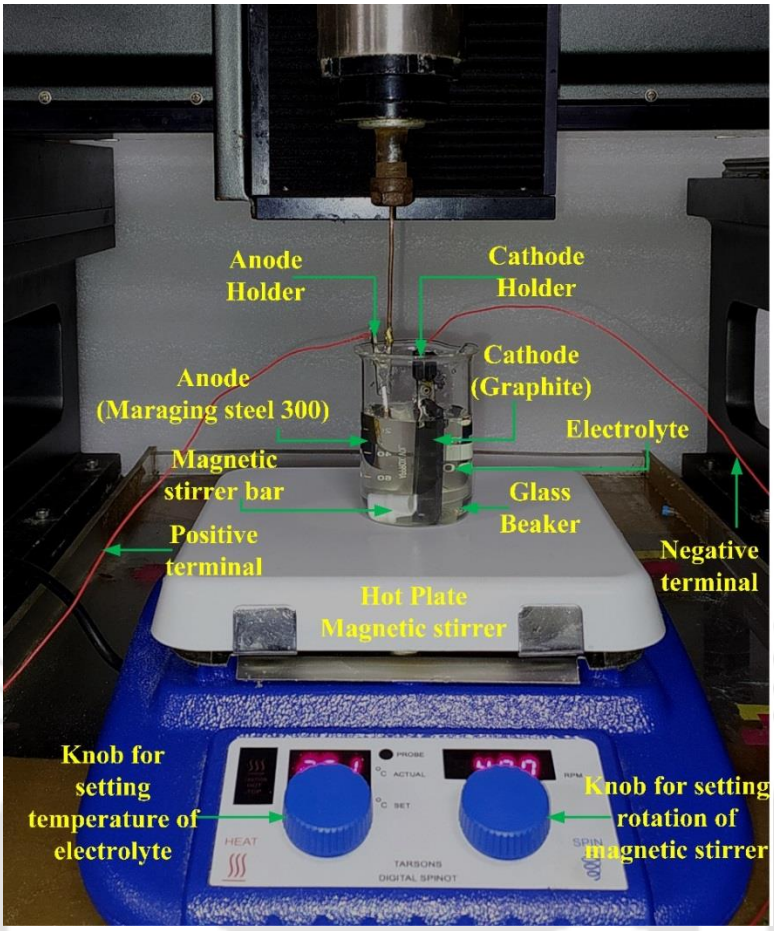

Fig. 4.2 Experimental setup for EP

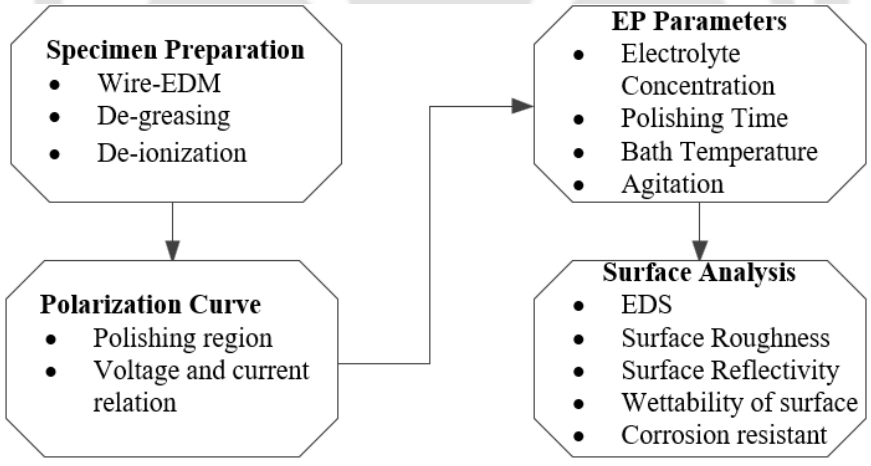

Fig. 4.3 Flow chart of electropolishing process

Table 4.1 shows the EP process parameters selected for polishing maraging steel. The major influencing parameters are electrolyte temperature, rotation of the magnetic stirrer, and polishing time. The actual electropolishing experimental setup is shown in Fig. 4.2. As shown in Fig. 4.3, the flow chart describes the step-by-step process of electropolishing. The first step is the preparation of the sample. The maraging steel is cut by wire-EDM and then mechanically polished consecutively with sandpapers of grit nos: 120, 400, and 600 to

eliminate scratch marks and deformed layers from the test samples. The surface is manually cleaned using acetone. Further cleaning is conducted with deionized water in an ultrasonic cleaner for 15 minutes. The initial surface roughness (R_a) of the specimen is about 0.272 µm.

4.2.2 Electrochemical Analysis

A polarization curve is drawn utilizing linear sweep voltammetry (LSV) to correlate voltage and current during electropolishing. The organic electrolyte, which consists of acetic acid and perchloric acid, are mixed in a volume ratio of 3:1. LSV provides three different zones such as active, passive, and transpassive. An electrochemical workstation (Gamry Instruments) with a three-electrode system, namely a working electrode (maraging steel sample), counter electrode (platinum electrode), and reference electrode (Ag/AgCl electrode), is used for LSV. The voltage is swept between 10 to 0 V with a scan rate of 10 mV/s [100]. The potential must be swept in the cathodic direction to avoid any pitting of the electrode surface while achieving reproducible measurements [101].

4.2.3 Analysis of Polished Surface

The polished surface microstructure and its morphology are analyzed with the help of an optical microscope and field emission scanning electron microscopy (FESEM). The sample is fixed in the epoxy resin using a cold setting to obtain the grain structure. The specimens were first mechanically polished with sandpapers of grit nos. 120, 400, and 600 to eliminate the test samples' scratch marks and deformed layers. Finally, it is polished in buff cloth with 1 µm diamond paste. For visualizing the micro-structure, the sample should be etched. A modified fry reagent consisting of 75 ml of deionized water (DI), 25 ml of hydrochloric acid (36 wt.%), 12.5 ml of nitric acid (68 wt.%), and 0.5 g of copper (II) chloride ($CuCl_2$) is prepared as the etchant. For the etching of the cold-mounted sample, the surface is scrubbed for approximately 60s with cotton, which is dipped in the solution, and then the surface is cleaned with deionized water and ethanol, followed by hot, dry air [102]. The metallographic structure is inspected with the help of a metallographic optical microscope.

The surface roughness (R_a) is measured with the help of a non-contact optical profilometer. The elemental composition is characterized with the help of Energy-dispersive X-ray spectroscopy (EDS). Further, the contact angle is measured for the wettability study, i.e., hydrophilicity and hydrophobicity of the polished surface. It is inspected using a goniometer utilizing the sessile method of contact angle measurement. For this purpose, a

water drop of 2 µl is placed over the workpiece surface before and after EP [103]. The contact angle can be utilized to calculate the surface energy of the metallic workpiece surface [104]. An angle greater than 90º signifies a hydrophobic surface, and a lesser than 90º signifies hydrophilic.

X-ray photoelectron spectroscopy (XPS) analysis is carried out to study the surface elemental composition before and after EP. The measured XPS spectra are calibrated with respect to C 1s (284.8 eV) adventitious peak, and the samples were scanned from 0 to 1200 eV with a step size of 1 eV. Higher-resolution spectra are conducted for iron, nickel, and oxygen elements. The Gaussian function is used for background correction.

Corrosion analysis is performed by utilizing the Tafel polarization curve by conducting experiments in potentiostat. The potential is varied from −250 mV to +250 mV vs. Ag/AgCl with respect to the corrosion potential at a scan rate of 10 mVs^{-1} using 3.5 wt.% of NaCl solution [105]. Various parameters like corrosion potential (E_{corr}) and corrosion current density (I_{corr}) are evaluated from the experimental curve. Table 4.2 shows the operating conditions during various operations performed to analyze the electropolished surface.

Table 4.2 Operating conditions

Experiments	**Value**
Linear sweep voltammetry	Potential range: 10 V to 0 V; Scan rate: 10 mV/s
Surface reflectance	UV light with wavelength between 200 to 1000 nm
Contact angle	Waterdrop of 2 µl
Tafel polarization	Potential range: −250 mV to +250 mV; Scan rate: 10 mV/s
Electrolyte for corrosion analysis	3.5 wt.% NaCl solution

4.3 Results and Discussion

Electropolishing (EP) is performed on the maraging steel 300 sheet. The organic electrolyte consisting of acetic acid and perchloric acid is mixed in a volume ratio of 3:1. The setup for EP is indigenously designed and fabricated. It consists of electrolytes with electrodes. The effect of different parameters such as polishing time, temperature, agitation on surface roughness, and surface reflectance are investigated. The results are discussed in the following sub-sections.

4.3.1 Anodic Polarization Behavior of Maraging Steel

Linear sweep voltammetry (LSV) is performed to determine the anodic polarization behavior of maraging steel, as shown in Fig. 4.4. Three electrodes system is used to select the region of

EP. The polarization curve is conducted by varying the potential from 10 to 0 V with a scan rate of 10 mV/s [106]. The polarization curve obtained in acetic acid and perchloric acid solution in maraging steel consists of three regions (Fig. 4.4). The region between 3 to 4 V is the active region (I) in which current increases with increased potential. The corresponding potential of 3 V is termed as activation potential (E_a). The region between 4 to 6.2 V is the passive region (II), where the current is stable for an increase in voltage. The corresponding potential of 4 V is termed as passivation potential (E_p). After this region, the current increases rapidly in the transpassive region (III). The corresponding potential of 6.2 V is termed as breakdown potential (E_b). Three sets of experiments are performed to measure the breakdown voltage. Almost similar anodic polarization behavior of maraging steel in acetic and perchloric acid is observed for all three experimentations, with the breakdown voltage measured at 6.2±0.3 V.

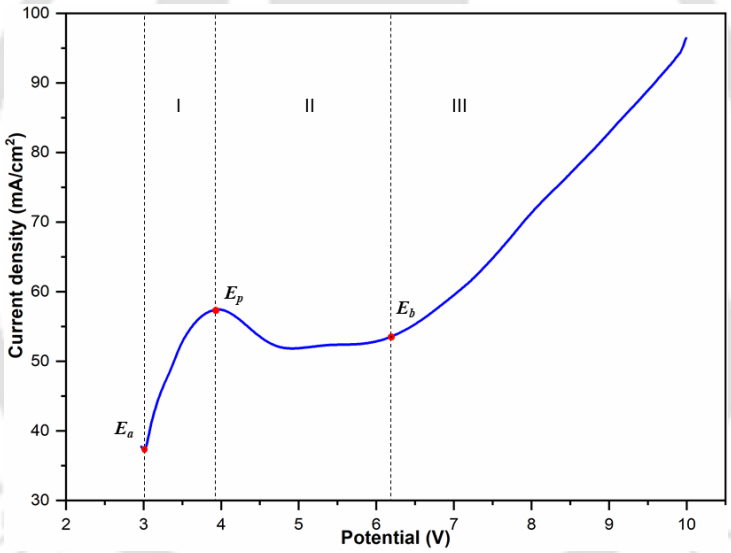

Fig. 4.4 Anodic polarization behavior of maraging steel in acetic acid and perchloric acid with breakdown voltage at 6.2±0.3 V

As per the literature, EP occurs only in the passive region. A viscous film having higher resistance than the electrolyte is formed in the passive region [100]. Region (III) is also termed as gas evolution region where oxygen gas bubbles are evolved. The reactions that take place during EP are discussed below in Eqs. (4.1) to (4.4) [75].

$$M \rightarrow M^{n+} + ne^{-} \quad \text{(at workpiece surface)} \tag{4.1}$$

$$nH_2O + ne^{-} \rightarrow \frac{n}{2}H_2 + nOH^{-} \quad \text{(at tool surface)} \tag{4.2}$$

$$M^{+n} + nOH^{-} \rightarrow M(OH)_n \quad \text{(Near anode surface towards bulk electrolyte)} \tag{4.3}$$

$$M + nH_2O \rightarrow M(OH)_n + \frac{n}{2}H_2 \text{ (Net process reaction)} \quad (4.4)$$

During EP, the metal (M: Fe, Ni) is dissolved by releasing electrons (n, valency of metal M) (Eq. (4.1) [55], and these electrons are gained on the cathode surface to produce hydrogen gas (H_2) and hydroxyl ions (OH^-) (Eq. (4.2)) [107]. These hydroxyl ions combine with metal ions near the anode surface and form metal hydroxides (Eq. (4.3)). The overall reaction to the EP process is expressed as Eq. (4.4). The chemical reactions (i.e., Eqs. (4.1-4.4)) are the proposed generalized reactions that occur during electropolishing. These equations show the proposed formation of metal hydroxides. XPS analysis has been performed to find the generated final products (i.e., metal hydroxides and oxides), which are discussed later in section 4.3.7.

4.3.2 Effect of EP on Elemental Composition of Surface

Energy-Dispersive X-Ray Spectroscopy analysis is performed to investigate the elemental composition of maraging steel 300 surfaces before and after EP. The initial surface is cleaned with acetone, followed by an ultrasonic cleaner. EDS analysis of maraging steel before and after EP is shown in Fig. 4.5 (a & b). EP is performed at 60 ºC with magnetic stirrer bar rotation at 400 rpm.

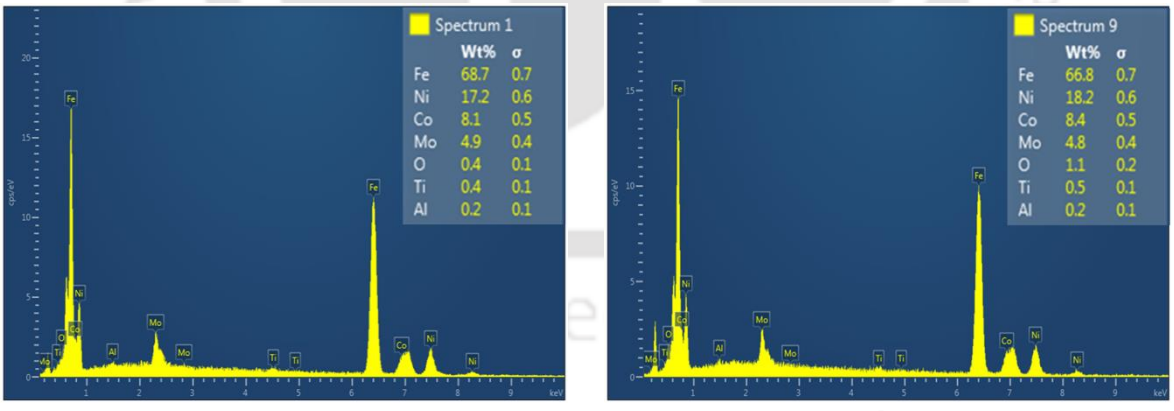

(a) (b)

Fig. 4.5 EDS analysis of maraging steel at 60 ºC with 400 rpm stirrer rotation (a) before and (b) after EP

Table 4.3 shows the changes in the surface's elemental compositions before and after EP, which are negligible [77]. However, the sub-surface composition is not measured with EDS. An increase in % oxygen composition indicates that an oxide layer is formed on the surface after EP, increasing corrosion resistance [108]. EDS analysis suggests that after EP,

the concentration of Ni^+ increases, and Fe^+ decreases at the passive layer [52]. The surface microstructural images of maraging steel before and after EP are shown in Fig. 4.6(a) and (b), respectively. The microstructure consists of martensite and austenite phases [109]. However, distinct grain boundaries with no scratch marks are visible after EP [71].

Table 4.3 Elemental compositions (Wt.%) of maraging steel before and after EP

Process / Element	Before EP		After EP	
	% Wt.	S.D (σ)	% Wt.	S.D (σ)
Fe	68.7	0.7	66.8	0.7
Ni	17.2	0.6	18.2	0.6
Co	8.1	0.5	8.4	0.5
Mo	4.9	0.4	4.8	0.4
O	0.4	0.1	1.1	0.2
Ti	0.4	0.1	0.5	0.1
Al	0.2	0.1	0.2	0.1

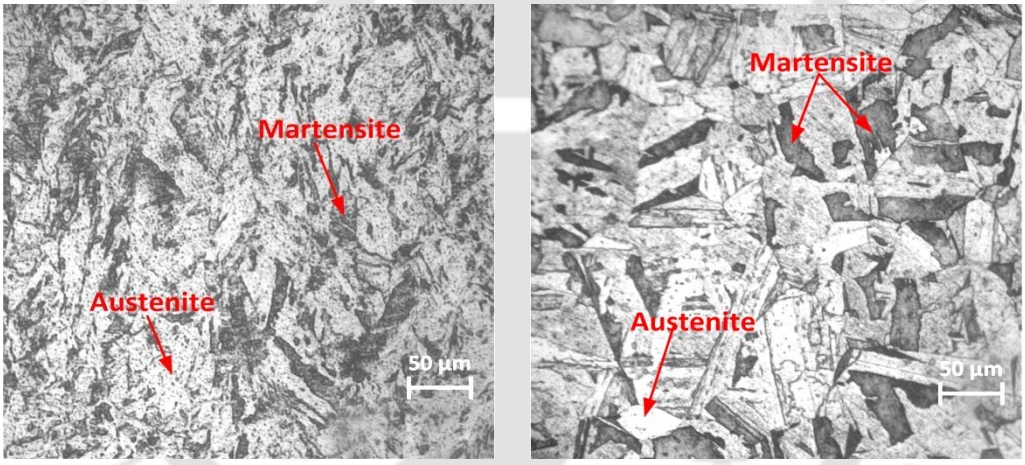

(a) (b)

Fig. 4.6 The surface microstructural images using an optical microscope of maraging steel 300 (a) before and (b) after EP

4.3.3 Effect of Temperature on Surface Roughness and Surface Reflectance

During electropolishing, the temperature has a significant effect on the surface roughness. As the temperature increases, the conductivity of electrolytes increases, which increases the anodic dissolution [110]. The percentage improvement in the surface roughness with temperature has been shown in Fig. 4.7. As temperature increases, the surface roughness decreases. A maximum gain of 55.47±3% is observed at 60 ºC (out of 5 repeated experimentations at the same condition). At higher temperatures, faster anodic dissolution occurs, which leads to pitting the surface. Hence, the surface finish deteriorates. It can be

inferred from Fig. 4.7 that beyond 60 ºC, the percentage improvement in surface roughness decreases.

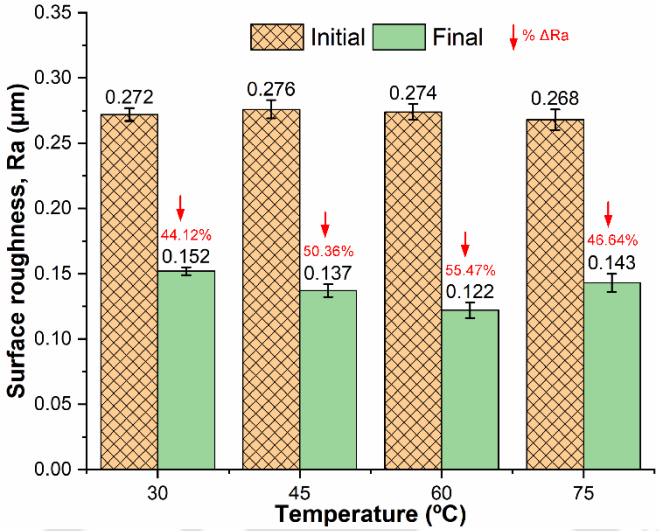

Fig. 4.7 Effect of temperature on surface roughness with maximum roughness improvement of 55.47±3% at 60 ºC

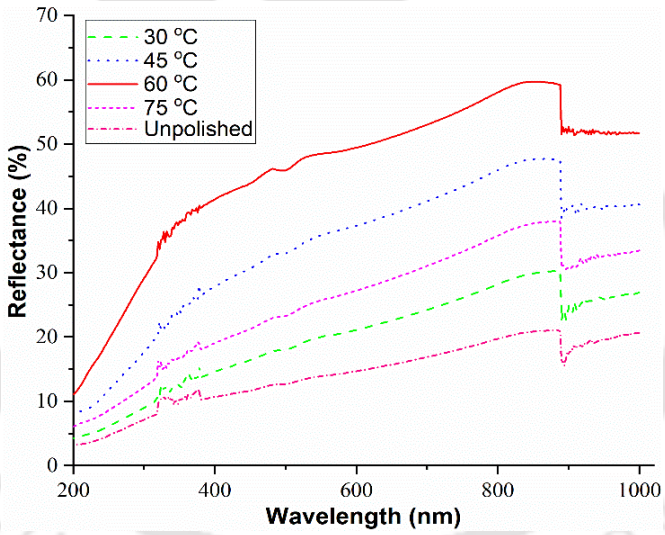

Fig. 4.8 Effect of temperature on surface reflectance with maximum reflectance of 58.6±2% at 60 ºC

The temperature has a significant effect on surface reflectance during EP. The surface reflectance at various temperatures is shown in Fig. 4.8. The relative surface reflectance is measured with reference to a highly polished silver surface having 100% reflectivity. The magenta dot line shows the surface reflectance of the unpolished base material. The ultra-violet (UV) light is varied between 1000 to 200 nm. It can be inferred from Fig. 4.8 that better surface reflectance is observed at 60 ºC, having a maximum surface reflectance value of 58.6±2% (out of 5 repeated experimentations at the same condition). At a higher temperature, above 60 ºC, pitting occurs, decreasing surface reflectance.

4.3.4 Effect of Agitation on Surface Roughness and Surface Reflectance

The effect of agitation on surface roughness is shown in Fig. 4.9. A magnetic stirrer is used to provide agitation to the solution during EP. The magnetic bar is rotated from 0 to 600 rpm to see its effect on the workpiece surface roughness. Electropolishing was performed at 60 ºC for 6 minutes with a varied magnetic stirrer rotation between 0 to 600 rpm. It can be inferred from Fig. 4.9 that as the rotational speed increases from 0 to 400 rpm, surface roughness decreases during EP due to the stirring of the electrolyte and further easy removal of the gas bubbles. The maximum improvement in surface roughness is observed as 56.25±2% at 400 rpm magnetic bar rotation (out of 5 repeated experimentations at the same condition). With increased rotational speed from 400 to 600 rpm, the viscous layer formed on the anode surface becomes unstable, increasing surface roughness [46].

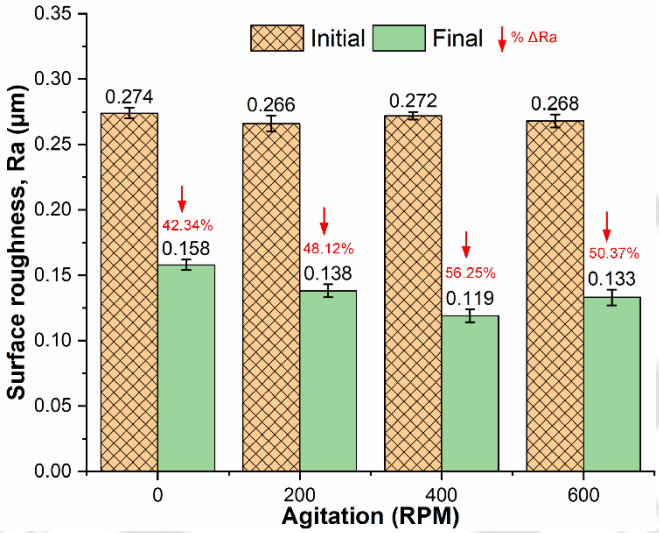

Fig. 4.9 Effect of magnetic stirrer agitation (i.e., rotation) on surface roughness with maximum improvement of 56.25±2% at 400 rpm

A comparison of surface reflectance between unpolished and electropolished samples at different rotations (between 0 to 600 rpm) of the magnetic stirrer is shown in Fig. 4.10. Electropolishing is performed at 60 ºC for 6 minutes. The magenta dot line shows the surface reflectance of the unpolished base material. The higher the surface finish, the higher will be the surface reflectance. It can be inferred from Fig. 4.10 that at 400 rpm, maximum reflectance of 60.3±3% is observed (out of 5 repeated experimentations at the same condition).

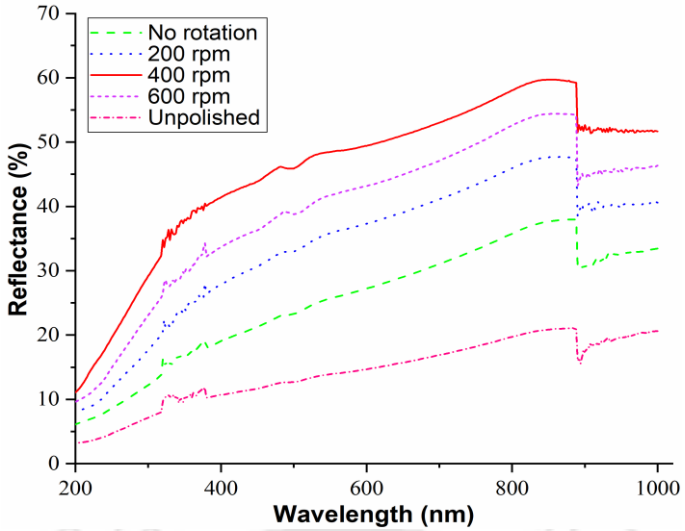

Fig. 4.10 Effect of magnetic stirrer agitation (i.e., rotation) on surface reflectance with maximum reflectance of 60.3±3% at 400 rpm

4.3.5 Effect of Polishing Time on Surface Roughness and Surface Reflectance

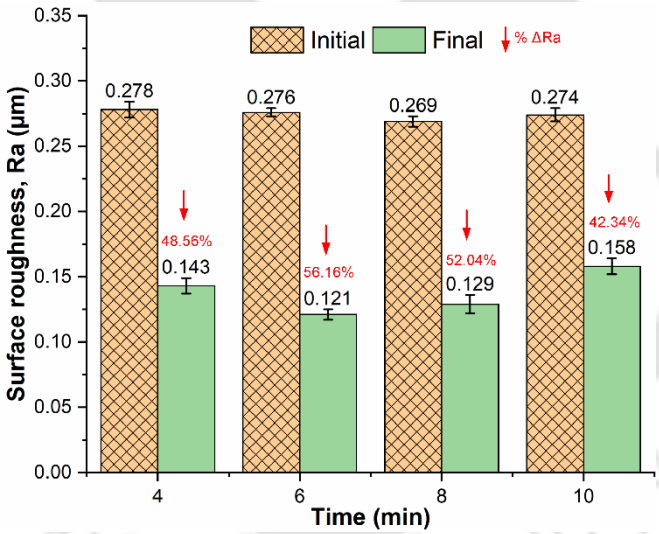

Fig. 4.11 Effect of polishing time on surface roughness with maximum roughness improvement of 56.16±2% at 6 minutes

The percentage improvement of the surface roughness with polishing time is shown in Fig. 4.11. The polishing time is varied between 4 to 10 minutes at an interval of 2 minutes. It can be inferred from Fig. 4.11 that as polishing time increases, surface finish increases. However, the amount of material removal also increases with the rise in polishing time. The maximum improvement in surface roughness is obtained as 56.16±2% at 6 minutes of EP (out of 5 repeated experimentations at the same condition). For a longer duration of EP, the amount of

anodic dissolution increases, and alloying elements start leaving the surface, creating pits and deteriorating surface finish [56].

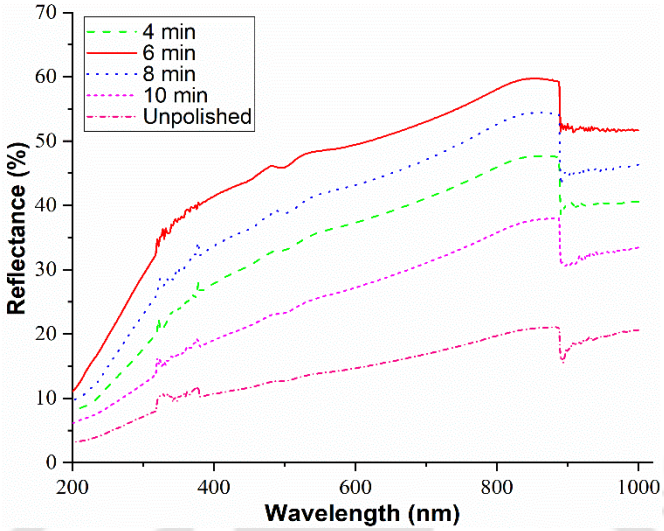

Fig. 4.12 Effect of polishing time on surface reflectance with maximum reflectance of 59.7±3% at 6 minutes

A comparison between the surface reflectance of the electropolished samples at different polishing durations with the unpolished ones is represented in Fig. 4.12. Electropolishing is performed at 60 ºC at a magnetic stirrer rotation of 400 rpm while varying the polishing time between 4 to 10 minutes. The maximum reflectance of 59.7±3% (out of 5 repeated experimentations at the same condition) is observed for 6 minutes of electropolishing, as inferred from Fig. 4.12. The reflectance property of the surface is of great importance for industries that require a radiant surface. Higher the reflectance, the higher the ability to reflect visible, infrared, and ultraviolet light.

4.3.6 Effect of EP on Workpiece Surface Wettability

From the present study, the best EP parameters are 60 ℃ temperature, 400 rpm of magnetic stirrer rotation, and 6 minutes of polishing time, at which experimentation is performed for contact angle analysis. The contact angle is measured by dropping a 2 µL water droplet on the workpiece surface before and after EP, as shown in Fig. 4.13. Five repeated sets of experimentations are performed. An angle of 111.2±0.7º (> 90º) is formed on the surface before EP (Fig. 4.13(a)), which signifies that the surface is hydrophobic. An angle of 68.6±0.5º (<90º) is formed after EP (Fig. 4.13(b)), which indicates that the surface is hydrophilic. Electropolishing reduces surface irregularities and increases the wettability of

the surface. Thus, EP changes the surface contact angle and makes it hydrophilic, which can be used in anti-fogging applications, biomedical, filtration, heat pipes, etc. [46].

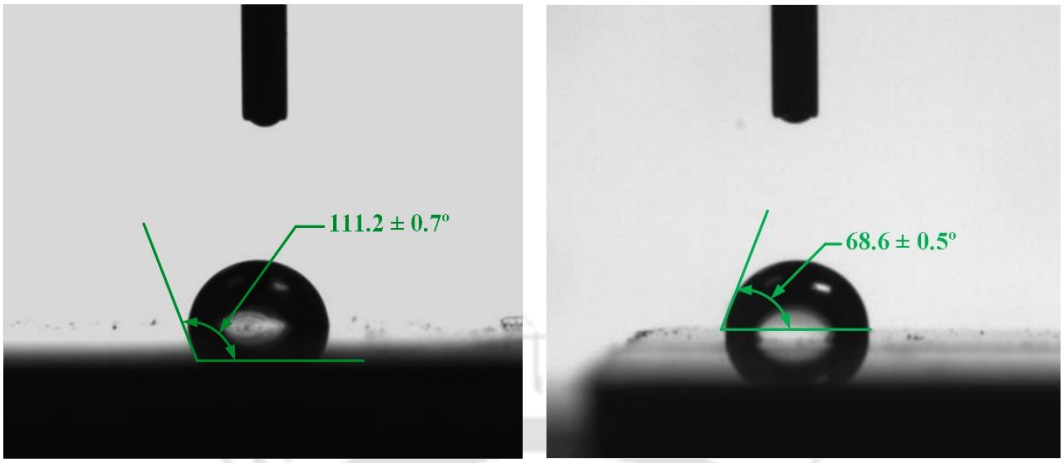

(a) (b)

Fig. 4.13 Measured contact angles (a) before and (b) after EP

4.3.7 XPS Analysis of Maraging Steel

The surface elemental compositions of maraging steel before and after EP is studied with the help of XPS analysis, and the same is shown in Fig. 4.14. The surface scan is performed between 0–1200 eV with a step size of 1 eV. The surface consists of all the elements before and after EP. The peaks are matched with the results available in the literature [111].

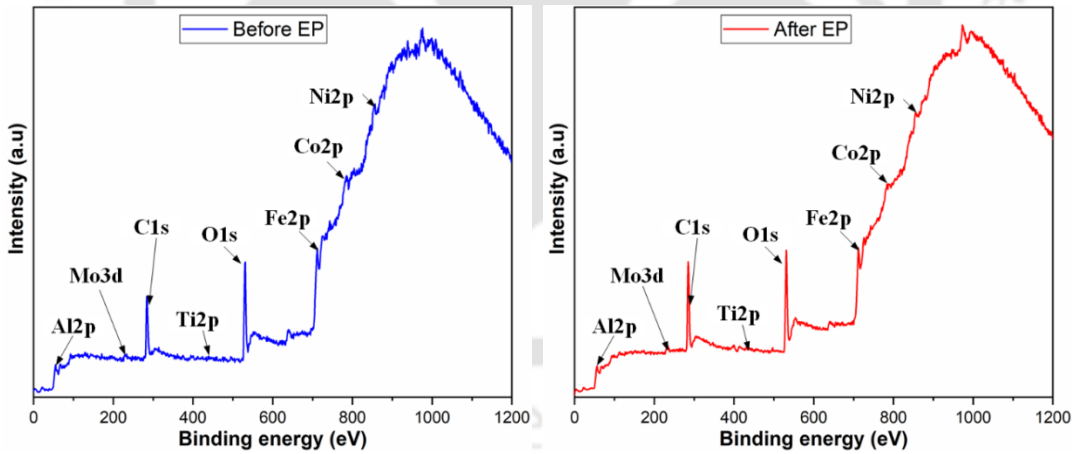

(a) (b)

Fig. 4.14 XPS spectra of maraging steel (a) before and (b) after EP

Table 4.4 shows the elemental compositions of maraging steel obtained from the XPS spectra. It is noted that the oxygen O 1s is the dominant element on both surfaces (both before and after EP) due to the passive oxide film present on the surface. From XPS analysis, it has been found that the percentage of the O 1s element on the maraging steel surface is increased to 37.66% after electropolishing from its initial value of 29.3% (before

electropolishing), which signifies that a thicker passive layer is formed after electropolishing. A similar observation was also found in the literature [108].

Table 4.4 Elemental compositions of maraging steel from XPS spectra

Elements	Before EP		After EP	
	Binding energy (eV)	Atomic %	Binding energy (eV)	Atomic %
Fe2p	711.03	3.21	710.19	5.09
Al2p	70.28	0.37	74.09	0.7
Co2p	782.02	1.2	782.87	1.62
Mo3d	232.86	0.49	228.6	0.52
Ni2p	854.42	1.33	852.75	2.73
O1s	531.23	29.3	530.65	37.66
Ti2p	456.06	0.42	459.29	0.55
C1s	284.28	63.67	284.62	51.12

The major elements that participate in the passive layer formation are iron and nickel. The high-resolution spectra of (i) iron, (ii) nickel, and (iii) oxygen (a) before and (b) after EP are presented in Fig. 4.15 to analyze the surface composition.

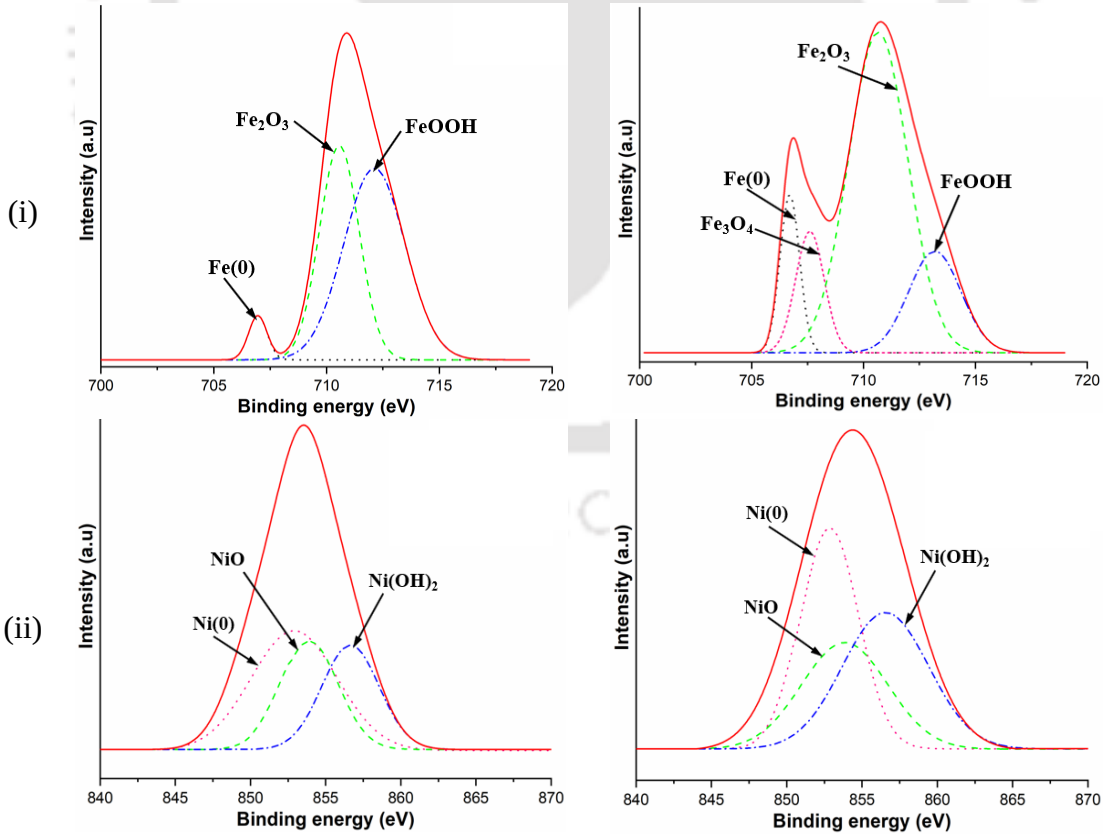

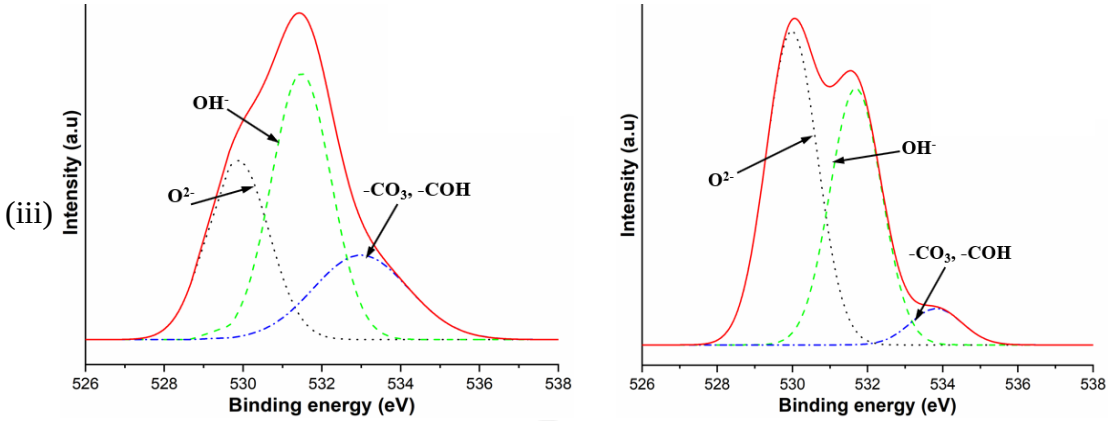

Fig. 4.15 High-resolution spectra of (i) Iron, (ii) Nickel, and (iii) Oxygen elements (a) before and (b) after EP

The high-resolution spectra of iron consist of three and four peaks before and after EP, respectively, as shown in Fig. 4.15i (a) & (b). However, the peak of Fe(0) and Fe_2O_3 has been increased after EP with a new peak of Fe_3O_4. Similar results were obtained by Han and Fang [108]. The high-resolution spectra of nickel before and after EP are shown in Fig. 4.15ii (a) & (b), respectively, with the major compositions of Ni(0), NiO, and $Ni(OH)_2$. After EP, all the major compositions are increased, which signifies a thicker passive layer. The high-resolution spectra of oxygen before and after EP are shown in Fig. 4.15iii (a) and (b), respectively with the major compositions of O^{2-} and OH^-. However, after EP, the composition of O^{2-} and OH^- increases, leading to the generation of metal oxides/hydroxides [63]. The newly formed oxide layer increases the corrosion resistance after EP.

4.3.8 Effect of EP on Corrosion Behaviour

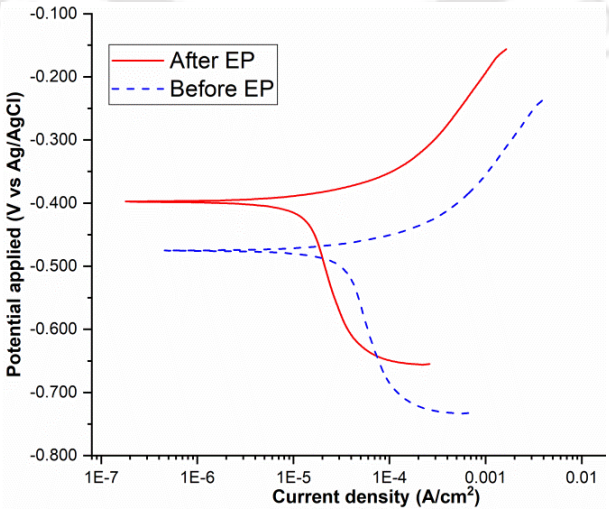

Fig. 4.16 Tafel polarization curve before and after EP

The corrosion resistance of the maraging steel is an essential parameter for practical application. Potentiodynamic polarization curves measure the corrosion resistance of maraging steel before and after EP with 3.5 wt.% NaCl solution [105]. As shown in Fig. 4.16, a higher value of corrosion potential of maraging steel is observed after EP. However, corrosion current density of maraging steel decreases from 16.5 µA/cm^2 to 6.84 µA/cm^2 after EP (Table 4.5), indicating higher corrosion resistance of electropolished maraging steel. Higher E_{corr} and lower I_{corr} values increase corrosion resistance [108], [112].

Table 4.5 Potentiodynamic corrosion test results

Conditions	**E_{corr} (V vs. Ag/AgCl)**	**I_{corr} (µA/cm^2)**
Before EP	-0.475	16.5
After EP	-0.397	6.84

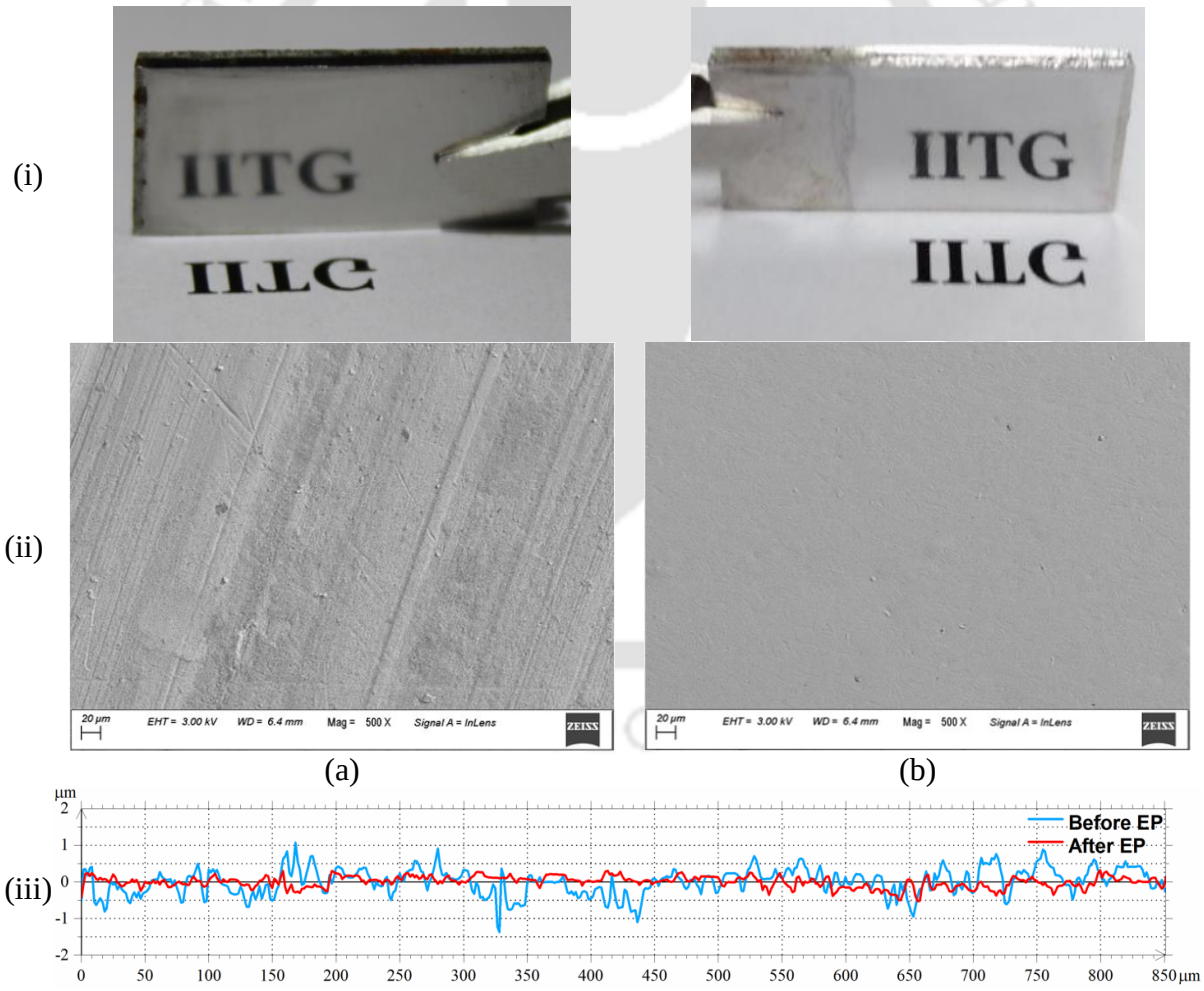

Fig. 4.17 (i) Surface reflectance, (ii) Surface morphology (a) before and (b) after EP; (iii) 2D surface roughness profiles

Surface reflectivity (Fig. 4.17(i)), surface morphology (Fig. 4.17(ii)) and corresponding 2D surface profiles (Fig. 4.17(iii)) are shown (a) before and (b) after EP. EP is performed at 6V, 60 ºC, and 400 rpm for 6 minutes. It can be inferred from Fig. 4.17(i) that the surface reflectance of the workpiece surface improved significantly (b) after EP compared to its (a) initial surface. The surface morphologies of the components are observed through FESEM images, as shown in Fig. 4.17 (ii) (a) before and (b) after EP. It can be inferred that all the surface defects, like scratches, undulation, etc., got removed after EP (Fig. 4.17 (ii) (b)).

To analyze the 2D surface roughness (R_a) profiles before and after EP, both the profiles are plotted in the same graph as shown in Fig. 4.17(iii). Electropolishing has reduced surface irregularities, and the corresponding surface roughness (R_a) value is reduced to 0.119 µm after EP from its initial value of 0.272 µm.

4.4 Summary

Maraging steel 300 is widely used in aircraft, tools, and automotive industries, which requires a polished surface for better performance. In conventional polishing methods, the abrasives directly contact the workpiece surface and deteriorate its property. Thus, a nonconventional method such as electropolishing (EP), is utilized to finish maraging steel with acetic acid and perchloric acid mixed in the volume of 3:1. Linear sweep voltammetry (LSV) is performed to determine the passive region that gives the best electropolishing performance. Different parameters, namely temperature, agitation, polishing time, and their effect on surface roughness and surface reflectance, are observed during EP. The process parameters, which give the best EP performance, are the temperature at 60 ºC, rotation of the magnetic stirrer at 400 rpm, and polishing time of 6 min. An improvement of 56.25% in surface roughness and 60.3% in surface reflectance from its initial value of 21% is observed. EP makes the surface hydrophilic as the contact angle changes from 111.2º to 68.6º. X-ray photoelectron spectroscopy analysis suggests that after EP, thick passive layer forms on the surface, which helps in increasing corrosion resistance.

Chapter 5 Investigation of EP Performance on Surface Residual Stress

5.1 Introduction

Electrical Discharge Machining (EDM) is a potential non-conventional thermoelectric machining process used to machine intricate shapes or cavities on hard (martensitic) and conductive alloys. One major disadvantage associated with EDM is the generation of tensile residual stress on the machined surface due to rapid cooling. Some adverse thermal effects, such as micro-cracks formation, voids, globules, and other defects due to rapid heating and cooling cycles, have also been associated with EDM, which leads to poor surface morphology. Micro-cracks may form due to tensile residual stress, propagates, and produces transgranular or intergranular fracture during component service under dynamic loading conditions. As a result, post-processing is required to eliminate the tensile residual stress and surface defects formed during EDM.

Electropolishing (EP) is an efficient post-processing technique that removes materials at a micron scale from the workpiece surface. It can also perform stress relaxation and improve the surface quality of ED machined surface without distorting the material's internal structure. This post-treatment process is selected in the current investigation due to its inexpensive setup and polishing medium with various advantages like ease of customization, improved residual stress, improved surface quality without grain distortion, and ability to effectively polish intricate-shaped features compared with other finishing techniques like *Magnetorheological Finishing* (MRF), *Abrasive Flow Finishing* (AFF), and shot peening.

The prime objective of this chapter is to investigate the change of surface residual stress and surface morphology following EP with organic electrolyte on an EDM-machined maraging steel alloy. The recent trend in this process is using eco-friendly organic electrolytes, an aqueous-based solution free from sulfuric acid used for the present investigation. The generated surface residual stress after EDM and after post-processing using EP was measured using "$\sin^2\psi$ method" of *X-ray Diffraction* (XRD). The current research presents a comprehensive surface characteristic such as morphological analysis on EDM and EP machined surfaces using SEM and AFM, compositional analysis using EDS, microstructural /recast layer thickness analysis using optical microscope (OM), and quantitative analysis including surface roughness improvement and thickness of recast layer removal using optical surface profilometer and stylus-based profilometer, respectively.

5.2 Experimental Procedure

The experimental investigation is presented in a flow chart, as shown in Fig. 5.1, explaining the steps from sample preparation to the surface characteristics analysis for EP.

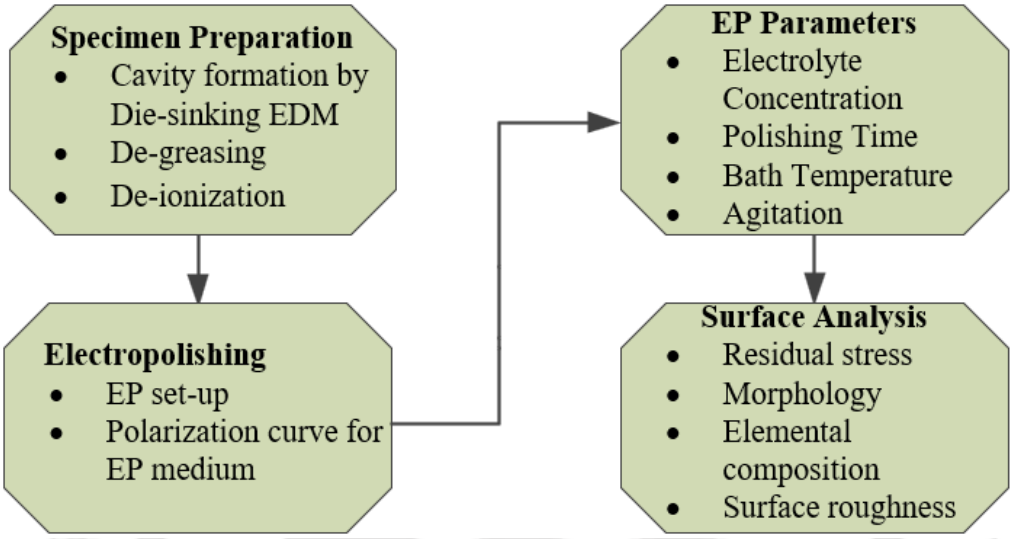

Fig. 5.1 Flow chart of experimental investigation for EP

The specimens are prepared from the maraging steel sheet in the first step. The specimen and the copper tool are used to form a cavity utilizing EDM. The surface of the specimens becomes oily as EDM oil is used as dielectric during EDM. Hence, the specimen surface is further cleaned in an ultrasonic bath after EDM. Before electropolishing, a linear sweep voltammetry test is conducted with the electrolyte on the specimen to determine the polarization curve for finding the polishing zone. After that, EP was performed in which the specimen was connected to the anode, and the graphite sheet was connected to the cathode. Further, a comparative study was conducted between EDM machined and EP polished specimens.

5.3 Materials and Measuring Instruments

The present study utilized maraging steel 300 sheet of dimension 25mm×12mm×2mm. Before machining on EDM, each specimen was ground and annealed (to remove residual stress). The chemical composition of maraging steel 300 was determined using EDS analysis and is presented in Table 5.1. The hardness of the workpiece measured using the Rockwell hardness tester is around 35 HRC having martensitic morphology.

Table 5.1 Elemental composition of Maraging steel 300

Element	Fe	Ni	Co	Mo	O	Ti	Al
Wt.%	68.7	17.2	8.1	4.9	0.4	0.4	0.2

Die-sinking EDM (make: Sparkonix, model: ZNC) was utilized to fabricate the cavity at the maraging steel surface. The pulse on duration can be varied from 0.5 to 1050 µs with a maximum current of 49A. The copper rod is used as the tool electrode, and EDM oil is used as the dielectric fluid during the EDM. The graphite sheet was used as tool material (cathode), and acetic acid and perchloric acid were used as an electrolyte during EP. The magnetic stirrer with a hot plate (make: Tarson) was utilized for providing agitation and maintaining a steady temperature for the electrolytic solution. The surface morphology with elemental composition was analyzed under FESEM equipped with EDS (make: Zeiss, model: Sigma). AFM (make: Oxford, model: Cypher) was also used to support the morphology analysis. For the residual stress analysis, the XRD facility (model: SmartLab, make: Rigaku) with CuK_{α} source of wavelength 1.54 Å, which operates at 45 V and 200 mA, was utilized. The material removed from the surface (i.e., the difference in height between the surfaces after EDM and EP) is measured with the help of a stylus surface profilometer (make: Veeco, model: Dektak150).

5.4 Fabrication of the Cavity by EDM

A cavity was formed on the workpiece by EDM with copper as the tool (Ø=10 mm). The workpiece was connected to the positive terminal and the tool to the negative terminal of the power supply. The schematic setup of EDM is shown in Fig. 5.2(a).

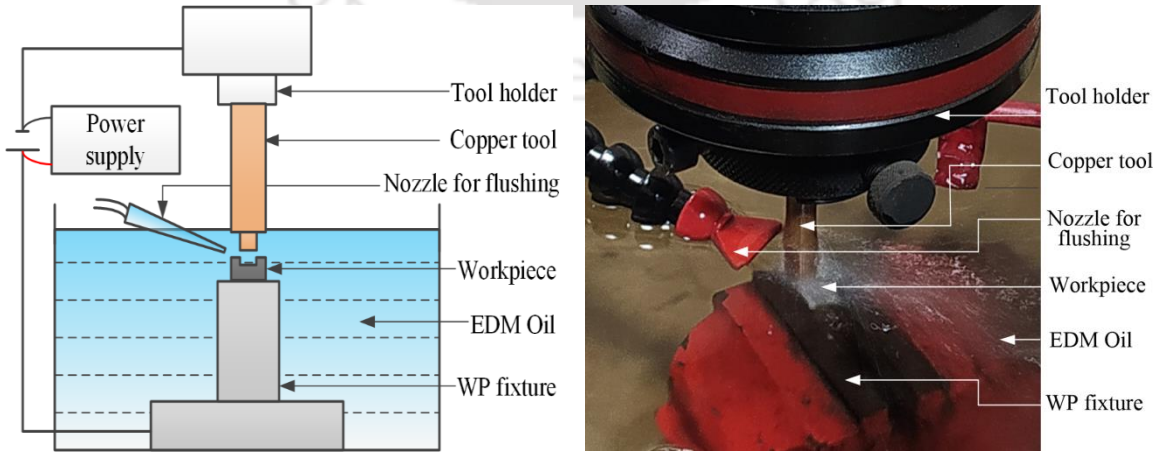

(a) (b)

Fig. 5.2 Setup for EDM (a) schematic and (b) actual

The copper tool was attached to the tool fixture, and the workpiece was held in the workpiece fixture. The machining began once the electrodes were submerged entirely in EDM oil, maintaining the inter-electrode gap (IEG), which aids in generating sparks. The nozzle was also placed in the machining zone to ensure proper debris removal from the IEG and avoid short-circuiting.

5.5 Polishing of the Cavity by EP

The circular cavity fabricated by EDM was electropolished. The setup arrangement is shown in Fig. 5.3. It consists of a container filled with electrolyte in which the workpiece (manufactured by EDM) acts as an anode. The copper tool acts as the cathode and is connected to the power supply's negative terminal. Hydrogen and oxygen gases are liberated during EP at the cathode and anode, respectively. The complete experimental setup was placed over a magnetic stirrer with a hot plate, as shown in Fig. 5.4. The magnetic stir bar is placed at the bottom, and it rotates, which helps to escape gases. The heat was delivered to the electrolyte via the magnetic stirrer with a hot plate during EP to boost its temperature at a constant value, which aids in attaining a superior surface finish [8].

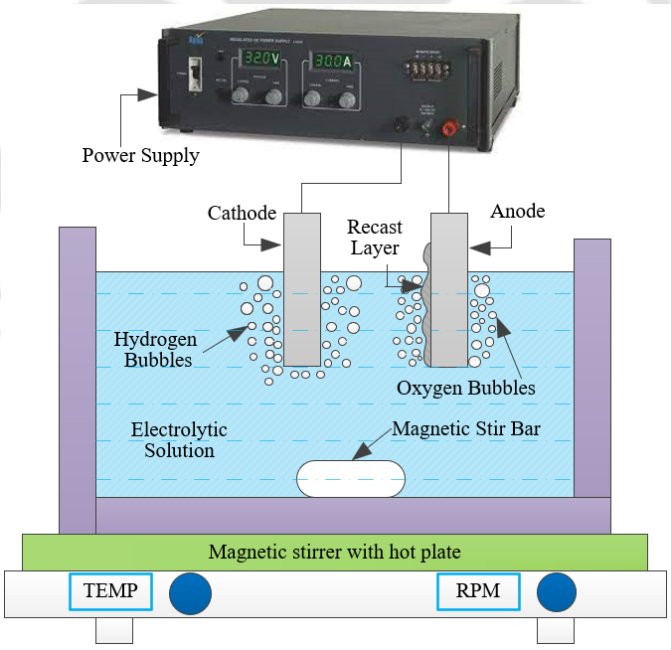

Fig. 5.3 Schematic experimental setup of EP

The die-sinking EDM and EP parameters for the present investigation are presented in Table 5.2. The prime objective of the current work is to get a finished surface with no recast layer. The parameters for EDM were selected such that a cavity can be formed. The EP

parameters are chosen based on preliminary experiments conducted previously on the present experimental setup, which gives the best surface finish without any recast layer [113].

Table 5.2 EDM and EP process parameters

EDM process parameters	**EP process parameters**
Peak current (A): 5 A Pulse on time (machine unit): 203 µs Duty factor (machine unit): 50% Discharge voltage (V): 40 V Dielectric medium: EDM Oil (DEF-92)	Voltage (V): 6 V Polishing time (min): 6 Agitation (rpm): 400 Temperature: 60 ºC Polishing media- Acetic acid: Perchloric acid (volume ratio) = 3:1

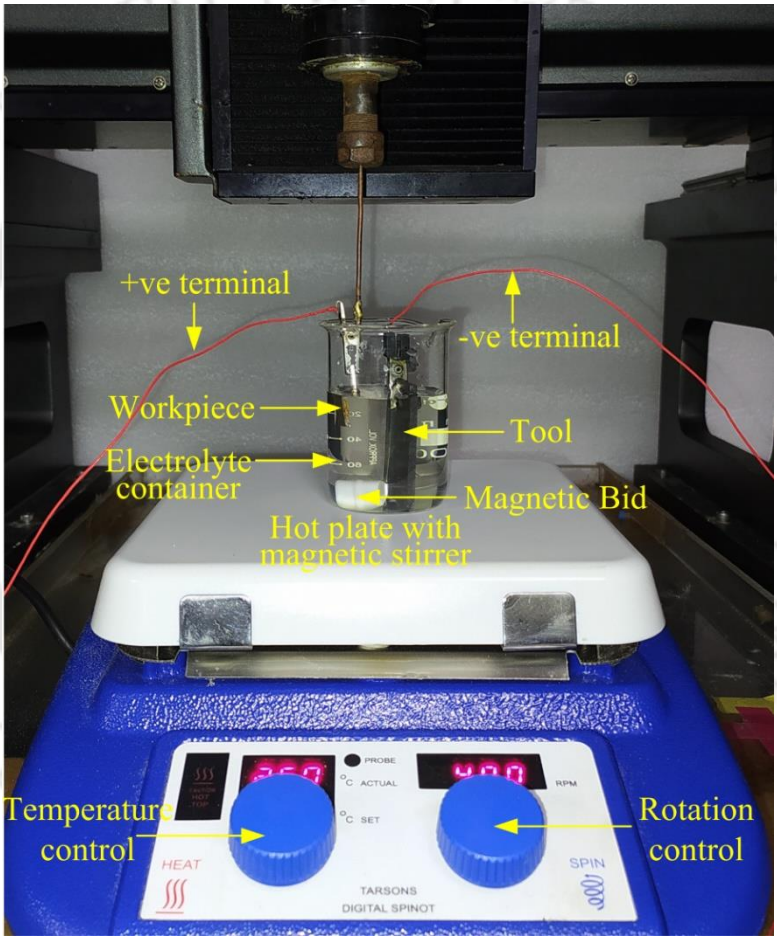

Fig. 5.4 Experimental setup of EP

5.6 Results and Discussion

This section presents the measured surface residual stress and EDM machined surface's morphological changes following EP. In the present study, the "$\sin^2\psi$" method of XRD technique is used to determine the residual stress on the maraging steel after EDM and EP.

The fundamental law of XRD techniques is Bragg's law, presented in Eq. (5.1), and a biaxial stress condition on the cavity surface was postulated using "$\sin^2\psi$" approach.

$$n\lambda = 2d\sin\theta \tag{5.1}$$

Where n denotes the diffraction order (integer), λ denotes the source's wavelength, and θ is the diffraction angle. The d spacing value varies when residual stress is present in the specimen. The strain generated by a change in d spacing is calculated and transformed to a residual stress value using Hooke's law.

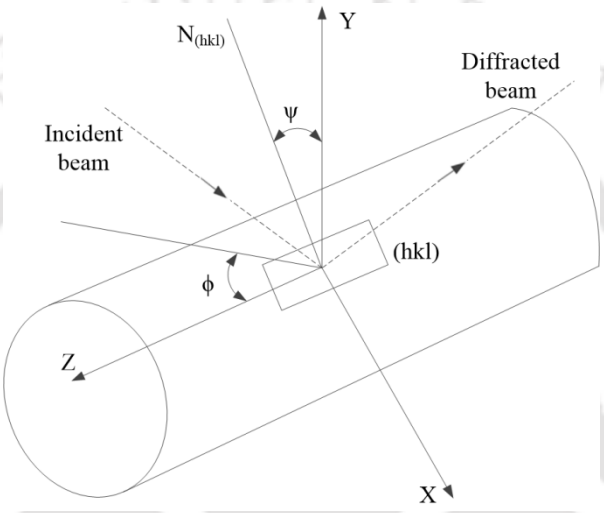

Fig. 5.5 Schematic of XRD setup for measurement of residual stress

The schematic setup of XRD for residual stress measurement for a plane (hkl), sample tilted by ψ and rotated by ϕ, is shown in Fig. 5.5. The workpiece was tilted through different tilt angles (ψ) once the 2θ angle was fixed (keeping 2θ and $\phi = 0$, constant).

Assuming maraging steel as isotropic material and biaxial state of stress, the residual stress was calculated using Eq. (5.2) [114].

$$\in_{\phi\psi} = \frac{d_{\phi\psi} - d_0}{d_0} = \frac{1+\nu}{E}\sigma_\phi \sin^2\psi - \frac{\nu}{E}(\sigma_{11} + \sigma_{22}) \tag{5.2}$$

$$d_{\phi\psi} = \left(\frac{1+\nu}{E}\right)\sigma_\phi d_0 \sin^2\psi - \frac{\nu}{E} d_0(\sigma_1 + \sigma_2) + d_0 \tag{5.3}$$

Where $\in_{\phi\psi}$ measures strain in the direction defined by the angles ϕ and ψ; $d_{\phi\psi}$ is the spacing between the lattice of planes (hkl), slant by ψ and rotated by ϕ; σ_ϕ is the stress in the direction of ϕ; unstressed d spacing is denoted by d_0; E is sample's Young's modulus

(190 GPa); ν is the Poisson's ratio (0.3); σ_1 and σ_2 denotes the biaxial principal stress components. Equation (5.4) determines the plot's slope [115].

$$\frac{\partial d_{\phi\psi}}{\partial \sin^2 \psi} = \left(\frac{1+\nu}{E}\right)\sigma_\phi d_0$$

$$m = \left(\frac{1+\nu}{E}\right)\sigma_\phi d_0 \tag{5.4}$$

$$\sigma_\phi = \frac{m}{d_0}\left(\frac{E}{1+\nu}\right) \tag{5.5}$$

Where m denotes the slope of the curve between d vs. $\sin^2\psi$, d_0 is unstressed d spacing. Equation (5.5) was used to determine the residual stress on the sample's surface. The d spacing determined at $\psi = 0$ was substituted for d_0 as the error is below 0.1% (assumption) of the Poisson's ratio contraction caused by the principal stresses [116].

The present study selected the 2θ range from 40º to 117º. The peaks were analyzed using the *JCPDS* data file. The (hkl) plane (220) was chosen at Bragg's peak angle of 98.7º to calculate the residual stress of maraging steel. The Bragg peak (2θ) was used to calculate d spacing values, and the graph is plotted against $\sin^2\psi$ values to determine the slope. The obtained slope and d spacing values were substituted in Eq. (5.5) to calculate the residual stress.

5.6.1 Surface Residual Stress Analysis

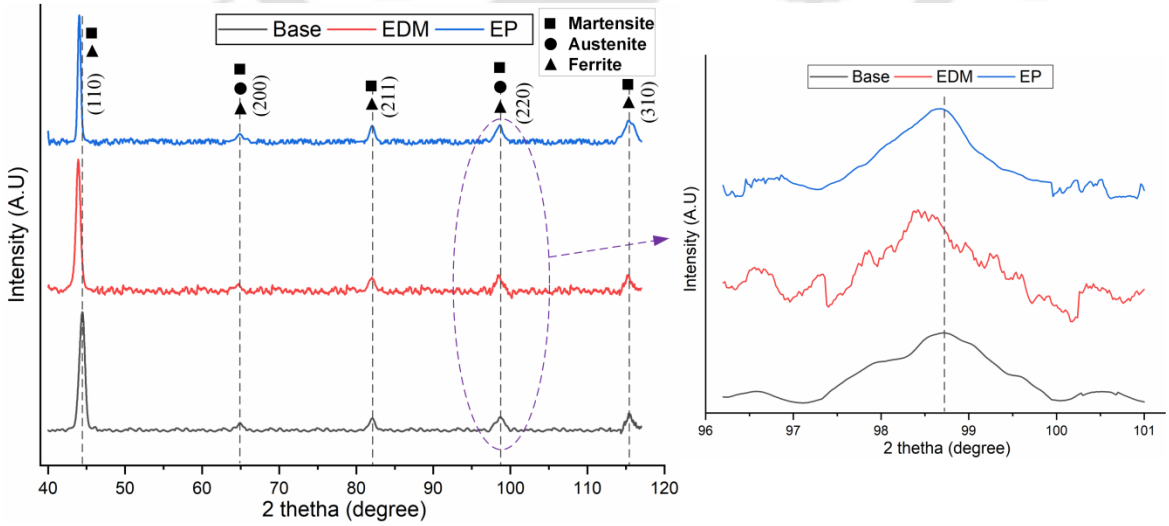

(a) (b)

Fig. 5.6 (a) XRD peaks for base material, after EDM and EP, and (b) shifting of peak at 98.7º

The XRD pattern with peaks after EDM and EP machined surface along with base material are presented in Fig. 5.6(a). The martensite, austenite, and ferrite phases in the ED machined surface have been analyzed qualitatively by matching peaks with reference numbers 44–1293, 31–0619, and 06–0696, respectively [117], [118]. The peak corresponding to a higher 2θ value (i.e., 98.7º) with the hkl plane (220) is selected for residual stress determination using Eq. (5.5). The shifting of peaks at 2θ=98.7º was visualized in Fig. 5.6(b), showing the left shifting of the peak after EDM.

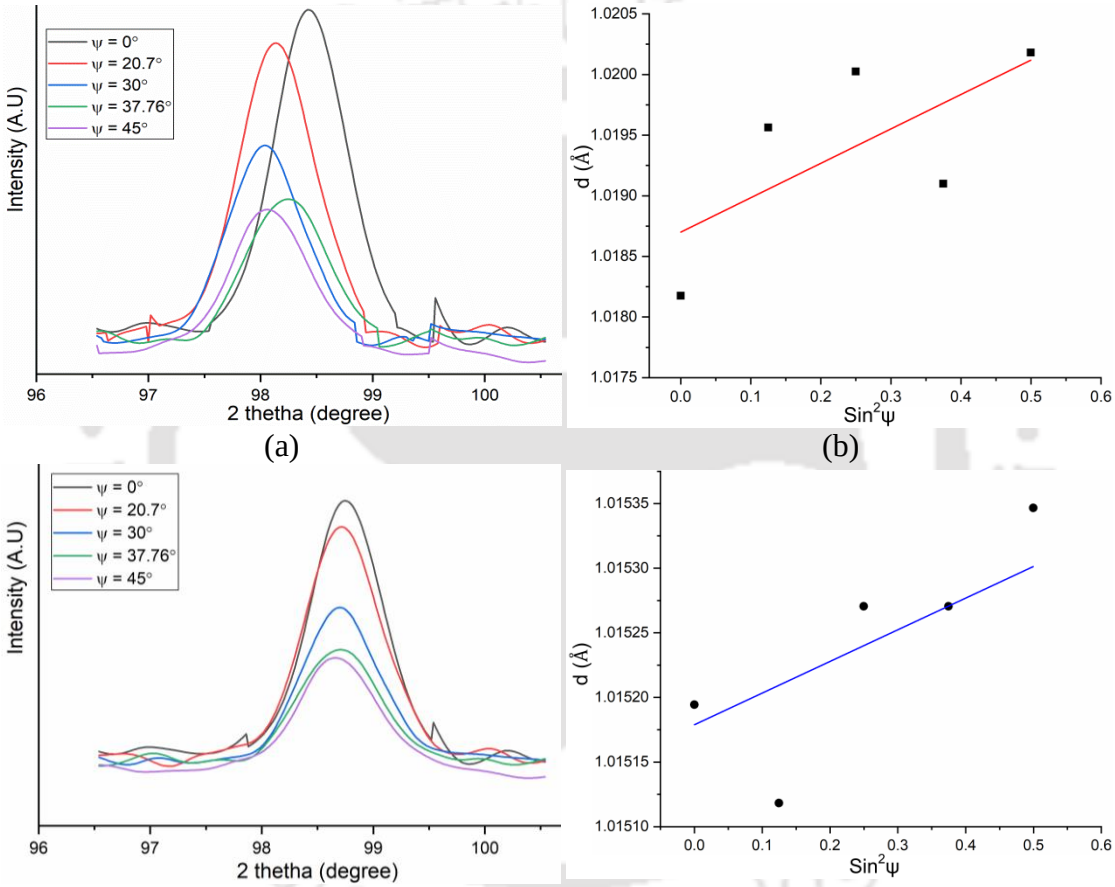

Fig. 5.7 Intensity vs. 2θ graph for plane (220) of maraging steel and d vs. $\sin^2\psi$ linear fitted graph after (a & b) EDM and (c & d) EP

Five different ψ values are selected while keeping 2θ constant and corresponding d-spacing values for all ψ values are determined. The intensity vs. 2θ graph for different ψ values is presented in Fig. 5.7(a) and (c). The d vs. $\sin^2\psi$ values are plotted in Fig. 5.7(b) and (d) to find the slope. These slope values are 0.00284 and 0.000245 for EDM and EP machined surfaces, respectively. The generated residual stresses on the maraging steel surface after EDM and EP are obtained as 407.17 MPa and 35.27 MPa, respectively, after

substituting the slope (m) values on Eq. (5.5). During EDM, tensile residual stress is generated on the white layer due to a steep temperature gradient caused by a rapid thermal cycle, non-homogeneity of heat flow, and metallurgical transformation. The martensitic transformation from austenite occurs when the material cool's down at a particular cooling rate [119] and shrinks because of negative temperature difference, causing tensile residual stress on ED machined surface [78]. This high amount of tensile residual stress may contribute to a surface crack on the white layer, which reduces the components' fatigue life of the components [120]. Electropolishing successfully removed the tensile residual stress on EDM machined surface after 6 min of polishing time and produced a crack-free surface (Fig. 5.8(b)).

5.6.2 Surface Morphology Analysis

The ED machined surface contains several globules, voids, craters, micro-crack, and pockmarks, as shown in Fig. 5.8(a). The high-temperature plasma melts and vaporizes the tiny region of the workpiece through continuous discharges, resulting in crater formation. The machined surface layer undergoes rapid cooling/quenching by the dielectric, resulting in the formation of a white layer and tensile residual stress. In the present study, the induced tensile residual stress (407.17 MPa) on the white layer does not exceed the workpiece's ultimate tensile strength (1034 MPa). A tensile sample was prepared to determine the ultimate tensile strength of the initial annealed workpiece, measured as 1034 MPa. The measured UTS results are almost similar to those obtained by Chakravarthi et al. [121]. However, micro-cracks appear on the white layer (Fig. 5.8(a)), which might be caused by a thermal cycle or a combination of process parameters [122].

The molten material not evacuated during EDM is resolidified after being rapidly cooled by the dielectric, forming globules of debris. Most globules appear to be partly evaporated debris rather than condensed material [123]. Some of the globules are quite small and stuck to the surface, giving them the appearance of pockmarks. The micro-voids are formed due to entrapped gas bubbles expelling during the solidification of molten material. FESEM micrograph of Fig. 5.8(b) reveals that the EP machined surface is free from cracks, voids, globules, and thermal pitting marks generated during EDM.

The 2D and 3D AFM image of the EP surface (Fig. 5.8(c&d)) also confirms the absence of micro-cracks, micro-voids, and pits, as the distinct grain boundary are clearly

visible. It indicates that the surface quality of the maraging steel sample after EP is excellent, and the visibility of the grain boundary is consistent with prior research [124].

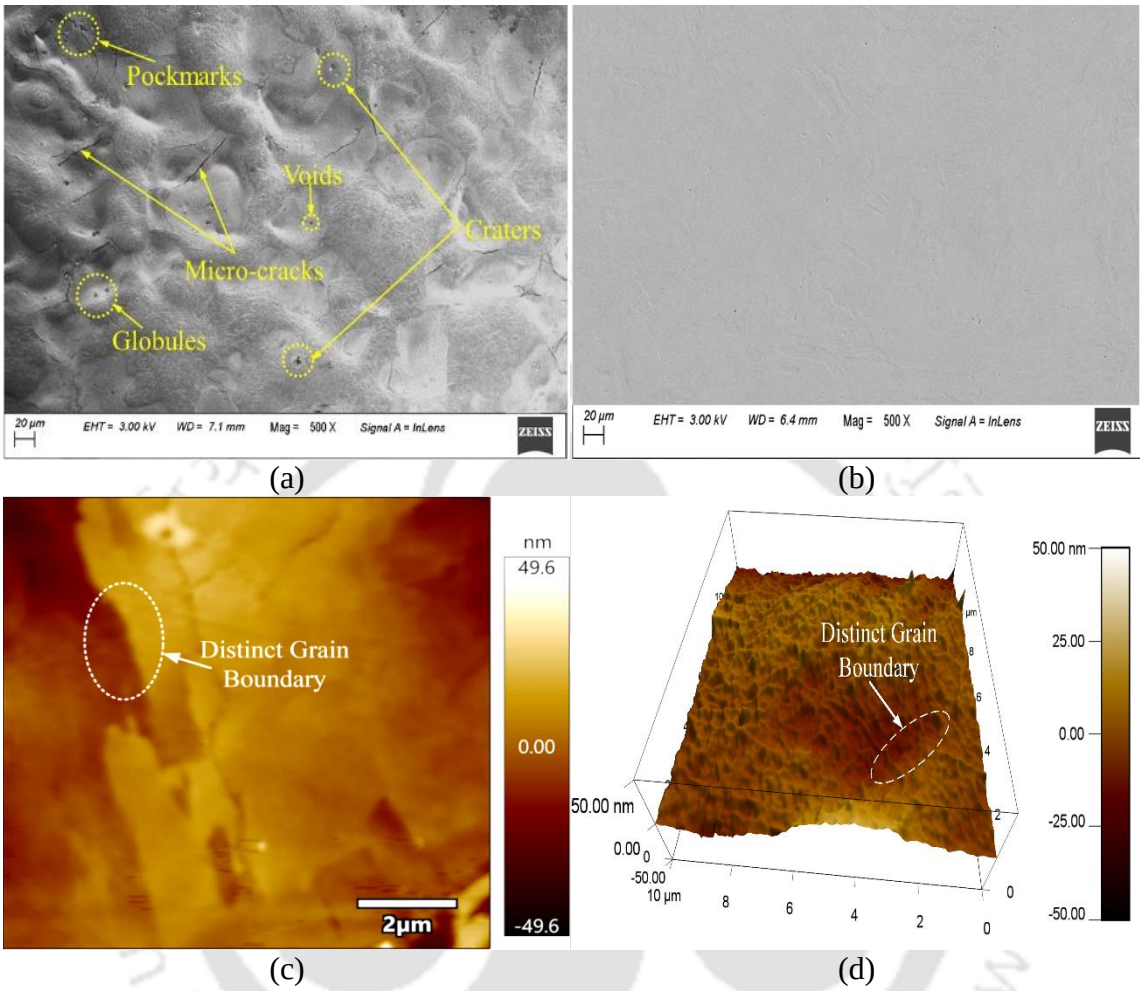

Fig. 5.8 Surface morphology (FESEM images) of (a) EDM and (b) EP surfaces; (c) 2D and (d) 3D AFM images of EP surface

5.6.3 Surface Elemental Composition Analysis

The surface elemental composition measured with EDX is shown in Fig. 5.9. The major constituents of maraging steel are Fe, Ni, Co, and Mo, with slight traces of Ti and Al. During EDM, the copper tool was used to fabricate the cavity. Due to sudden heating and cooling, the copper particles form globules and settle on the surface, and the traces of copper can be seen as shown in Fig. 5.9(a). The surface defects produced during EDM also change the elemental composition and also form carbide on the surface [78], [79]. This makes the surface hard and brittle, a favorable condition for the cracks to propagate.

To remove these surface defects and restore the base material's elemental composition, EP is performed. It can be inferred from Fig. 5.9(b) that all the formed carbides have been

removed along with copper globules. The increased percentage of oxygen signifies the oxide layer formed over the surface. This oxide layer also enhances corrosion resistance [63]. After EP, the surface elemental composition is similar to the base material.

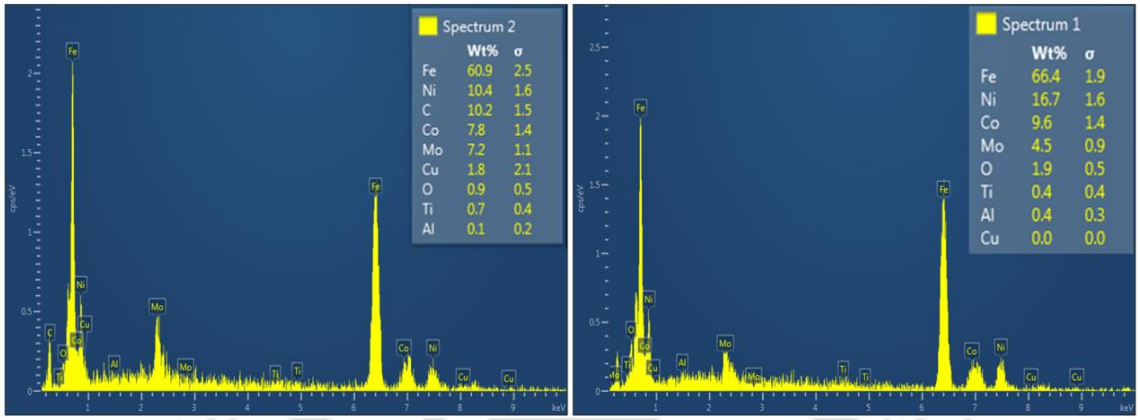

(a) (b)

Fig. 5.9 Maraging steel's elemental compositions after (a) EDM and (b) EP

5.6.4 Recast Layer Thickness Analysis

The maraging steel's microstructure is observed under an optical microscope after etching with modified Fry's reagent [125]. The surface defects on the EDM machined surface (i.e., cross-sectional view) appear as a layer over the surface, which is termed a recast layer (RCL), as shown in Fig. 5.10(a). It can be inferred that the recast layer thickness is not uniform over the surface and varies between 7.55 µm to 3.93 µm. A non-uniform heat-affected zone (HAZ) depth is also observed with the recast layer after EDM. EP is performed to altogether remove the recast layer and heat-affected zone. The recast layer is completely removed after EP; however, a fine layer of the heat-affected zone is still present, as shown in Fig. 5.10(b).

EP is performed on the cavity surface fabricated from EDM. An attempt has been made to measure the thickness of the removed material after EP from the cavity, as shown in Fig. 5.11. Electropolishing is performed on one-half of the cavity surface, i.e., only one-half of the cavity surface is dipped into the electrolyte for conducting EP, as shown in Fig. 5.11(a).

A stylus-based profilometer is utilized to measure the thickness of the layer removed after EP. A white line shows the region where the profilometer stylus has been moved, from unpolished to electropolished. The maximum movement of the stylus was 5000 µm. As shown in Fig. 5.11(b), large undulations have been observed due to the rough surface of the cavity (after EDM). As it reaches the electropolished region, very small undulations of the

stylus have been observed as EP improves the surface finish. An average thickness of 7.94 µm material is removed from the surface, removing all the surface defects.

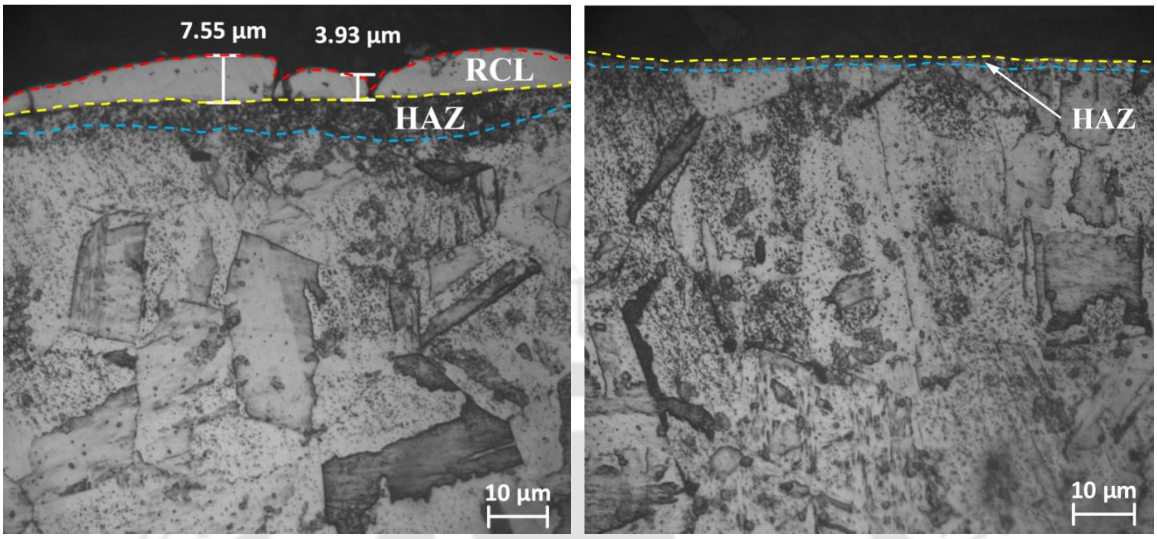

(a) (b)

Fig. 5.10 (a) Recast layer and heat-affected zone (HAZ) after EDM, and (b) no recast layer after EP

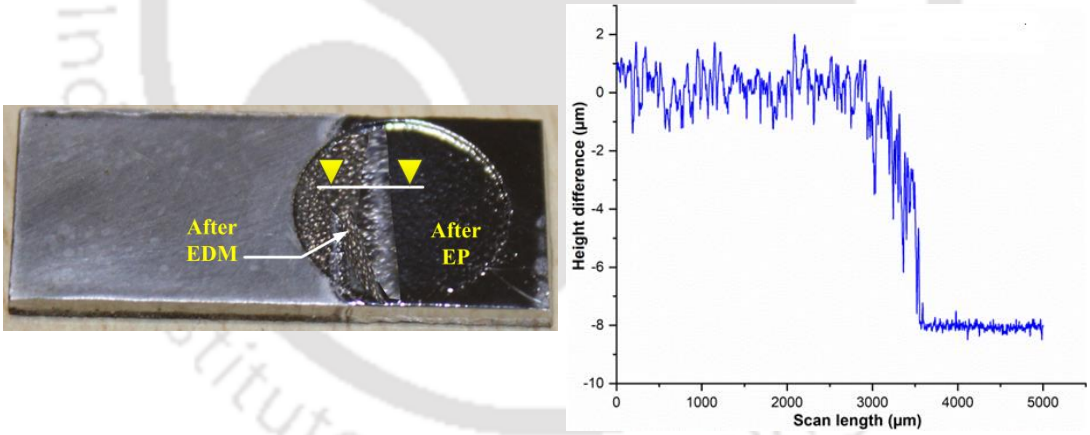

(a) (b)

Fig. 5.11 Thickness removed after EP (a) Optical image and (b) Surface profile measured with a stylus-based profilometer

5.6.5 Surface Roughness/Profile Analysis

The 2D surface roughness profiles of the cavity after EDM and EP are shown in Fig. 5.12. Talysurf non-contact CCI (coherence correlation interferometer) optical profilometer (make: Taylor Hobson), having an ISO 4287:1997 standard, is utilized for the surface roughness measurement. The sampling length for surface roughness measurement is 850 µm. It can be inferred that after EDM, the surface contains a lot of waviness with an average surface

roughness of 1.18 µm. During the cavity fabrication by EDM, the surface comprises many surface defects, resulting in increased surface roughness. Electropolishing has been performed on the EDM machined surface. It has been observed that all the surface defects are removed after EP. After EP, the measured surface roughness is 0.26 µm, with an improvement of about 78% from the EDM machined surface. During EP, a viscous layer forms on the workpiece surface with different dissolution rates for the peaks and valleys of the surface roughness profile. A polishing effect is created, which removes the surface irregularities. An improvement of 60-90% in surface roughness with a different set of parameters on different materials has been achieved by other researchers [46], [126].

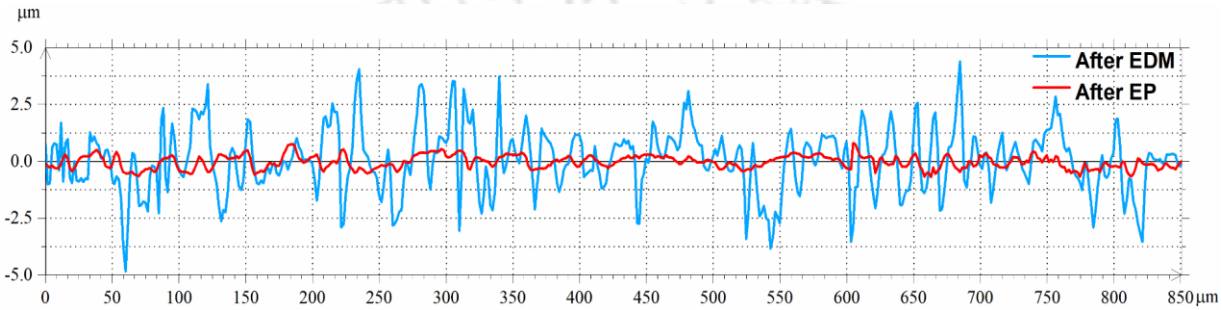

Fig. 5.12 2D surface roughness profiles after EDM and EP

5.7 Summary

In this chapter, the investigation of the electropolishing process on surface residual stress for the cavity fabricated by EDM is performed. After EDM, several surface defects like micro-cracks, globules, voids, craters, and pockmarks are generated. Due to alternate heating and cooling, tensile residual stress is generated and is calculated with the help of the "$\sin^2\psi$ method" of the XRD technique. The tensile stress of 407.17 MPa is generated on the EDM machined surface, which is reduced to 35.27 MPa after EP, all the surface defects are successfully removed, and a highly polished surface is obtained. A non-uniform thickness of the recast layer is formed on the surface after EDM, which is successfully removed after EP. Surface roughness after EDM on the specimen was recorded as 1.18 µm, reduced to 0.26 µm after EP.

Chapter 6 Surface Integrity Analysis of Electropolished Component

6.1 Introduction

Electropolishing is one of the promising post-processing techniques for improving surface integrity in EDM to remove damaged or recast layers utilizing anodic dissolution. This technique is advantageous over other post-treatment processes like mechanical-based processes (i.e., abrasive-based finishing or machining) in terms of enhanced corrosion resistance [127], reduced heat tint and oxide scale, better surface finish, and improved appearance [128]. Therefore, electropolishing is selected as a post-processing technique in the present study. Electropolishing of EDM-machined stainless steel alloy [129] and nickel-based alloys like nitinol [128] are available from a material perspective. The surface integrity improvement of EDM machined maraging steel components utilizing the electropolishing technique is not available in the literature. The present article presents a detailed investigation of EDM machined maraging steel's surface integrity enhancement by EP technique. The current study also focuses on surface integrity analysis, including chemical composition, microstructure, surface morphology and roughness, surface reflectance, crystallite size and lattice strain, surface wettability properties, and tribological properties of die-sinking EDM and EP surfaces.

6.2 Material and Experimental Procedures

This section explains the experimental setups for electrical discharge machining (EDM) and electropolishing (EP). The workpiece and tool material and the process parameters are also discussed. The measuring equipment and its operating parameters are also discussed, along with the steps involved during the experimental investigation.

6.2.1 Experimental Setup

The die-sinking EDM machine (Fig. 6.1) is used in the present investigation. The chemical composition of the Maraging steel 300 workpiece is provided in Table 6.1. The copper rod and the EDM oil (DEF–92) are used as tool and dielectric medium during EDM.

Table 6.1 Chemical composition of Maraging steel 300

Element	Fe	Ni	Co	Mo	O	Ti	Al
Wt.%	68.2	17.8	7.9	5.1	0.4	0.4	0.2

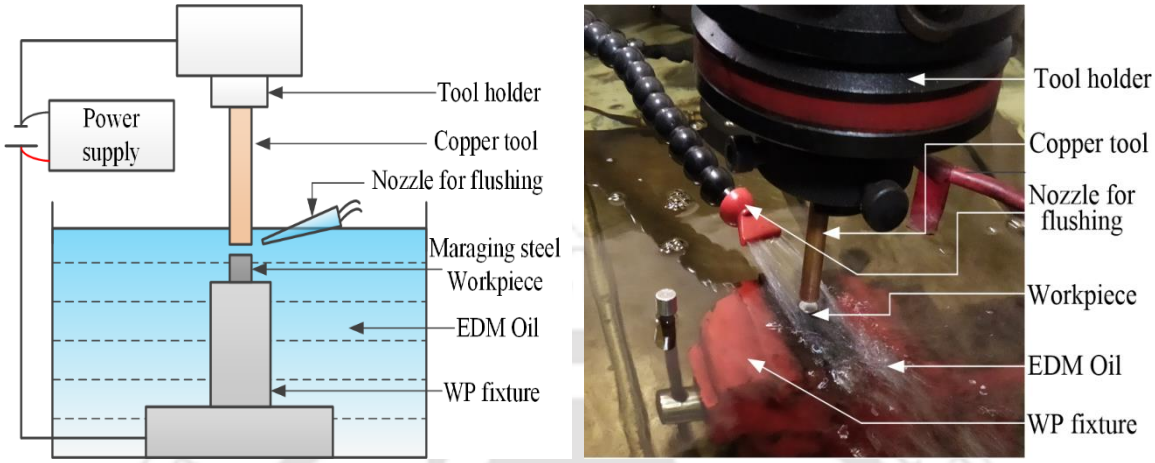

(a) (b)

Fig. 6.1 EDM setup (a) schematic diagram (b) actual photograph

A maraging steel rod of diameter 10 mm is workpiece material for EDM and it is machined using a copper tool (Ø=10 mm). The electrodes are dipped in EDM oil and switched to the terminals of the power supply, shown in Fig. 6.1. The workpiece and the copper tool are attached to the fixtures and the machining starts once the potential difference is applied across the electrodes, generating sparks. The flushing nozzle is placed closed to machining area to remove debris between the IEG while avoiding the short-circuiting condition.

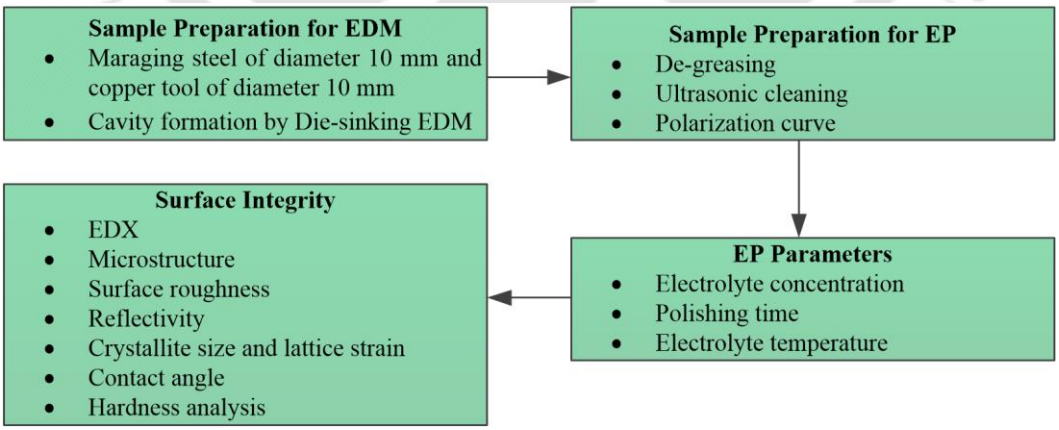

Fig. 6.2 Steps involved in the experimental investigation by EDM and EP

The investigation procedures are presented as a flow chart in Fig. 6.2. After EDM, the next step is the sample preparation. The EDM machined component surface is cleaned using acetone. Further, an ultrasonic bath in deionized water for 15 minutes is performed.

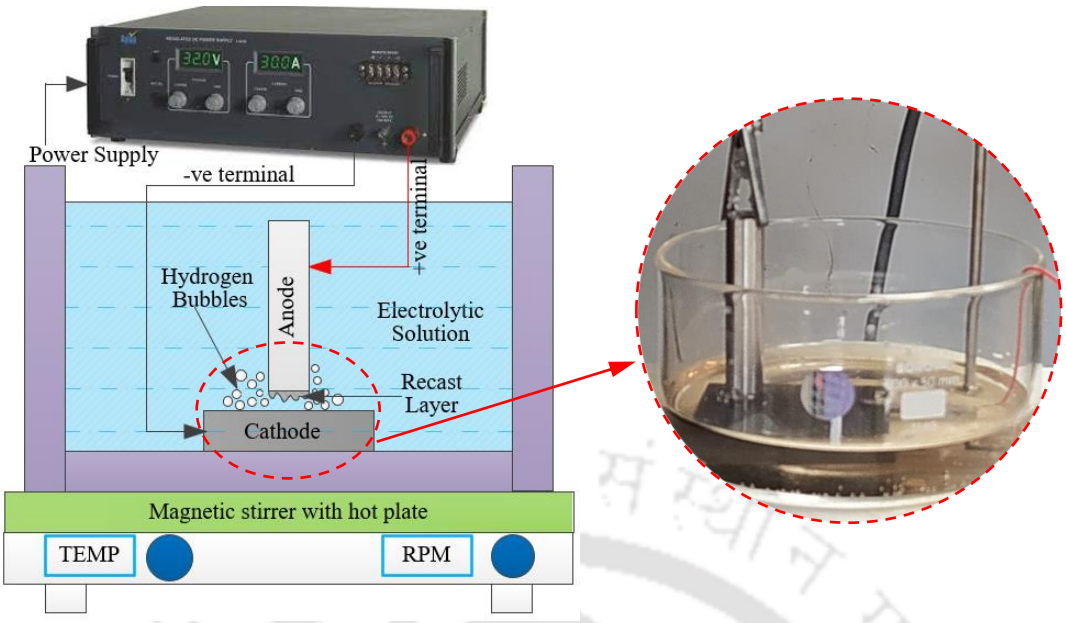

(a) (b)

Fig. 6.3 (a) Schematic of EP setup and (b) magnified view of polishing zone

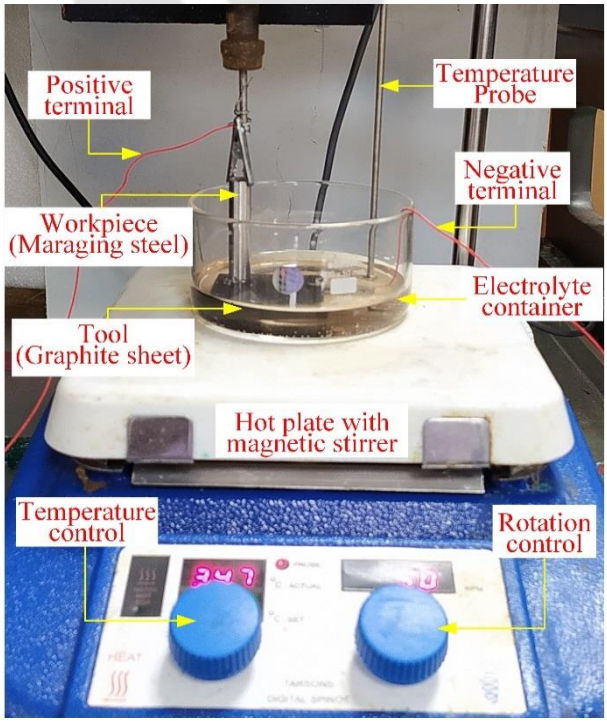

Fig. 6.4 Actual photograph of EP experimental setup

EP setup is indigenously designed and developed. The experimental setup schematic diagram is presented in Fig. 6.3. A 100 ml glass beaker consists of electrolyte is kept over the hot plate with a magnetic stirrer having a maximum temperature and rotational speed of 200 ºC and 2000 rpm, respectively. The negative (cathode) and positive terminal (anode) of the power supply are switched to the tool and workpiece. The maraging steel 300, machined by

die-sinking EDM, further polished by EP. The cathode and anode are dipped inside the electrolyte. The cathode made of a graphite plate of 3 mm thickness is chosen for performing EP as it is inert and does not react with the electrolyte. During EP, hydrogen gas bubbles are created at the tool surface. A power supply (Constant DC) with a specification of 60 V and 20 A is utilized to supply the potential difference between the electrodes. The actual setup for experiment is presented in Fig. 6.4.

6.2.2 Process Parameters for EDM and EP

In the present study, the die-sinking EDM parameters, as presented in Table 6.2, including peak current, pulse duration, duty cycle, and discharge voltage, are selected for the machining of maraging steel [130]. Based on the preliminary experiments, the parameters of EP are chosen [113].

Table 6.2 Process parameters for EDM and EP

EDM	EP
Peak current (A): 5 A Pulse duration (µs): 203 µs Duty cycle (%): 50 Discharge voltage (V): 40 Dielectric fluid: EDM oil (DEF-92)	Voltage applied (V): 6 Polishing time (s): 360 Current density (mA/cm^2): 55 Electrolyte's temperature: 60 ºC Polishing electrolyte: Acetic acid and perchloric acid (Vol. ratio 3:1)

6.2.3 Measuring Equipment and Operating Conditions

After EDM and EP, a detailed investigation of surface integrity is carried out by analyzing the surface morphology, surface roughness, microstructure, phase transformation, and hardness. The microstructure and surface morphology of ED and EP machined surfaces are analyzed using an optical microscope and FESEM. A non-contact type optical profilometer is used to measure the surface roughness of the machined surfaces. An average of three readings at different workpiece positions are considered to achieve high precision of the measured surface roughness. Energy-dispersive X-ray Spectroscopy (EDS) is employed to analyze the elemental composition/chemical composition of base material, EDM-damaged layer, and electropolished workpieces. The phases involved in the base material, ED, and EP machined surfaces are obtained using X-Ray diffraction (XRD) analysis. Hardness analysis is also performed using nanoindentation at the cross-sections of the EDM machined surfaces and EP polished surfaces to evaluate the hardness. The wettability properties are measured using apex instruments. A water drop of 2 µL is utilized to measure the surface's contact

angle. UV spectrometer measures the reflectance of the surfaces. The UV light is varied between 1000 nm to 200 nm, and the relative reflectance is calculated with respect to a polished silver surface having high reflectivity. The tribological performance of the machined surfaces is also evaluated using a pin-on-disc tribometer to determine the wear performance and coefficient of friction.

6.3 Results and Discussion

This section compares the surface integrity analysis of base material, after EDM and EP. The surface integrity analysis includes elemental composition, microstructure, surface morphology and roughness, surface reflectance, crystallite size and lattice strain, surface wettability properties, and tribological properties of die-sinking EDM and EP surfaces.

6.3.1 EDS Analysis

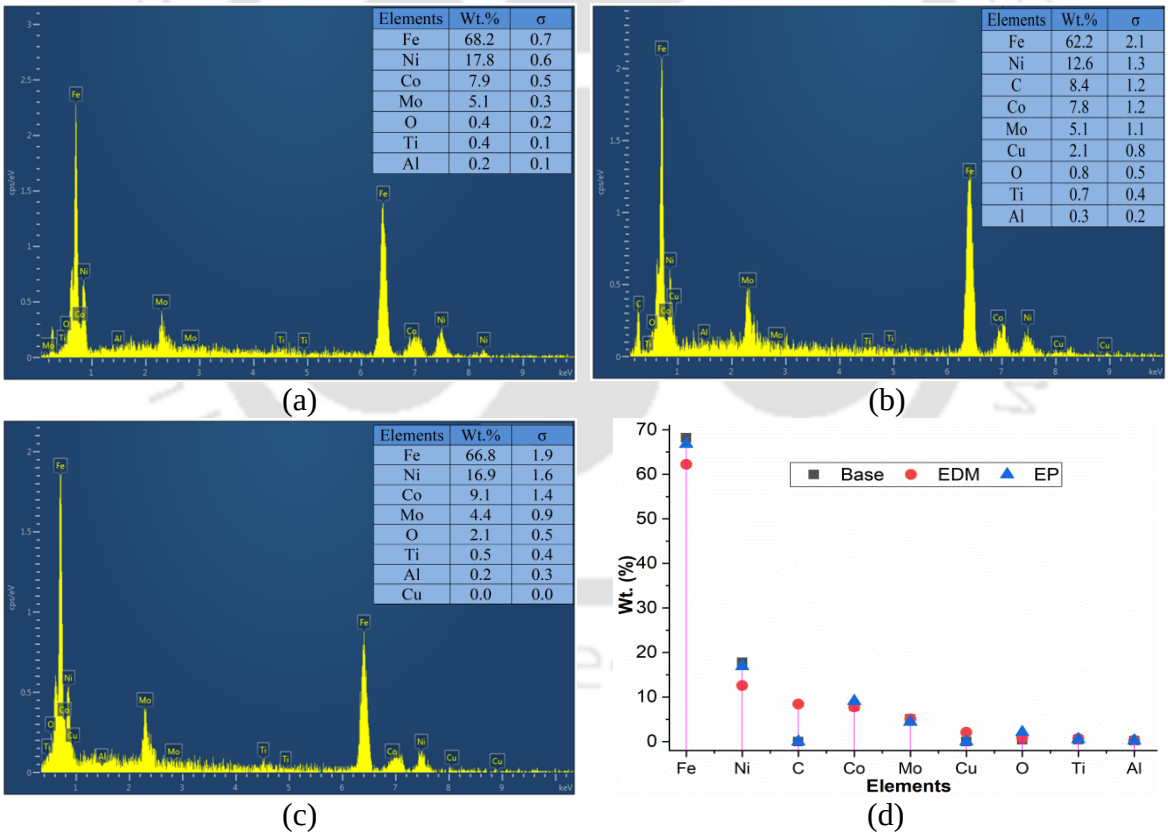

Fig. 6.5 EDS analysis of maraging steel (a) base material, (b) EDM machined (i.e., RCL), and (c) electropolished (EP) surfaces; (d) Drop lines plot showing elemental percentage (Wt. %) of base material, RCL, EP surface

The elemental weight percentage obtained from Energy-Dispersive X-Ray Spectroscopy (EDS) analysis of maraging steel base material, EDM machined (RCL), and EP polished

surfaces are presented in Fig. 6.5. After EDM, there is a change in the surface's elemental composition due to the formation of the RCL (Fig. 6.5). Due to the copper tool's wear during EDM, copper gets deposited over the workpiece surface, which reflects in Fig. 6.5(b). The surface defects induced during EDM, changes the elemental composition and lead to carbide formation. After electropolishing, RCL is wholly removed, and the original base material is obtained with an increased percentage of oxygen content (Fig. 6.5(c)), improving corrosion resistance [52]. Drop lines are plotted in Fig. 6.5(d). The elemental composition in base material changes after EDM. However, the elemental composition resembles the base material after EP.

6.3.2 Microstructural Analysis

A cylindrical maraging steel rod machined by EDM is cut via wire-EDM and cold-mounted to view under the optical microscope. An uneven RCL has been formed over the surface fabricated via EDM, which can be seen after etching with a modified Fry's reagent [102]. It consists of 75 ml of deionized water (DI), 25 ml of hydrochloric acid (36 wt.%), 12.5 ml of nitric acid (68 wt.%), and 0.5 g of copper (II) chloride ($CuCl_2$) is prepared as the etchant.

This RCL has a thickness of up to 13.46 µm, as shown in Fig. 6.6(a). This RCL is hard and brittle, changes the surface integrity of the material, and thus should be removed.

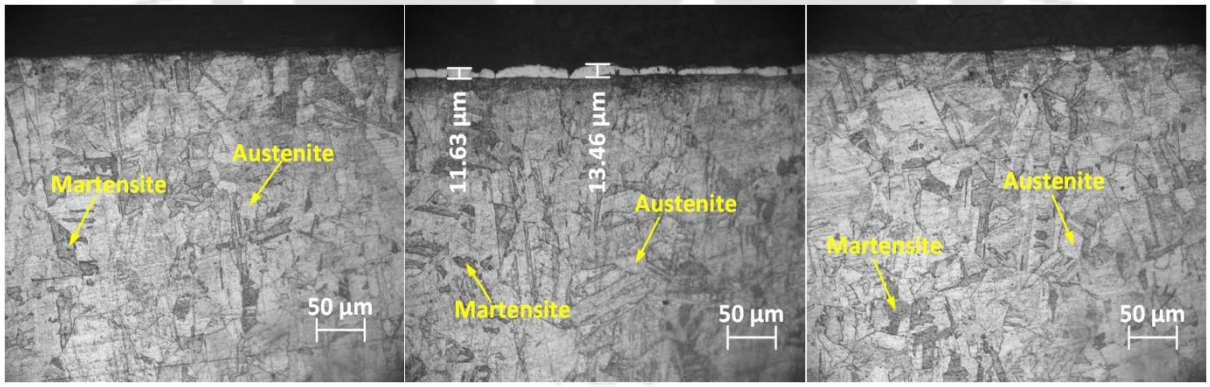

(a) (b) (c)

Fig. 6.6 Microstructure of maraging steel (a) base; after (b) EDM, and (c) EP

An electrolytic solution of acetic acid and perchloric acid, in the volume ratio of 3:1, is used to perform the EP. The sample fabricated by EDM is dipped into the electrolyte along with graphite as the tool. A potential difference of 6 V is applied across the electrodes for 6 mins to perform EP and remove the RCL. EP successfully removes the RCL, as shown in

Fig. 6.6(b), without affecting the microstructure of the base material. Furthermore, the maraging steel consists of austenite and martensite phases, as observed in Fig. 6.6 [113].

6.3.3 Surface Morphology Analysis

Surface morphology of the Maraging steel components is studied after EDM and EP using FESEM, as presented in Fig. 6.7. It has been observed that micro-cracks, voids, and craters are formed on EDM machined surface (Fig. 6.7(a)). The dielectric fluid rapidly quenches the EDM machined surface and produces hard RCL, leading to several surface defects that reduce the components' performance and premature failure. The defects present on the EDM machined surface are eliminated after EP, producing a smooth surface, as presented in Fig. 6.7(b) (at 500X magnification).

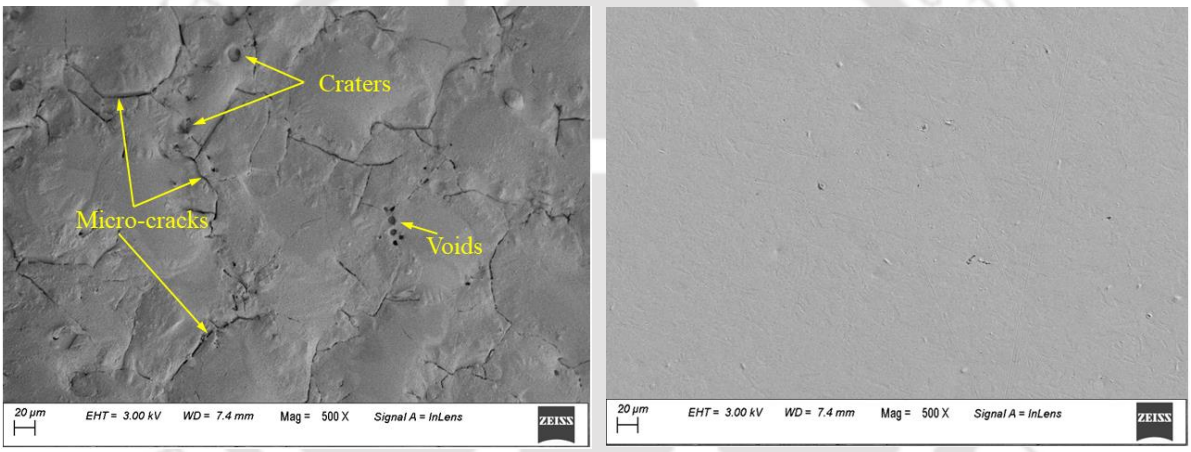

(a) (b)

Fig. 6.7 Surface Morphology of Maraging steel component surface after (a) EDM and (b) EP

6.3.4 Surface Roughness Analysis

Surface roughness, a quantitative measurement of machined surface characteristics, is essential to surface integrity. It can be inferred from Fig. 6.7 that surface after EDM contains several cracks causing surface roughness variation, which are removed after EP. A 2D surface roughness analysis has been presented in Fig. 6.8. Due to micro-defects on the surface after EDM, the 2D surface profile has a lot of variation, and an average surface roughness (R_a) of 1.14±0.05 µm is achieved. The high surface roughness increases wear undesirable for precision applications. The ED machined surface is electropolished to remove all the surface micro-defects, and a bright reflecting surface with average surface roughness (R_a) of 0.18 ±0.04 µm is obtained. An improvement of about 84% in surface roughness is

achieved. To visualize the reflectance after EP, surfaces are analyzed with a UV spectrometer, as presented in the following section.

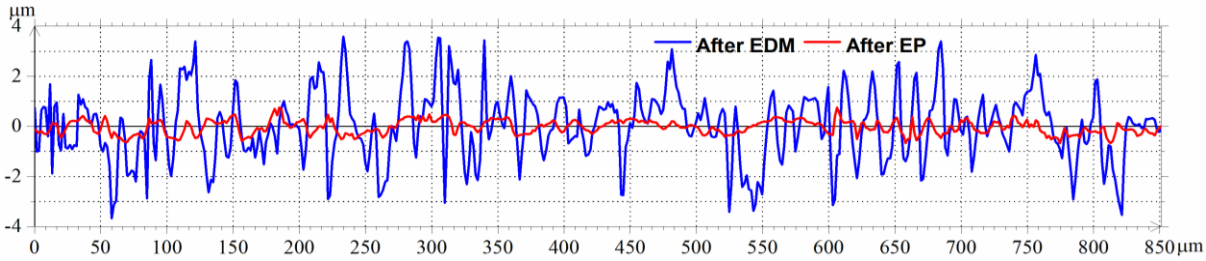

Fig. 6.8 2D surface roughness profiles after EDM and EP

6.3.5 Surface Reflectance Analysis

The UV light is incident on the machined surfaces with a wavelength variation from 1000–200 nm, and the reflectance has been recorded. Initially, a polished silver surface is placed for scanning, and its reflectance data is recorded. Its reflectance is assumed maximum, and its data acts as a reference for reflectivity analysis of the EDM and EP machined surfaces. The reflectance curve along the machined surfaces is shown in Fig. 6.9. The electropolished surface has a reflectance of 77±3%, compared to 13±2% of the EDM surface. As the EDM surface consists of several surface defects and due to diffusion of carbon from the dielectric fluid, the surface becomes blackish and shows negligible reflectivity. However, after EP, all the EDM machined surface defects have been removed, and a polished surface with improved reflectivity is observed.

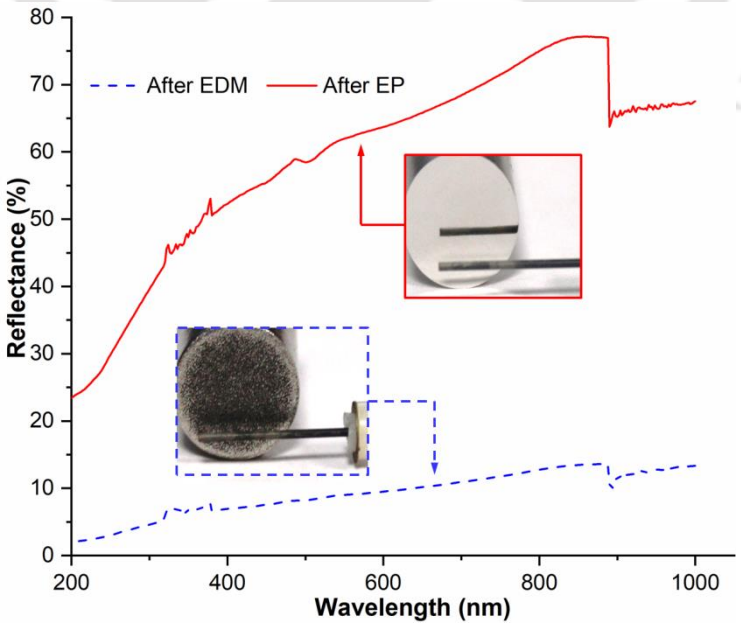

Fig. 6.9 Surface reflectance comparison after EDM and EP

6.3.6 XRD Analysis

6.3.6.1 Phase Analysis

X-Ray diffraction (XRD) analysis has been performed after EDM and EP to find the phases present in the maraging steel. A wavelength of 1.54 Å of Cu-Kα radiation source is employed to obtain Bragg's peaks for the material. Continuous scanning is performed for each specimen by undergoing rotation from 40º to 119º with a scan speed of 3º/min. As maraging steel is martensitic steel, the majority of the phase is martensite with little traces of austenite and ferrite, as observed in Fig. 6.10. The austenite, ferrite, and martensite phases in the maraging steel sample have been qualitatively analyzed by matching the peaks with reference numbers 31-0619, 06-0696, and 44-1293, respectively, from JCPDS data [117], [118].

The peaks are shifted to the left after the EDM process, signifying the formation of tensile residual stress [78]. The generated tensile residual stress on the white layer causes several surface defects and fatigue failure under dynamic loading conditions. Therefore, EP is employed to remove this layer or surface defects as a post-processing technique. The peaks are shifted back and almost match the base material peaks, which signify the stress relaxation after EP. The shifting of peaks indicates a probable elongation in the spacing of crystallographic planes after EDM due to induced tensile stress [79].

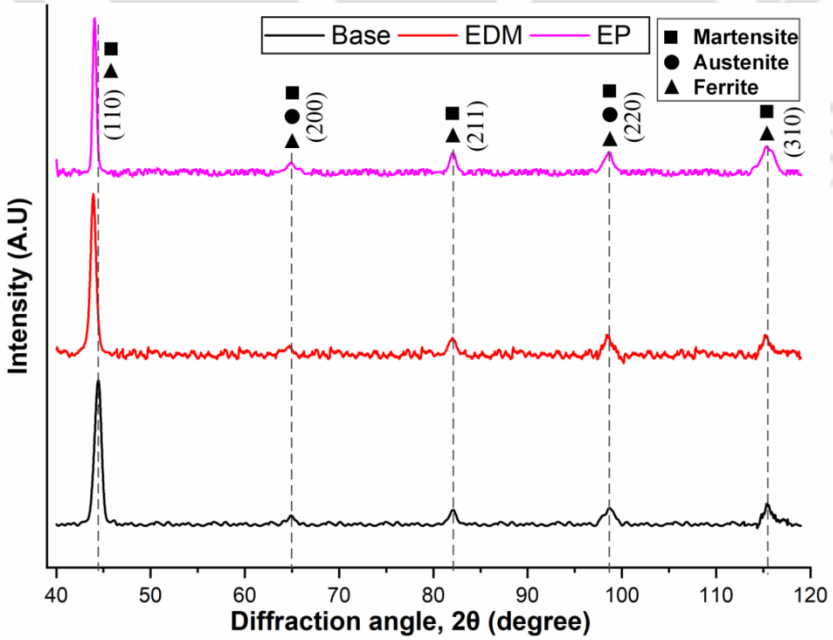

Fig. 6.10 XRD peaks of base material, after EDM and EP

6.3.6.2 Crystallite Size and Lattice Strain

The change in crystal size and the microstrain present on the surface can be explained by the Williamson Hall approach, as presented in Eq. (5.1) [131]. The model assumes the crystal is isotropic in all crystallographic directions with uniform strain.

$$\beta_{hkl}\,\mathrm{Cos}\,\theta_{hkl} = 4\varepsilon\,\mathrm{Sin}\,\theta_{hkl} + \frac{K\lambda}{D} \tag{5.1}$$

In Eq. (5.1), β_{hkl} is full width at half maximum (FWHM) intensity, θ_{hkl} is Bragg's angle, λ is the wavelength of the radiation source (1.54 Å, Cu-Kα), D is the average crystallite size, K is constant as 0.9 (assumed), and ε is the lattice strain in the maraging steel sample. The Bragg's peak angle (2θ) and FWHM (β_{hkl}) of base material, EDM machined, and EP polished workpiece surfaces are presented in Table 6.3.

Table 6.3 XRD data of base material, EDM machined, and EP polished workpiece surface

hkl	Bragg's peak angle (2θ)			FWHM (β_{hkl})		
	Base	EDM	EP	Base	EDM	EP
110	44.41	43.92	44.18	0.715	0.472	0.712
200	64.89	64.52	64.82	0.996	0.985	0.988
211	82.04	81.82	82.01	0.925	0.799	0.914
220	98.66	98.23	98.56	1.211	1.191	1.218
310	115.51	115.31	115.46	1.445	1.596	1.512

The Williamson-Hall equation is linear ($y = mx + c$) in which y, x, m, and c denotes $\beta_{hkl}\,\mathrm{Cos}\,\theta_{hkl}$, $4\mathrm{Sin}\,\theta_{hkl}$, ε, and $K\lambda/D$, respectively. For the calculation of the microstrain and crystallite size, the data is plotted, i.e., $4\mathrm{Sin}\,\theta_{hkl}$ on the x-axis and $\beta_{hkl}\,\mathrm{Cos}\,\theta_{hkl}$ on the y-axis, as shown in Fig. 6.11. The data are linearly fitted to find the slope and intercept, which helps in finding the microstrain (ε) and average crystallite size (D).

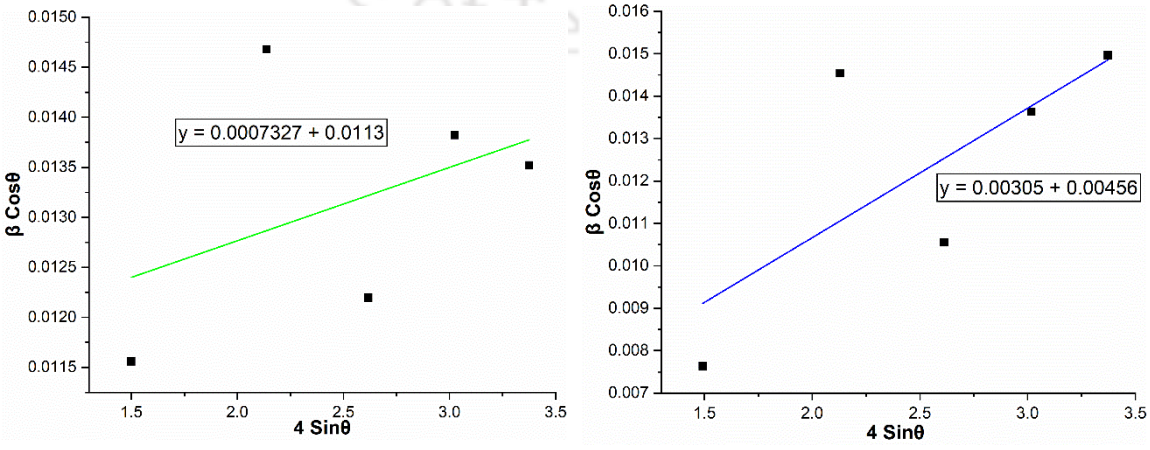

(a) (b)

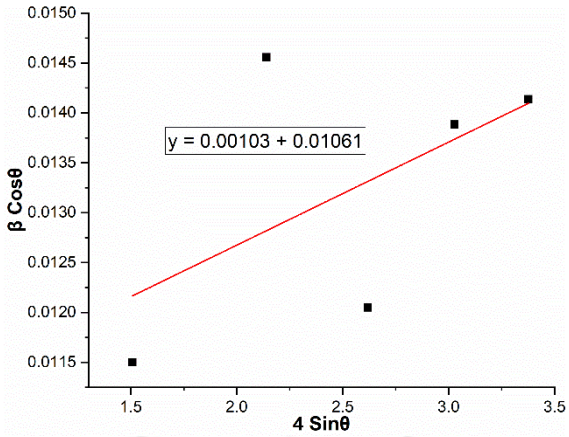

(c)

Fig. 6.11 Williamson-Hall plot for maraging steel (a) Base; (b) after EDM and (c) EP

Table 6.4 presents the average crystallite size and lattice strain using the Williamson-Hall method of base material, EDM machined, and EP polished workpiece surface. As EDM induces tensile stress in the material, average crystallite size and the lattice strain increase to 30.39 nm and 3×10^{-3} (after EDM), from 12.26 nm and 7.3×10^{-4} (base material), respectively, compared to the base material. This indicates a probable increase in the spacing of crystallographic planes due to induced tensile stresses after EDM. The post-processing technique, i.e., EP, removes this RCL, reduces the residual surface stress, and brings average crystallite size and lattice strain close to the base material.

Table 6.4 Average crystallite size and microstrain

Specimen-Maraging steel	Average crystallite size (*D*)	Microstrain (ε)
Base	12.26 nm	7.3×10^{-4}
After EDM	30.39 nm	3×10^{-3}
After EP	13.06 nm	1.03×10^{-3}

6.3.7 Hardness Analysis

Nanoindentation utilizing the Berkovich tip has been used to measure the hardness, as the thickness of the RCL is at the micron level. A comparative hardness analysis of base material, RCL, and EP surfaces is exemplified. A low load of 9 mN is fixed, and the study is performed under displacement control mode. The process begins with a load applied on the surface, and the depth at which it can indent is then analyzed, is presented in Fig. 6.12(a). It is evident that the indentation depth on the RCL surface is approximately 225 nm, lesser than that of the base and electropolished surface. The indentation depths of the base material and electropolished surfaces are ~300 nm and almost coinciding.

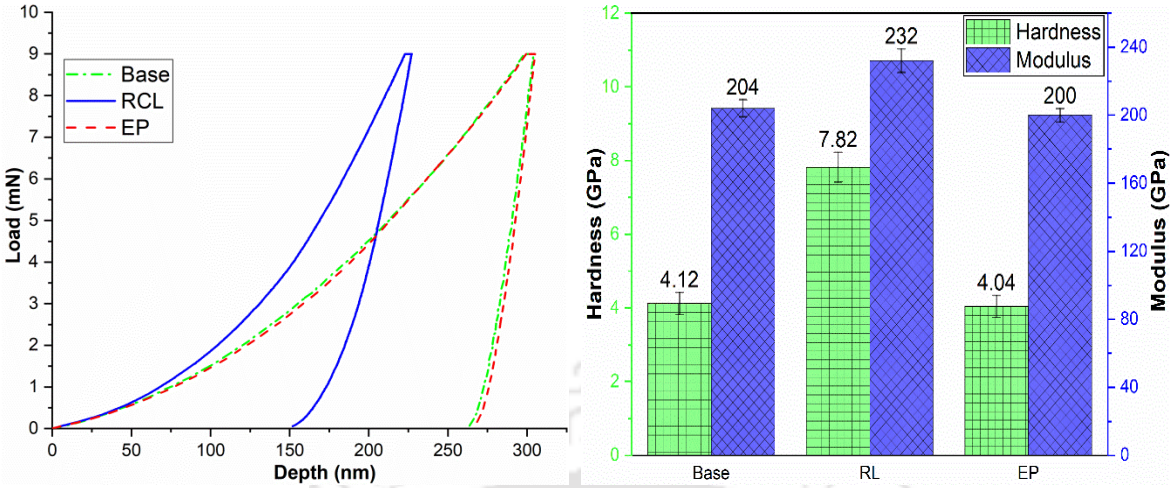

(a) (b)

Fig. 6.12 (a) Load Vs. displacement (b) Hardness and Modulus at base material, EDM machined, and EP polished workpiece surface

The hardness and the elastic modulus data for the base material, RCL, and the electropolished surface are also plotted, as represented in Fig. 6.12(b). Because of the shallower indentation, it may be deduced that the RCL's hardness and Young's modulus (7.82 GPa and 232 GPa) are higher than the base material (4.12 GPa and 204 GPa). As the indentation depth is low, the area of the indent will be small. Thus, as the area of the indent shrinks, hardness rises. Phase transformation takes place during EDM process, which results in the formation of martensite, thereby increases hardness. The hardness and elastic modulus values of the electropolished surface (4.04 GPa and 200 GPa) are almost equivalent to the base material, as EP successfully eradicates the EDM-damaged layer. However, the hardness value of the surface after EP is slightly lesser than the base material, due to the formation of an oxide layer over the surface [63].

6.3.8 Wettability Analysis

The wettability property of the workpiece surfaces has been analyzed by measuring the contact angle. With the help of a goniometer [113], the contact angle is measured by dropping a 2 µL water drop on the base material, EDM machined, and EP polished surfaces, as shown in Fig. 6.13. A contact angle of 77.7±0.3º (<90º) is measured on EDM machined surface, compared to 64.1±0.3º on the base material (Fig. 6.13(b) and (a)), which signifies that the surface is hydrophilic. However, following EP, the contact angle decreases to 56.5±0.4º (Fig. 6.13(c)), indicating that the surface becomes more hydrophilic. It is

advantageous for the food industries to have a hydrophilic surface to avoid the growth of bacteria [46].

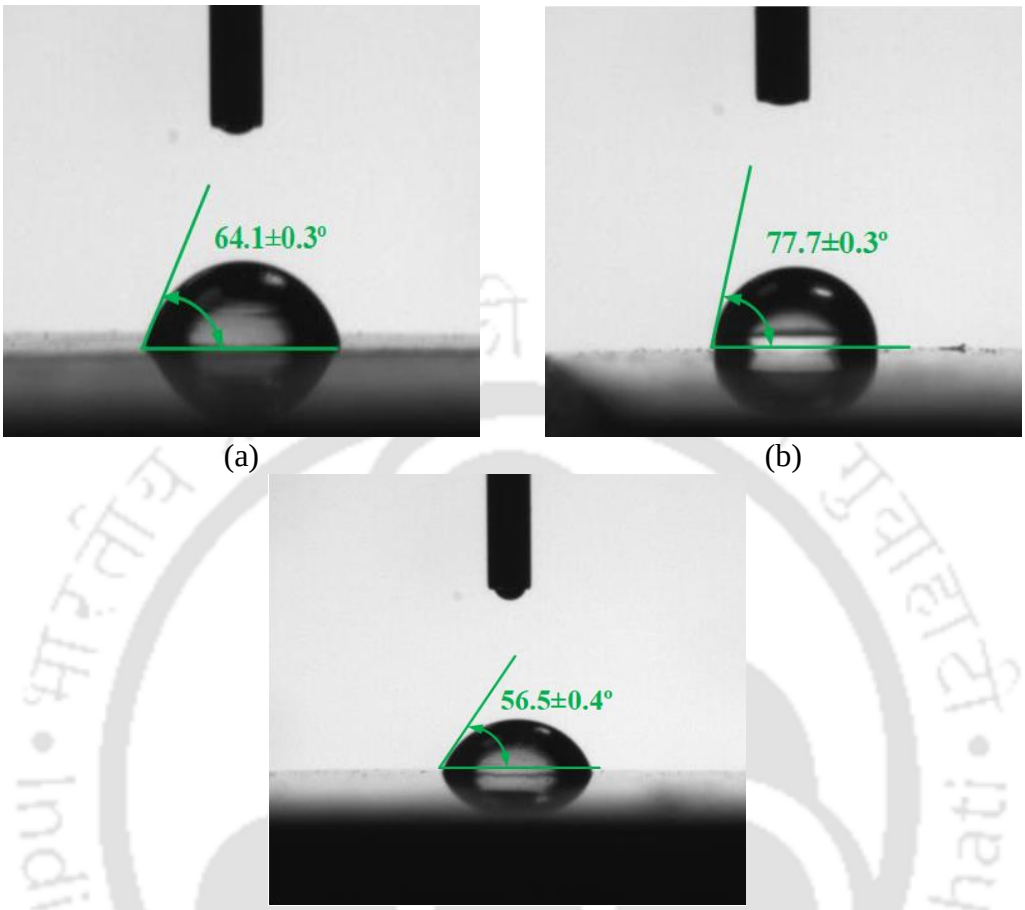

(a) (b)

(c)

Fig. 6.13 Measured contact angle of (a) base material, (b) EDM machined, and (c) EP polished workpiece surface

6.3.9 Tribological Performance

The tribological performance of the metal workpiece plays a vital role in their service life. EP reduces the components' coefficient of friction and enhances service life [85]. With the help of a tribometer (pin on disk), dry sliding friction and wear test are conducted at room temperature. The counter sink disk, made of EN31 steel alloy having a hardness of ~ 60 HRC, is selected for the test. Before the test starts, the sample and the counter disk are cleaned with acetone to remove contamination. The sliding speed (ν) of 2 m/s with a 15N load is applied for 10 mins. The coefficient of friction is calculated by dividing the friction force by the normal force [132].

The tribometer on which the wear test was performed is shown in Fig. 6.14(a). The variation of coefficient of friction with time for base material, EDM machined, and EP polished workpieces are demonstrated in Fig. 6.14(b). The coefficient of friction of the EDM

machined surface is increased to 0.376 from 0.256 of the base material due to the increased surface roughness after EDM. However, surface roughness decreases after EP, reducing the coefficient of friction to a lower value of 0.212.

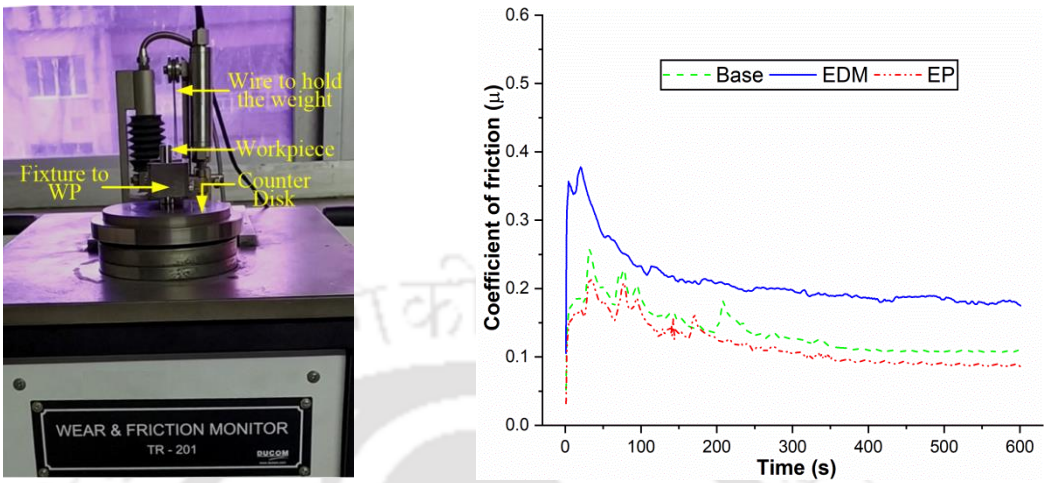

(a) (b)

Fig. 6.14 (a) Tribometer and (b) coefficient of friction for base material, after EDM and EP

After EDM and EP, the workpiece material's wear rate (mm^3/m) is calculated using the relation described in Eqs. (5.2)–(5.4) where k represents the wear rate in mm^3/m. The wear volume (ΔV mm^3) is calculated from the change in mass (ΔW) during the wear test and the density (ρ) of the maraging steel. The sliding distance (s, meter) is covered in 10 minutes. A weighing balance with a precision of 0.001 mg is utilized to measure the mass loss during the wear test, from which wear volume is calculated. Table 6.5 represents the tribological performance of base material, EDM machined, and EP polished maraging steel surface.

$$\Delta V = \frac{\Delta W}{\rho} \ (mm^3) \tag{5.2}$$

$$s = v \times t \ (m) \tag{5.3}$$

$$Wear\ rate\ (k) = \frac{\Delta V}{s} (mm^3 / m) \tag{5.4}$$

Table 6.5 Tribological performance of base material, EDM machined, and EP polished maraging steel workpiece surface

Parameter name	Base material	After EDM	After EP
Maximum value of frictional force (N)	3.85	5.64	3.19
Maximum value of coefficient of friction (μ)	0.256	0.376	0.212
Wear volume, ΔV (mm^3)	0.0645	0.114	0.0486
Wear rate, k (mm^3/m)	5.37×10^{-5}	9.5×10^{-5}	4.05×10^{-5}

The formation of hard and non-uniform layer of recast layer after EDM is the major cause for high wear volume. However, the smooth surface after EP significantly reduces the wear volume.

6.4 Summary

The present study proposes an electropolishing (EP) process to improve the surface integrity of the EDM-machined surface. The surface integrity improvement is demonstrated through the investigation of surface quality, morphology, mechanical properties, including hardness, phases present, crystallite size, physical properties, including reflectance and wettability, and tribological performance, including friction and wear. The surface defects over the EDM machined surfaces are removed, and a minimum surface roughness of 0.18 µm is achieved after electropolishing for 6 mins. Copper from the tool electrode and carbon from hydrocarbon-based EDM oil is deposited on the EDM machined surfaces, as verified from the EDX analysis. Furthermore, average crystallite size increases after EDM, and then it reduces after EP, almost similar to base material, as evident from XRD analysis. The peak shifting and phases present for a crystallographic plane have been observed from the XRD pattern. After EDM, hardness was increased from 4.12 to 7.82 GPa, and the coefficient of friction was increased from 0.256 to 0.376. However, the hardness and coefficient of friction are reduced to 4.04 GPa and 0.212 after EP. Also, increased surface reflectivity and hydrophilicity are achieved after EP. Based on the present findings, the EP process remarkably improved the component's surface integrity, offering a promising hybrid alternative technique.

Chapter 7 Electropolishing of Thin-Cruciform Gimbal Flexure of Gyroscope

7.1 Introduction

Gyroscope finds its application in instruments such as automatic pilots on aircraft and ships, compasses, torpedoes for the steering mechanism, and satellite launch vehicles, ballistic missiles, and orbiting satellites as inertial guidance systems. It also acts as a sensor in determining the orientation, and the most critical part is the gimbal flexure. The shape of the gimbal flexure is cruciform with thin flexure members. The gimbal flexure is generally made of maraging steel 300, providing sufficient strength to the thin flexure during its operation. Maraging steel is martensitic steel which is very difficult to machine via a conventional machining process. It consists of iron-nickel alloys with low-carbon content. It provides a very high strength-to-toughness ratio and high ductility, which is suitable for use in industries such as aircraft, molds, and tools.

In the present study, the cruciform-shaped ~119.75 µm thin gimbal flexure of a gyroscope is fabricated by EDM from maraging steel. EDM is a thermoelectric machining process that induces surface defects like recast layer and micro-cracks and changes the microstructural property. These surface defects deteriorate the performance of the gyroscope. Electropolishing is performed to remove these surface defects. An experimental setup is designed and developed to electropolish the cruciform-shaped thin gimbal flexure fabricated by EDM. An experimental investigation based on the statistical design of experiments (DOE) is performed, and experimental results are analyzed to find the influence of process parameters on surface roughness. With the help of optimum process parameters, further electropolishing experiments are performed. The analysis includes elemental composition, surface morphology, recast layer, and hardness tests on the workpiece surface after EDM and EP.

7.2 Materials and Methods

The cruciform-shaped thin gimbal flexure of the gyroscope is made of maraging steel fabricated by EDM. A rod of maraging steel having a diameter of 10 mm is selected as the base material for the gyroscope. With the help of a wire-cut EDM, its height is reduced to 5 mm. A tungsten copper rod of 10 mm diameter is selected as tool material for the fabrication of a cruciform shape on the maraging steel workpiece via die-sinking EDM. A negative

replica (as required on the workpiece surface) of the cruciform slot has been fabricated on the tungsten copper tool using a wire-cut EDM, as shown in Fig. 7.1. The wire diameter of 120 µm is used to cut the slots, and due to the overcut, the final slot dimension of 190±4 µm is achieved on the tool (Fig. 7.1). The cruciform-shaped thin gimbal flexure of the gyroscope is made of maraging steel. A cylindrical workpiece of 10 mm diameter and 5 mm height is prepared, and further, the cruciform shape is fabricated on it by a precision EDM machine.

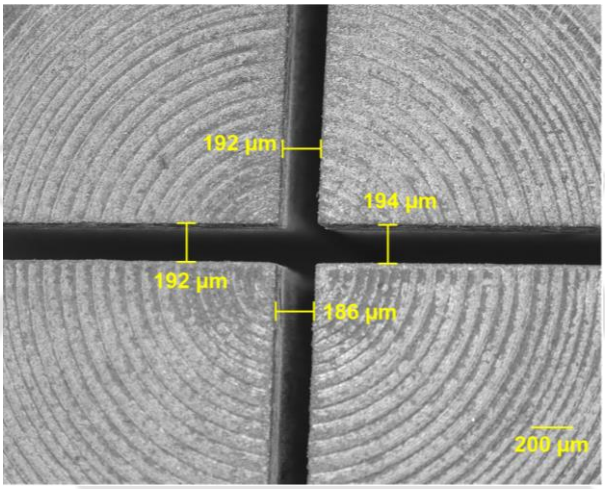

Fig. 7.1 Cruciform slot on tungsten copper tool

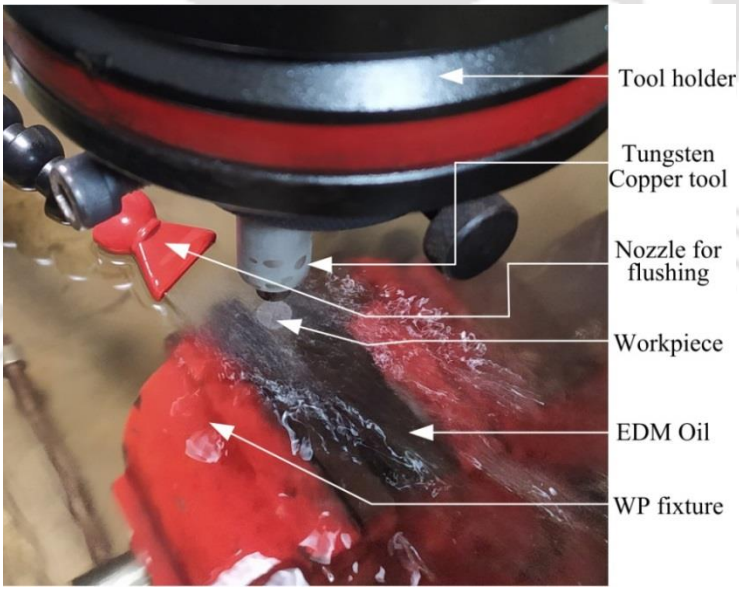

Fig. 7.2 Fabrication of cruciform-shaped thin gimbal flexure by EDM

The experimental setup of EDM for fabricating thin flexures using the tungsten copper tool is shown in Fig. 7.2. The tungsten copper tool works well for the EDM process with less tool wear. The tool fabricated, as shown in Fig. 7.1, is utilized to fabricate the gyroscope's

cruciform-shaped thin gimbal flexure. The EDM process parameters based on preliminary experiments are presented in Table 7.1 to fabricate the cruciform-shaped thin gimbal flexure.

Table 7.1 EDM process parameters

Parameters	**Value**
Peak current	5 A
Duty cycle	50 %
Pulse on time	200 µs
Discharge voltage	40 V
Dielectric medium	EDM Oil (DEF-92)

The cruciform-shaped thin gimbal flexure fabricated by EDM is shown in Fig. 7.3. The average size of the thin gimbal flexure is ~119.75 µm (Fig. 7.3(a)). The recast layers and burrs (Fig. 7.3(b)) are visible on the optical micrographs of EDM machined surfaces of thin gimbal flexure due to the formation of temperature gradient during EDM, damaging the microstructural and mechanical properties of maraging steel, which degrades the performance of the gyroscope.

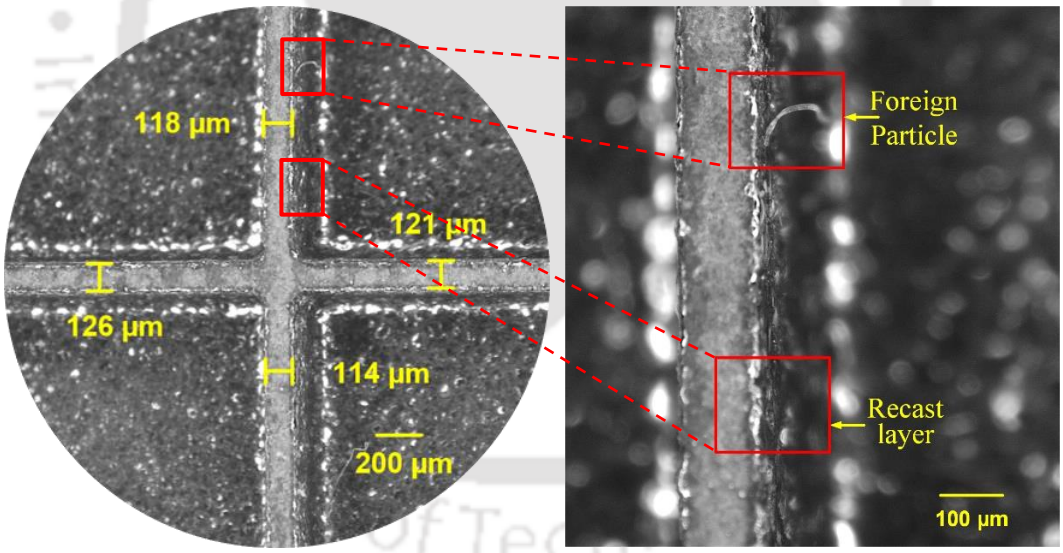

(a) (b)

Fig. 7.3 Optical microscopic views of (a) cruciform-shaped thin gimbal flexure fabricated by EDM and (b) surface defects

For the removal of surface defects after EDM, an indigenous electropolishing setup has been designed and developed to perform the experimentation, and the same has been shown in Fig. 7.4(a). A glass beaker of 100 ml has been considered as the container for electrolytes, in which the workpiece and the tool are dipped. A dedicated fixture has been designed for the gyroscope, as shown in Fig. 7.4(b). The workpiece (maraging steel) is made as an anode that

will undergo electropolishing, and the tool (graphite rod) is made as the cathode. The shape of the graphite tool is similar to the tungsten copper tool fabricated using wire-EDM, as shown in Fig. 7.1. During EP, some gas bubbles are formed in the electrolyte, which slows down the process. These gas bubbles need to be removed from the EP region. A magnetic bid is placed in the electrolyte and rotated to escape the gas bubbles. The EP setup is placed over the hot plate, which has the provision for a magnetic stirrer. It provides heat to the electrolyte to raise its temperature and rotates the magnetic bid. The electrolyte selected for the EP of maraging steel is a mixer of acetic acid and perchloric acid in the volume ratio of 3:1.

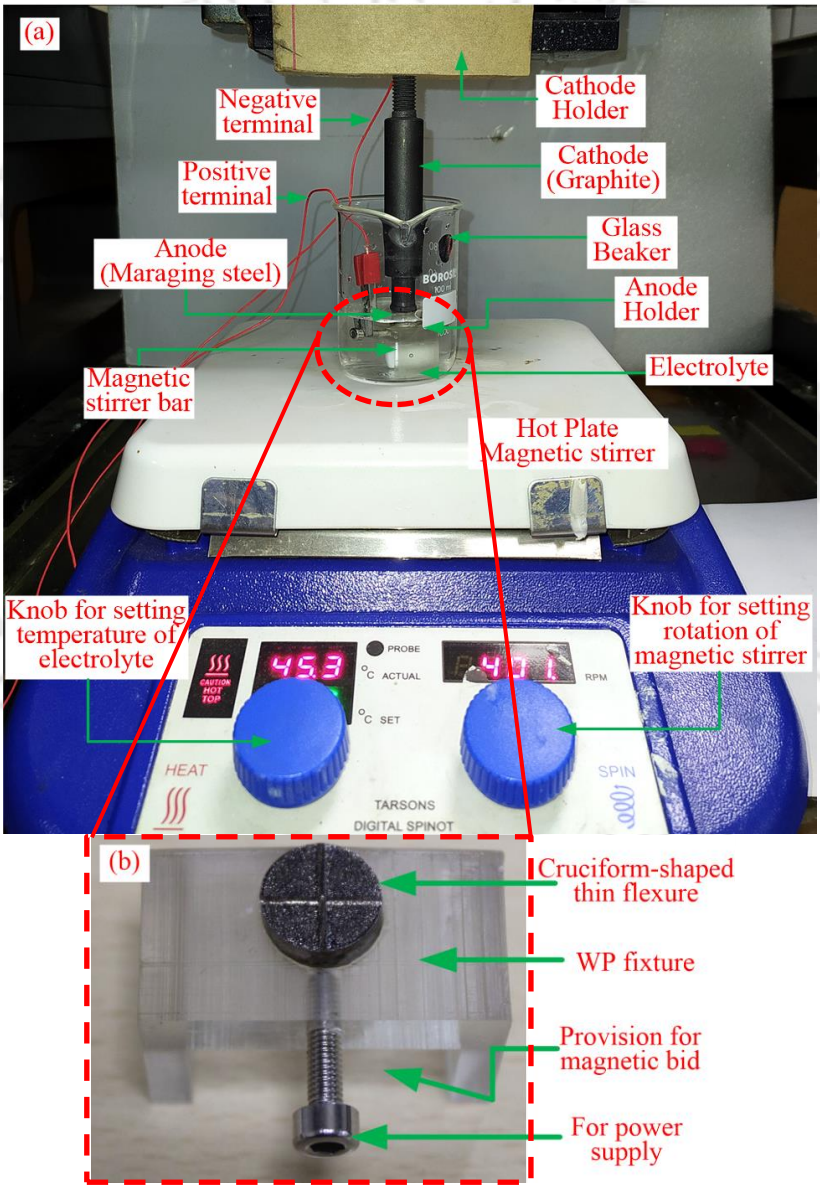

Fig. 7.4 (a) Experimental setup for EP and (b) gyroscope fixture

The process parameters, i.e., electrolyte temperature, agitation of magnetic bid, and polishing time, are selected from trial experiments to investigate their effect on the surface roughness. A statistical design of experiments (DOE) is conducted to analyze the impact of process parameters and their interactions on surface roughness. The process parameters with their levels are presented in Table 7.2.

Table 7.2 Process parameters and 3-level design of DOE

Factor symbol	Process Parameters	Levels		
		-1	**0**	**+1**
A	Temperature (°C)	30	60	90
B	Agitation (rpm)	200	500	800
C	Polishing time (s)	120	300	480
Constant Parameters				
Voltage			6 V	
Electrolyte concentration			Acetic acid: Perchloric acid=3:1	

Table 7.3 3-level factorial design of experiments with output responses

	Process Parameters			Output response
Exp. No.	**Temperature (°C)**	**Agitation (rpm)**	**Polishing time (s)**	**Surface roughness (μm)**
1.	60	500	300	0.107
2.	30	500	120	0.144
3.	90	500	120	0.172
4.	30	200	300	0.123
5.	60	200	120	0.146
6.	90	200	300	0.144
7.	60	500	300	0.118
8.	60	800	480	0.110
9.	30	500	480	0.125
10.	90	800	300	0.138
11.	30	800	300	0.117
12.	60	500	300	0.112
13.	60	800	120	0.131
14.	60	500	300	0.113
15.	60	500	300	0.106
16.	90	500	480	0.144
17.	60	500	300	0.112
18.	60	200	480	0.128

A three-level factorial design based on Box–Behnken RSM technique is carried out to design the experiment (DOE), and the corresponding experimental plan is presented in Table 7.3. In this technique, twelve points corresponding to the midpoints of the edges and six center nodes are considered design points required to fit a polynomial. It includes three levels of input parameters with one output response. The surface roughness (output response) of the

polished samples is measured with the help of the "Talysurf CCI non-contact surface profilometer". The roughness value is measured at the base of gimble flexure.

7.3 Results and Discussion

This section discusses the experiments performed as per the design of experiment (DOE) and the analysis of data. A total of eighteen experiments (Table 7.3) are performed to determine the influence of temperature, agitation, and polishing time on surface roughness. Analysis of Variance (ANOVA) study of surface roughness has been presented with the test for the model to be significant and for the lack-of-fit to be insignificant. The F-value in the ANOVA table shows whether the model obtained is relevant or not. The P-value signifies the confidence level ($\alpha = 0.05$) of the developed model [133]. The regression equation explains the correlation between the input factors (i.e., electrolyte temperature, agitation of magnetic bid, and polishing time) and the output factor (surface roughness). With the help of parameters, which gives the minimum surface roughness after electropolishing, several characteristics such as elemental composition, surface morphology and mechanical behavior were analyzed before and after EP.

Table 7.4 presents the study of ANOVA for surface roughness. The p-value is termed significant (p-value <0.05), the preferred condition for a model. The coefficient of determination (R^2) for the surface roughness is 0.9699. These values suggest that the regression equation explains the correlation between the input factors (i.e., temperature, agitation, and polishing time) with the output factor (i.e., surface roughness). The influence of input parameters on the surface roughness (R_a) results in a quadratic model. The quadratic model suggests the regression equation presented in Eq. (6.1).

$$R_a = 0.228505 - 0.001949A - 0.000024B - 0.000335C + 4.32673\times10^{-21}AB - 4.16667\times10^{-7}AC - 1.38889\times10^{-8}BC + 0.000020A^2 + 9.25926\times10^{-9}B^2 + 5.11831\times10^{-7}C^2 \quad (6.1)$$

Where A, B, and C signify temperature, agitation, and polishing time, respectively, in Eq. (6.1) presented by the model. The comparison between the experimental and predicted (calculated from the regression equation, i.e., Eq. (6.1)) surface roughness values for different experiments is shown in Fig. 7.5. The experimental surface roughness values match very well with the predicted values (Fig. 7.5) with a minimal variation. The model's determination

coefficient (R^2) value for the quadratic model obtained from the regression equation is used to confirm it, as it provides 96.99 % accuracy.

Table 7.4 ANOVA for surface roughness

Source	Sum of Squares	DOF	Mean Square	F-value	p-value	% contribution
Model	0.0052	9	0.0006	28.64	< 0.0001	
A-Temperature	0.0010	1	0.0010	49.02	0.0001*	20.13
B-agitation	0.0003	1	0.0003	12.53	0.0076*	5.14
C-time	0.0009	1	0.0009	45.77	0.0001*	18.79
AB	0.0000	1	0.0000	1.95	0.3460**	0.80
AC	0.0000	1	0.0000	1.95	0.3460**	0.80
BC	2.25×10^{-06}	1	2.25×10^{-06}	0.1114	0.7471**	0.04
A^2	0.0015	1	0.0015	72.61	0.0001*	29.81
B^2	3.030E-06	1	3.030E-06	0.1500	0.7086**	0.06
C^2	0.0012	1	0.0012	59.41	0.0001*	24.39
Residual	0.0002	8	0.0000			
Lack of Fit	0.0001	3	0.0000	1.16	0.4120**	

* Significant (p-value<0.05), ** Not Significant (p-value>0.05), R^2=0.9699

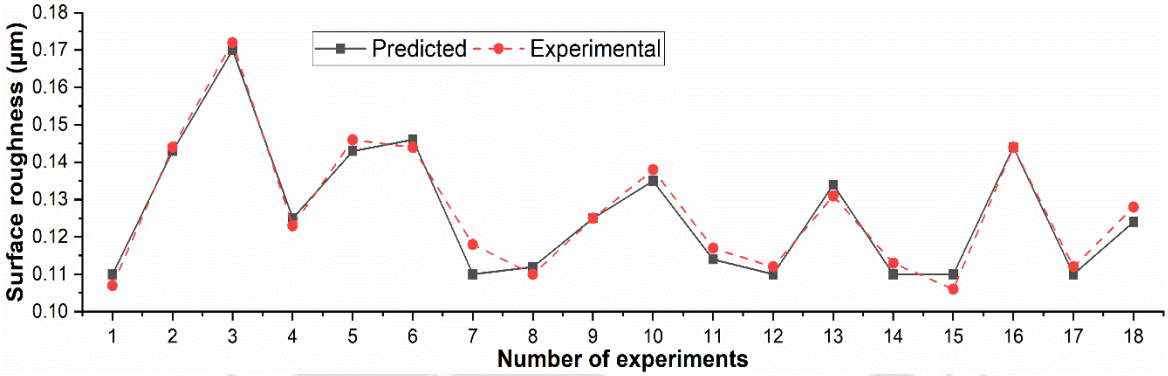

Fig. 7.5 Variation between experimental and predicted values of surface roughness for different experiments

After ANOVA, an optimization study to minimize surface roughness (keeping process parameters in the range) is carried out to determine the optimum combination of process parameters. The optimized process parameter values are 50 ºC temperature, 650 rpm agitation, and 350 sec polishing time, predicting 0.105 µm surface roughness. Three experiments are performed to validate the ANOVA model; Exp. I: at optimum condition, Exps. II and III: parameters are randomly selected within the range (Table 7.2). The experimental surface roughness values are compared with predicted results (calculated from the regression equation (Eq. (6.1)), as shown in Table 7.5. An error of 8.13% (maximum) is

observed from the three validation tests, which suggests the feasibility of the proposed ANOVA model.

The percentage contribution of each input factor (linear and non-linear) on surface roughness with the individual and combined parameters is shown in Fig. 7.6. The combined contribution of temperature (A and A^2) on surface roughness is 49.94% (Fig. 7.6). The influence of change in temperature keeping other parameters constant is shown in Fig. 7.7(a). Increasing the temperature increases the electrolyte's conductivity, which enhances the anodic dissolution process [71]. It is observed that when the temperature increases up to 50 ºC, the surface roughness value decreases as more ions start to dissolve, making the anode surface smooth. However, after 50 ºC, it is observed that surface roughness starts to increase. The possible reason may be the uncontrolled anodic dissolution due to increased electrolyte conductivity.

Table 7.5 Validation tests comparing predicted and experimental surface roughness values

Input parameters				**Response**		
	Temp (ºC)	Agitation (rpm)	Polishing time (sec)	Predicted R_a (µm)	Experimental R_a (µm)	**% Error**
EXP I	50	650	350	0.105	0.112	6.25
EXP II	40	400	300	0.112	0.118	5.08
EXP III	70	750	400	0.113	0.123	8.13

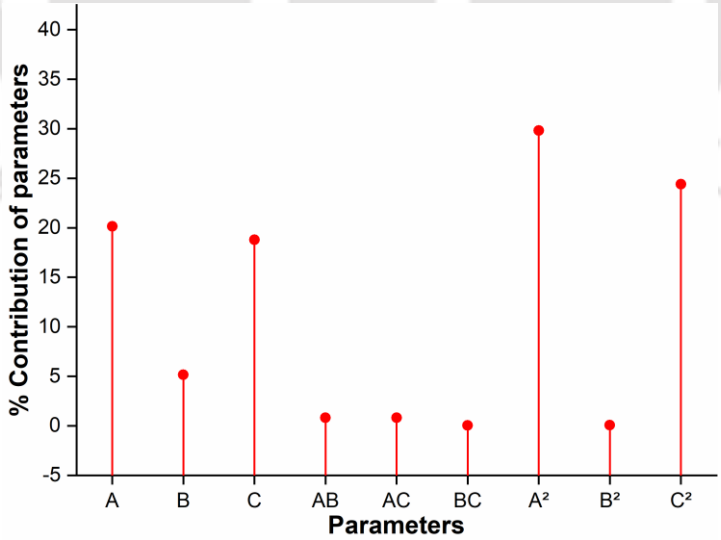

Fig. 7.6 Percentage contribution of process parameters on surface roughness during EP

The combined contribution of agitation (B and B^2) is 5.2% (Fig. 7.6) on surface roughness. The influence of change in agitation, keeping other parameters constant, is shown in Fig. 7.7(b). The agitation is provided by the magnetic bid via the magnetic stirrer. It helps

in removing the gas bubbles formed at the cathode surface during electropolishing. It can be inferred (Fig. 7.7(b)) that as agitation increases, surface roughness decreases. The possible reason may be that agitation helps in removing the gas bubbles, which act as a potential barrier between the electrodes [99].

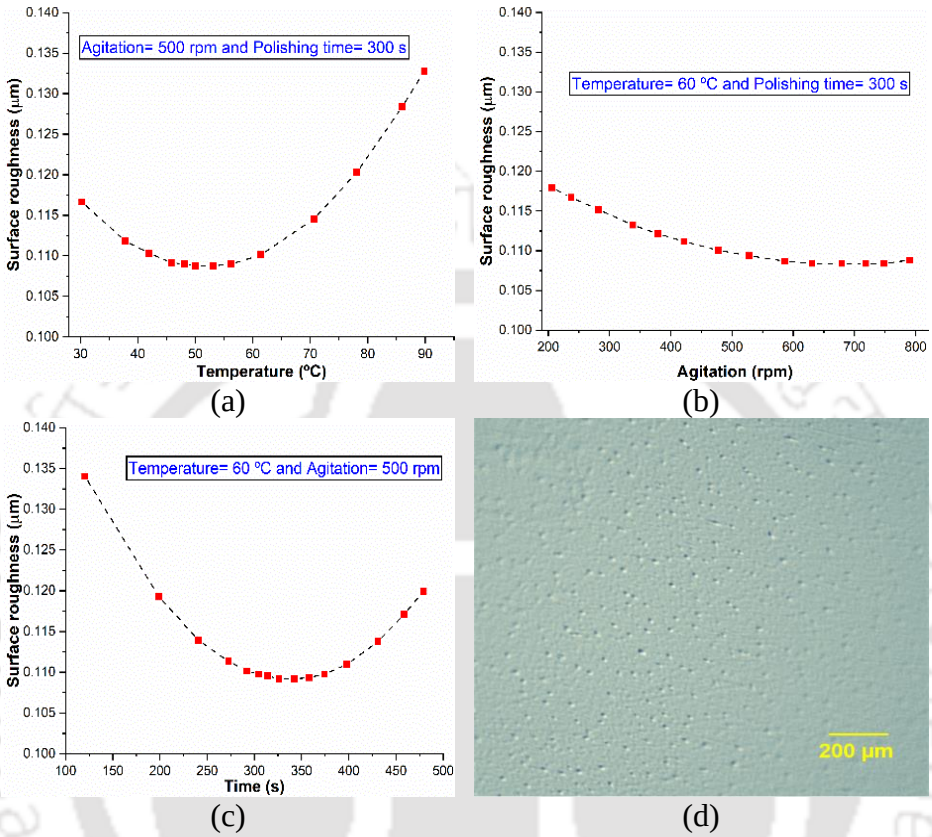

Fig. 7.7 Effect of EP process parameters (a) temperature, (b) agitation, (c) polishing time on surface roughness, and (d) pits on the surface after 350 sec of polishing time

The combined contribution of polishing time (C and C^2) on surface roughness is 43.18% (Fig. 7.6). The influence of change in time, keeping other parameters constant, is shown in Fig. 7.7(c). As the polishing time increases, the protruding part on the surface undergoes anodic dissolution, and irregularities present on the workpiece surface decrease. Surface roughness decreases with an increased polishing time, but after attaining an optimum roughness value at 350 sec polishing time, it starts to increase due to pitting on the surface. The possible reason may be the differential dissolution rates of elements present in the maraging steel alloy, which leads to the pitting and increases surface roughness beyond 350 sec polishing time, as shown in Fig. 7.7(d).

The combined influence of electrolyte temperature and magnetic bid agitation on workpiece surface roughness, keeping polishing time constant at 300 sec is shown in Fig. 7.8(a). For the temperature around 50 °C, increasing the magnetic bid agitation up to 650

rpm, the surface roughness decreases and attains a minimum value. However, on increasing temperature, surface roughness increases rapidly for lower agitation, and for higher agitation, a comparatively slower increase in surface roughness is observed.

The combined influence of electrolyte temperature and polishing time on the surface roughness of the gyroscope, keeping magnetic bid agitation fixed at 500 rpm, is shown in Fig. 7.8(b). The surface roughness decreases and attains a minimum value for the temperature around 50 ºC, increasing the polishing time up to 350 sec. However, on increasing the temperature beyond 50 ºC, surface roughness increases rapidly for a shorter polishing time and at a slower rate for a higher polishing time. However, on increasing the polishing time, for lower temperatures, surface roughness decreases to its lower value and for the higher temperature at a comparatively slower rate.

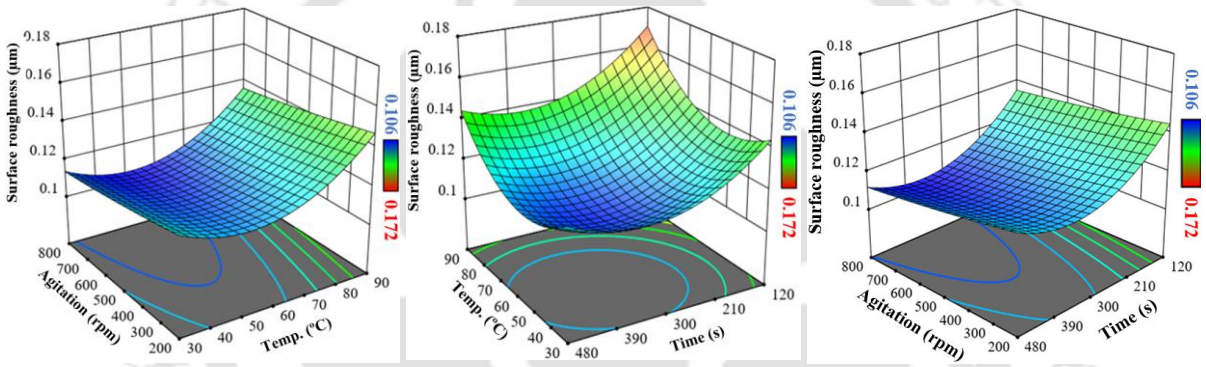

(a) (b) (c)

Fig. 7.8 3D plots showing combined effect of (a) temperature and agitation, (b) temperature and time, and (c) time and agitation on surface roughness

The combined effect of polishing time and magnetic bid agitation on the surface roughness of the workpiece, keeping electrolyte temperature constant at 60 ºC is shown in Fig. 7.8(c). For the polishing time up to 350 sec and magnetic bid rotation upto 650 rpm, the surface roughness decreases and attains a minimum value. However, at a lower polishing time and lower agitation, higher surface roughness is observed compared to the higher polishing time and higher agitation.

Energy-Dispersive X-Ray Spectroscopy (EDS) has been conducted to determine the surface elemental compositions of maraging steel 300 on base metal, and EDM and EP machined surface as shown in Fig. 7.9. It is cleaned with acetone to remove all the contaminants from the initial surface. EP on the gimbal flexure has been performed at the optimum experimental condition of 50 ºC temperature, 650 rpm of magnetic stirrer bar for 350 sec polishing time. The EDS analysis of the maraging steel 300 base metal is shown in

Fig. 7.9(a). The elements are shown in Fig. 7.9(b) after processing with EDM due to the diffusion of copper and tungsten from the tool. The recast layer is the solidified layer on the top surface of the workpiece after EDM. This layer is hard and brittle due to the continuous and rapid quenching. After EP, the recast layer is removed from the top surface, and the surface elemental composition is almost similar to the base material (Fig. 7.9(c)). The drop line graph for the variation of each element when compared to the base metal after EDM and EP is shown in Fig. 7.9(d). The elemental composition varies after EDM; however, it becomes almost similar to the base material after EP (Fig. 7.9(d)).

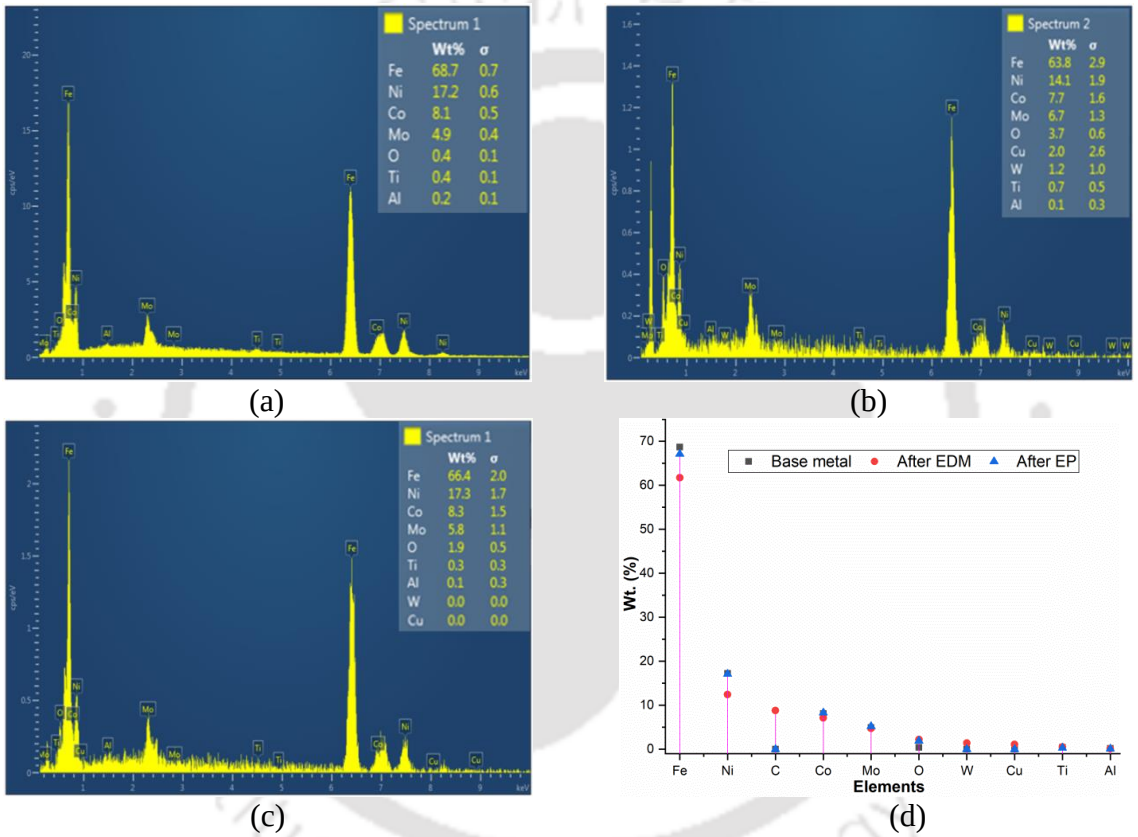

Fig. 7.9 EDS analysis of maraging steel on (a) base metal, (b) EDM machined, (c) electropolished surface, and (d) variation of each element during the process

The effect of EP on the hardness of the workpiece surface is conducted. Nanoindentation having a Berkovich tip has been utilized to measure the hardness as the thickness of the recast layer after EDM is in microns. A comparative study has been performed on the base material, recast layer (RCL), and the electropolished surface. Due to the availability of low load, a load of 9 mN has been fixed, and the study has been performed under displacement control. Initially, the load is applied to the surface, and the depth up to which it can indent is studied, as shown in Fig. 7.10(a). It can be inferred that the indentation

depth for the RCL surface (shown in the dashed orange line) is much lower than the base metal (shown in the dash-dot black line) and electropolished surface (shown in the solid blue line). The indentation depth for the base material and electropolished surface almost coincides.

The hardness and the elastic modulus data are also plotted for the base material, recast layer, and the electropolished surface, as shown in Fig. 7.10(b). It is inferred from Fig. 7.10(b) that the hardness value at the RCL increases from the base material due to lesser indentation depth. As the indentation depth is low, the indentation area is small. The hardness value is calculated by dividing the indentation area to the load. Hence, as the indentation area decreases, the hardness value of the workpiece increases. Phase transformation takes place during EDM process, which results in the formation of martensite, thereby increases hardness. Electropolishing removes the RCL of the EDM machined surface, achieving the base material. Therefore, the hardness of the electropolished surface is almost similar to the base material. However, an oxide layer is formed over the EP surface, hardness value after EP is marginally smaller than the base material [63].

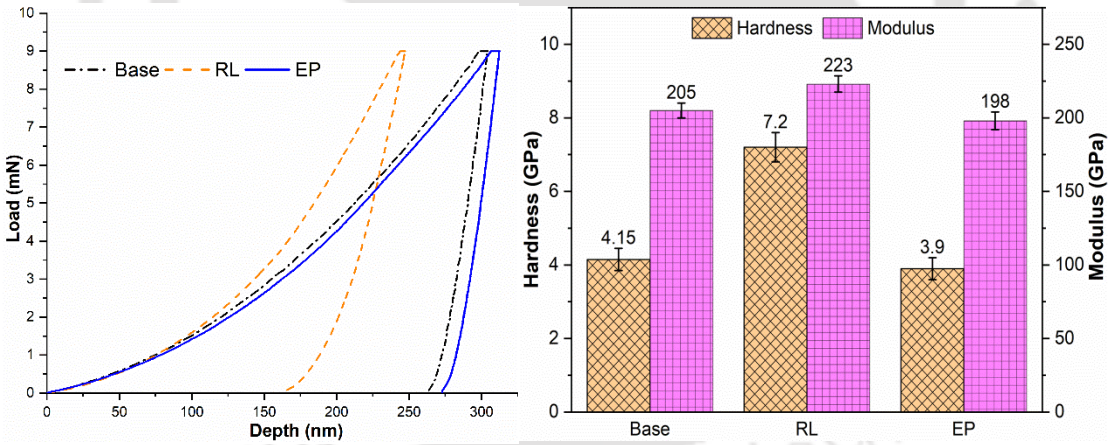

(a) (b)

Fig. 7.10 (a) Load Vs. displacement curve and (b) hardness and modulus of elasticity values of base metal, recast layer, and EP polished surface

Surface morphology has been studied after EDM and EP by field emission scanning electron microscope (FESEM), as shown in Fig. 7.11. It is observed that several micro-cracks, craters, and voids are present on the surface after EDM (Fig. 7.11(a&c)). The material removal by melting and evaporation mechanism by EDM and rapid heating and cooling leads to the formation of the recast layer, which is brittle and contains defects. These defects are in the micron level and can only be seen when magnified. The gimbal flexures fabricated with

these defects have lesser performance, and there are chances of premature failure. To remove these defects, EP has been performed after EDM. It is observed from Fig. 7.11(b&d) that after EP, the defects present on the surface after EDM have been removed and made the surface smooth.

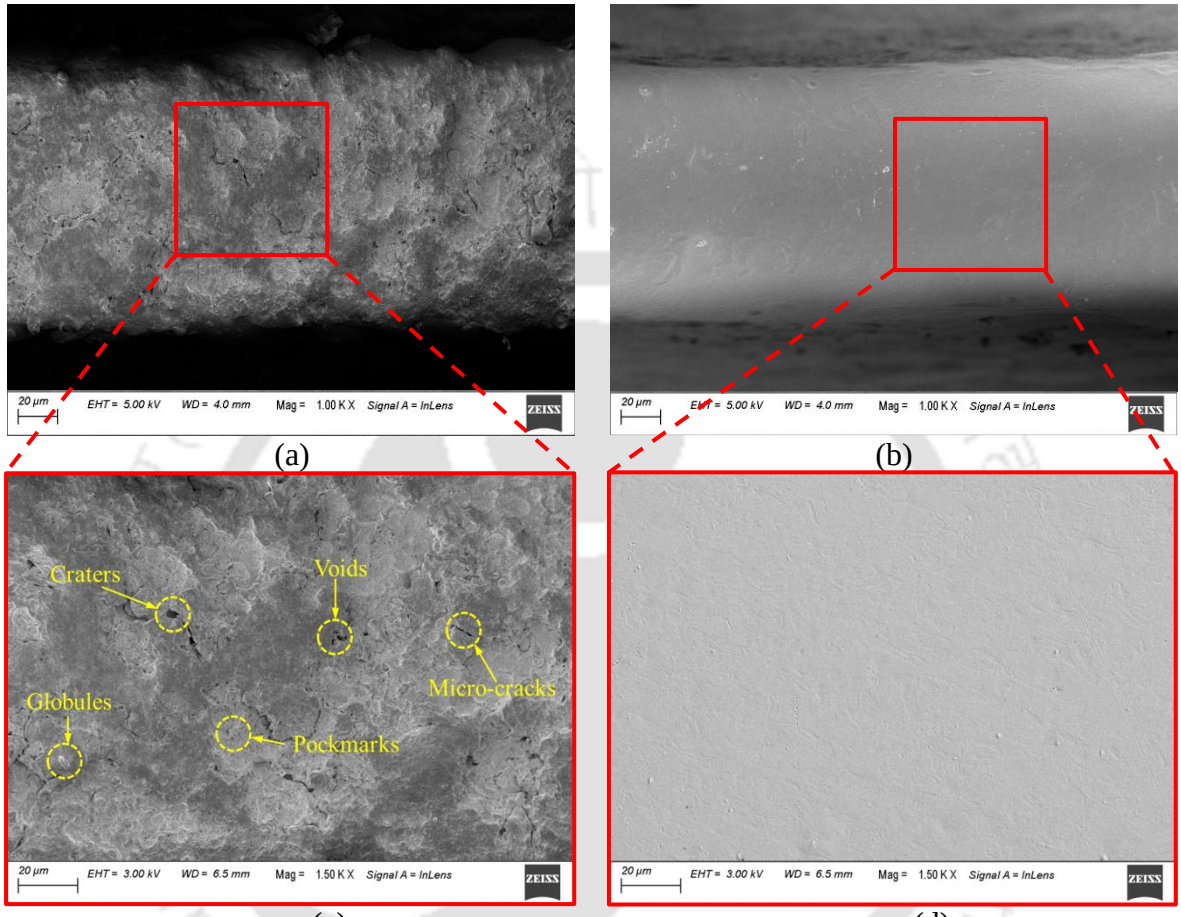

Fig. 7.11 Surface Morphology (a & c) after EDM, and (b & d) after EP

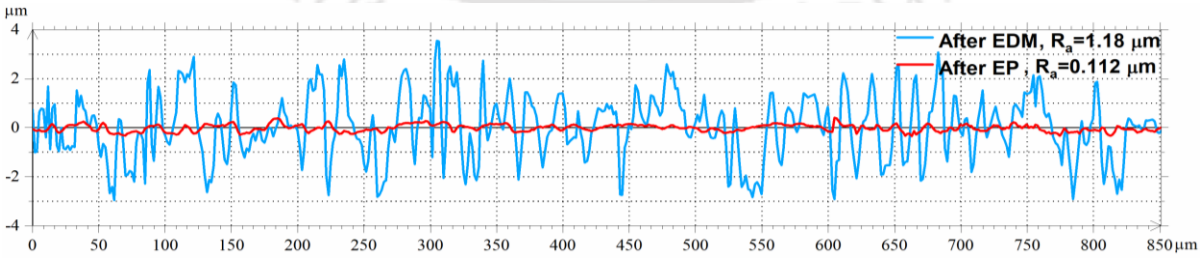

Fig. 7.12 2D Surface roughness profile after EDM and EP

The 2D surface roughness profiles of the workpiece after EDM and EP are shown in Fig. 7.12. It can be inferred from Fig. 7.12 that a surface roughness of 1.18 µm is obtained after machining with EDM due to defects on the surface. After EP, the surface roughness of 0.112 µm is obtained as all surface defects are removed.

7.4 Summary

Electrical discharge machining (EDM), a non-traditional process, is widely used for micro-fabrication, such as the thin-cruciform gimbal flexure of a gyroscope. Due to the thermoelectric process of EDM, it induces surface defects and alters the base material's property, degrading its performance. In the present study, electropolishing (EP) has been performed on a cruciform-shaped ~119.75 µm thin gimbal flexure to remove its surface defects. The gimbal flexure is made by maraging steel 300, and it is electropolished with an electrolyte mixture of acetic acid and perchloric acid in a volume ratio of 3:1. The main EP process parameters, namely electrolyte temperature, agitation of magnetic bid, and polishing time, are optimized using the response surface method of statistical design of experiments (DOE). Also, experiments are performed at optimum process parameter conditions to validate the model obtained from DOE. Surface elemental composition changes after EDM, which regain its base composition after EP. The formation of the recast layer on the surface after EDM, which increases hardness, is removed after EP and brings the surface hardness below the base material due to the formation of an oxide layer. Surface morphology after EDM contains several defects, which are completely removed after EP.

Chapter 8 Conclusions and Scope for Future Work

8.1 Conclusions

In the present work, the electrochemical-based manufacturing process is utilized to resolve micro-manufacturing challenges, i.e., fabrication of microtools and good surface integrity of fabricated micro-components. An electrochemical micromachining setup has been designed and developed to manufacture the microtool. The surface integrity of the micro-components fabricated by EDM is poor and requires post-processing to improve its performance. An experimental setup of electropolishing is developed, and a feasibility study is done with the organic electrolyte to improve the surface integrity of the thin cruciform-shaped gimbal flexure of a gyroscope fabricated by EDM. The following conclusions are drawn from the work reported in the thesis.

8.1.1 Electrochemical Micromachining (EMM)

8.1.1.1 Development of EMM Setup

An experimental setup of EMM has been designed and developed to fabricate micro-features. The developed setup consists of subsystems: the power supply unit, tool and workpiece holding unit, electrolyte and filtration unit, and the CNC controller for precise movement. The following conclusions are drawn from the present study.

- The power supply unit consists of a DC power supply, pulse generator, digital oscilloscope, and multimeter. DC power supply provides the constant direct current of set potential. The pulse generator consists of waves like sine, square, triangular, etc., with different frequencies and duty cycles. A digital oscilloscope and multimeter are used to visualize the pulse and the potential difference.
- A tool-holding unit consists of a spindle and a mechanical pencil arrangement to rotate and hold the microtools. A carbon brush arrangement is also designed to provide a power supply to the rotating tool.
- The workpiece fixture is made of Perspex, non-reactive to electrolytes, and non-conductive, thus no loss of charge. Allen bolts are used to fix the workpiece at the desired location and provide a power supply.

- An electrolyte container is also made of Perspex, which is readily machinable and transparent. It holds the electrolyte as well as the workpiece fixture. A filtration unit is also attached to filter the electrolyte mixed with debris particles.
- A CNC XYZ machine bed consists of servo motors. It is connected to the controller unit for precise movement with a resolution of 0.1 µm. The controller is connected to the desktop computer via Mach3 software.

8.1.1.2 Fabrication of Microtool

EMM is utilized for the fabrication of microtools. Two techniques are used: the tool inside the hole and the tool adjacent to a flat workpiece. The effect of tool rotation inside the hole during microtool fabrication is analyzed. Two methods have been utilized for the side tool: fixed tool and fixed IEG. Simulation results from Comsol® Multiphysics help to understand the current density behavior in IEG. The following conclusions are drawn from the present study.

- The tool inside the hole without rotation gives a poor surface finish as debris particles stick to the tool surface.
- The tool inside the hole with rotation gives a better surface finish than without rotation, as debris particles are easily removed from the tool surface.
- Due to eccentricity in placing the tool inside the hole, the conical shape of the microtool is produced.
- In fixed tool configuration, current density decreases during machining as IEG increases. It results in the formation of an oxide layer over the fabricated tool surface. An average of 105.5 µm microtool diameter is fabricated by this technique. An error of 12.83% in the diameter is observed from the simulation study due to the assumption.
- Fixed IEG configuration leads to a constant current density during machining as IEG is constant. It gives a better surface finish due to the constant machining rate. This technique fabricates an average of 86.26 µm microtool diameter. The simulation observes an error of 14.26% in the diameter due to the assumption.

8.1.2 Electropolishing

8.1.2.1 Parametric Investigation of EP

Electropolishing of maraging steel is performed with acetic acid and perchloric acid mixed in a volume ratio of 3:1. Effects of various input parameters of EP are investigated, and results

are compared before and after EP. The following conclusions are drawn from the present study.

- Electropolishing at 60 ºC, with the magnetic stirrer rotation at 400 rpm and polishing time of 6 minutes, gives a maximum improvement of 56.25% in surface roughness and 60.3% in surface reflectance.
- EDS analysis shows that the nickel and oxygen concentrations on EP polished surface increase.
- The contact angle is changed from 111.2º to 68.6º after EP. It is observed that EP makes the surface hydrophilic.
- XPS analysis suggests that the passive layer is formed after EP, improving corrosion resistance.
- EP improves the corrosion resistance as E_{corr} shifts from -0.475 V to -0.397 V, and I_{corr} shifts from 16.5 µA/cm^2 to 6.84 µA/cm^2 after EP. A more positive E_{corr} and lesser I_{corr} signify increased corrosion resistance.

8.1.2.2 Investigation of EP Performance on Surface Residual Stress

The effect of EP on surface morphology and residual stress of ED machined maraging steel is investigated with the aid of XRD, FESEM, and AFM. The concept of residual stress calculation with the help of the "$\sin^2\psi$ method" of the XRD technique and morphological changes of the machined surface was also emphasized. The following conclusions are drawn from the present study.

- The ED machined surface on maraging steel induces tensile strain as the peaks are shifted to the left. The tensile stress of 407.17 MPa was generated on the EDM machined surface. This residual stress was successfully removed from the surface with the help of electropolishing, having a final stress level on the surface of 35.27 MPa.
- The EDM machined surface's morphology generates many surface defects like micro-cracks, globules, voids, craters, and pockmarks. After EP, all the surface defects were successfully removed, and a highly polished surface was obtained.
- A recast layer had been formed over EDM machined surface with a maximum layer height of 7.55 µm. This hard-recast layer was successfully removed after EP, with an average layer removed from the surface of 7.94 µm.
- The surface elemental compositions are changed after EDM due to the inclusions of carbon and copper on the maraging steel surface, mainly present in the recast layer. The

elemental composition was similar to the base material on successfully removing the recast layer after EP.

- Surface roughness after EDM on the specimen was recorded as 1.18 µm, reduced to 0.26 µm after EP.

8.1.2.3 Surface Integrity Analysis of Electropolished Component

In the present study, cylindrical maraging steel 300 is machined by EDM. It is polished by electropolishing to remove the surface defects like micro-cracks, voids, craters, etc., formed on the EDM machined surface. The electrolyte used for EP is acetic acid and perchloric acid mixed in a volume ratio of 3:1. The surface integrity of ED and EP machined surface has been studied by various analyses such as EDS, microstructure, surface morphology, surface reflectance, crystallite size and lattice strain, hardness, wettability, and tribological performance. The following critical findings are observed from the present study.

- EDS analysis suggests that the elemental composition of maraging steel after EDM changes. Copper from the tool material and carbon from the hydrocarbon of dielectric fluid is diffused on the EDM surface. All the elements of the base material are restored with an increase in oxygen content after EP.
- The optical microstructure shows the formation of a recast layer on the EDM machined surface. This RCL is wholly removed after EP without affecting the base material's microstructure.
- The surface morphology of the EDM machined surface shows several surface defects like micro-cracks, craters, voids, etc. Differential heating and cooling cycles and rapid quenching generate tensile strain and hard RCL, which are responsible for surface defects. These defects are successfully removed following EP.
- Due to several surface defects after EDM, the average surface roughness of 1.14 µm is obtained. EP removes all these defects, which reduces the surface roughness to 0.18 µm.
- The surface reflectance has been measured by varying the UV light from 1000 to 200 nm. The EDM machined surface's reflectance is improved from 13% to 77% after EP.
- Crystallite size and lattice strain increase after EDM compared to base material signifying the surface is under tensile strain. However, EP relaxes the induced stresses that bring the crystallite size and lattice strain closer to the base material.
- In hardness analysis, the indentation depth is minimum for ED machined surface, followed by base material and EP surface, and the respective hardness values are 7.82

GPa, 4.12 GPa, and 4.04 GPa. Due to the formation of the oxide layer, the hardness of the electropolished surface is slightly reduced from the base material.

- The contact angle increases from 64.1º to 77.7º after EDM, making the surface hydrophilic (<90º). EP further enhances the hydrophilicity by further decreasing the contact angle to 56.5º.
- Tribological performance tests have been performed, and it is observed that the coefficient of friction increases from 0.256 to 0.376 and the wear rate from 5.37×10^{-5} to 9.5×10^{-5} after EDM. However, EP reduces the coefficient of friction to 0.212 and the wear rate to 4.05×10^{-5}.

8.1.2.4 Electropolishing of Thin Gimbal Flexure of Gyroscope

In the present study, electropolishing is performed on the thin cruciform-shaped gimbal flexure of a gyroscope fabricated by an electrical discharge machining process. The cruciform-shaped thin gimbal flexure is made by maraging steel 300, which acts as an anode and the graphite rod acts as the cathode for the electropolishing in an electrolytic mixture of acetic acid and perchloric acid in the volume ratio of 3:1. The parameters of EP are optimized using the statistical design of experiments. The ANOVA model is validated with the help of optimized process parameters. Surface elemental composition, hardness of the surface, and surface morphology after EDM and EP have been investigated. The following conclusions are drawn from the present study.

- Electropolishing of thin cruciform-shaped gimbal flexure of gyroscope fabricated from maraging steel by EDM is successfully performed using an electrolyte combination of acetic acid and perchloric acid in the volume ratio of 3:1.
- The ANOVA study of basic EP process parameters suggests that all three parameters, namely electrolyte temperature, agitation of magnetic bid, and polishing time, are significant, having percentage contributions of 49.67%, 5.18%, and 42.98%, respectively, on surface roughness.
- The optimized parameters that provide the best electropolishing effect are at 50 ºC temperature, at 650 rpm of magnetic bid, and at 350 sec of polishing time, which offers the best surface roughness value of 0.112 µm.
- A maximum error of 8.13% is observed between predicted (obtained from regression equation) and experimental surface roughness values, which shows the effectiveness of the DOE model.

- The surface elemental composition suggests that the tool material diffuses to the surface after EDM over the recast layer; however, after electropolishing, the surface elemental composition is almost similar to the base material.
- The nanoindentation study provides information about the hardness of the surface. The maximum indentation at base material, EDM machined surface (on recast layer), and electropolished surface are 300 nm, 250 nm, and 310 nm, respectively. The harder the surface, lesser indentation is observed. The hardness and Young's modulus values of electropolished surfaces are slightly reduced compared to the base material as the oxide layer is formed after EP.
- The surface morphology study suggests that all the surface defects, like micro-cracks, voids, etc., which degrades the performance of thin cruciform-shaped gimbal flexure of gyroscope after EDM, have been removed after EP.

8.2 Scope for Future Work

- A robust EMM setup with an in-house arrangement, like a rotary union, to supply the power to the tool while rotating and a high-speed camera to monitor the behavior of the bubble in the interelectrode gap can be developed.
- Image processing can be utilized to analyze the circularity error of fabricated micro-hole.
- A numerical model can be developed to analyze the effect of electropolishing on the electrical discharge machined component.
- A robust EP setup can be made so that the harmful fumes can be liberated in an open space. It should not affect the operator and the instrument nearby.
- A numerical model for monitoring the surface roughness of the electropolished component can be developed.
- Image processing can be utilized to analyze the surface morphology after EP.

References

[1] S. Hoseinzadeh and D. A. Garcia, "Numerical Analysis of Thermal, Fluid, and Electrical Performance of a Photovoltaic Thermal Collector at New Micro-Channels Geometry," *J. Energy Resour. Technol. Trans. ASME*, vol. 144, no. 6, Jun. 2021, doi: 10.1115/1.4052672/1121172.

[2] M. Singh, P. Tripathi, and J. Ramkumar, "Electrical discharge micro-texturing using compound tool electrodes for tribological and wettability applications," *Surf. Eng.*, pp. 1–17, 2022, doi: 10.1080/02670844.2022.2089801.

[3] D. S. Patel, A. Singh, V. K. Jain, J. Ramkumar, and A. Shrivastava, "Investigations into insertion force of electrochemically micro-textured hypodermic needles," *Int. J. Adv. Manuf. Technol.*, vol. 100, no. 5–8, pp. 1311–1326, 2019, doi: 10.1007/s00170-017-1265-2.

[4] B. Bhattacharyya, M. Malapati, and J. Munda, "Experimental study on electrochemical micromachining," *J. Mater. Process. Technol.*, vol. 169, no. 3, pp. 485–492, 2005, doi: 10.1016/j.jmatprotec.2005.04.074.

[5] M. Hackert-Oschätzchen, G. Meichsner, M. Zinecker, A. Martin, and A. Schubert, "Micro machining with continuous electrolytic free jet," *Precis. Eng.*, vol. 36, no. 4, pp. 612–619, Oct. 2012, doi: 10.1016/J.Precisioneng.2012.05.003.

[6] "https://blog.ableelectropolishing.com/topic/electropolishing-solutions." .

[7] "https://dipnsteel.com/2019/10/30/electro/." .

[8] W. Han and F. Fang, "Fundamental aspects and recent developments in electropolishing," *Int. J. Mach. Tools Manuf.*, vol. 139, no. April, pp. 1–23, 2019, doi: 10.1016/j.ijmachtools.2019.01.001.

[9] O. Dubrovski, Oles and Tietze, Sabrina and Zigelman, Anna and Drese, Klaus S and Lindner, Gerhard and Manor, "The Enhancement of Ion Transport in an Electrochemical Cell Using High Frequency Vibration for the Electropolishing of Copper," *J. Electrochem. Soc.*, vol. 165, no. 5, p. E256, 2018.

[10] B. Bhattacharyya, S. Mitra, and A. K. Boro, "Electrochemical machining: New possibilities for micromachining," *Robot. Comput. Integr. Manuf.*, vol. 18, no. 3–4, pp. 283–289, 2002, doi: 10.1016/S0736-5845(02)00019-4.

[11] T. Kurita, K. Chikamori, S. Kubota, and M. Hattori, "A study of three-dimensional shape machining with an ECμM system," *Int. J. Mach. Tools Manuf.*, vol. 46, no. 12–13, pp. 1311–1318, Oct. 2006, doi: 10.1016/J.IJMACHTOOLS.2005.10.013.

[12] M. A. H. Mithu, G. Fantoni, and J. Ciampi, "A step towards the in-process monitoring

for electrochemical microdrilling," *Int. J. Adv. Manuf. Technol.*, vol. 57, no. 9, pp. 969–982, May 2011, doi: 10.1007/S00170-011-3355-X.

[13] Z. Zhang, Y. Wang, F. Chen, and W. Mao, "A Micro-machining system based on electrochemical dissolution of material," *Russ. J. Electrochem.*, vol. 47, no. 7, pp. 819–824, 2011, doi: 10.1134/S1023193511070172.

[14] K. Mishra, D. Dey, B. R. Sarkar, and B. Bhattacharyya, "Experimental investigation into electrochemical milling of Ti6Al4V," *J. Manuf. Process.*, vol. 29, pp. 113–123, 2017, doi: 10.1016/j.jmapro.2017.07.014.

[15] K. Mishra, B. R. Sarkar, and B. Bhattacharyya, "Influence of inner-spraying rotating tool during electrochemical milling of Nimonic-263 alloy," *Mater. Manuf. Process.*, vol. 34, no. 7, pp. 807–813, 2019, doi: 10.1080/10426914.2019.1594277.

[16] S. Kunar and B. Bhattacharyya, "Investigation on surface structuring generated by electrochemical micromachining," *Adv. Manuf.*, vol. 5, no. 3, pp. 217–230, 2017, doi: 10.1007/s40436-017-0186-5.

[17] D. Li, D. Zhu, and H. Li, "Microstructure of electrochemical micromachining using inert metal mask," *Int. J. Adv. Manuf. Technol.*, vol. 55, no. 1–4, pp. 189–194, 2011, doi: 10.1007/s00170-010-3025-4.

[18] V. Rathod, B. Doloi, and B. Bhattacharyya, "Influence of electrochemical micromachining parameters during generation of microgrooves," *Int. J. Adv. Manuf. Technol.*, vol. 76, no. 1–4, pp. 51–60, 2013, doi: 10.1007/s00170-013-5304-3.

[19] S. Ayyappan and K. Sivakumar, "Experimental investigation on the performance improvement of electrochemical machining process using oxygen-enriched electrolyte," *Int. J. Adv. Manuf. Technol.*, vol. 75, no. 1, pp. 479–487, 2014, doi: 10.1007/s00170-014-6096-9.

[20] V. Rathod, B. Doloi, and B. Bhattacharyya, "Experimental investigations into machining accuracy and surface roughness of microgrooves fabricated by electrochemical micromachining," *Proc. Inst. Mech. Eng. Part B J. Eng. Manuf.*, vol. 229, no. 10, pp. 1781–1802, Oct. 2015, doi: 10.1177/0954405414539486.

[21] D. S. Patel, V. K. Jain, A. Shrivastava, and J. Ramkumar, "Electrochemical micro texturing on flat and curved surfaces: simulation and experiments," *Int. J. Adv. Manuf. Technol.*, vol. 100, no. 5–8, pp. 1269–1286, 2019, doi: 10.1007/s00170-016-9700-3.

[22] S. N. B. Oliaei, Y. Karpat, J. P. Davim, and A. Perveen, "Micro tool design and fabrication : A review," *J. Manuf. Process.*, vol. 36, pp. 496–519, 2018, doi: 10.1016/j.jmapro.2018.10.038.

[23] J. O'Hara and F. Fang, "Advances in micro cutting tool design and fabrication," *Int. J. Extrem. Manuf.*, vol. 1, no. 3, p. 032003, 2019, doi: 10.1088/2631-7990/ab3e7f.

[24] B. R. Acharya, A. Sethi, P. Saha, and D. K. Pratihar, "A Comparative Study of Micro-Tool Fabrication Methods Using Micro-EDM," in *Proceedings of 10th International Conference on Precision, Meso, Micro and Nano Engineering (COPEN 10), Indian Institute of Technology Madras, Chennai, India*, 2017, pp. 210–213.

[25] G. Malayath, A. M. Sidpara, and S. Deb, "Fabrication of micro-end mill tool by EDM and its performance evaluation," *Mach. Sci. Technol.*, vol. 24, no. 2, pp. 169–194, 2020, doi: 10.1080/10910344.2019.1636269.

[26] S. S. Das and P. K. Patowari, "Fabrication of serpentine micro-channels on glass by ultrasonic machining using developed micro-tool by wire-cut electric discharge machining," *Int. J. Adv. Manuf. Technol.*, vol. 95, no. 5–8, pp. 3013–3028, 2018, doi: 10.1007/s00170-017-1441-4.

[27] Y. Wang *et al.*, "Micro Electrochemical Machining of Array Micro-Grooves Using In-Situ Disk Electrode Fabricated by Micro-WEDM," *Micromachines*, vol. 11, no. 1, p. 66, 2020.

[28] S. N. Bhavsar, S. Aravindan, and P. V. Rao, "A critical review on microtools fabrication by focused ion beam (FIB) technology," in *Proceedings of the World Congress on Engineering*, 2009, vol. 2, pp. 1–3.

[29] Y. N. Picard, D. P. Adams, M. J. Vasile, and M. B. Ritchey, "Focused ion beam-shaped microtools for ultra-precision machining of cylindrical components," *Precis. Eng.*, vol. 27, no. 1, pp. 59–69, 2003.

[30] D. P. Adams, M. J. Vasile, and A. S. M. Krishnan, "Microgrooving and microthreading tools for fabricating curvilinear features," *Precis. Eng.*, vol. 24, no. 4, pp. 347–356, 2000.

[31] P. Dutta, A. Barman, A. Kumar, and M. Das, "Design and Fabrication of Electrochemical MicroMachining (ECMM) Experimental Setup for Micro-hole Drilling," in *Advances in Mechanical Engineering*, Springer, 2020, pp. 561–573.

[32] V. K. Jain *et al.*, "Micromachining : An overview (Part I)," *J. Micromanufacturing*, vol. 3, no. 2, pp. 142–158, 2020, doi: https://doi.org/10.1177/2516598419895828.

[33] A. Kumar, M. Kumar, A. Alok, and M. Das, "Surface Texturing by Electrochemical Micromachining: A Review," *IOP Conf. Ser. Mater. Sci. Eng.*, vol. 804, no. 1, p. 012011, 2020, doi: 10.1088/1757-899X/804/1/012011.

[34] V. K. Jain, S. Kalia, A. Sidpara, and V. N. Kulkarni, "Fabrication of micro-features

and micro-tools using electrochemical micromachining," *Int. J. Adv. Manuf. Technol.*, vol. 61, no. 9–12, pp. 1175–1183, Aug. 2012, doi: 10.1007/s00170-012-4088-1.

[35] A. Sethi, B. R. Acharya, P. Kumar, R. Chakraborty, and P. Saha, "Realization of Green Manufacturing Using Citric Acid Electrolyte for WC--Co Alloy Micro-tool Fabrication in Micro-WECM," in *Advances in Unconventional Machining and Composites*, Springer, 2020, pp. 211–223.

[36] V. Rathod, B. Doloi, and B. Bhattacharyya, "Parametric Investigation Into the Fabrication of Disk Microelectrodes by Electrochemical Micromachining," *J. Micro Nano-Manufacturing*, vol. 1, no. 4, p. 041005, 2013, doi: 10.1115/1.4025977.

[37] S. Sangeethakrishnan, E. Rajkeerthi, P. Hariharan, and G. Bhavesh, "Design and Development of Tool Electrode for Electrochemical Micromachining Using Reverse EMM Technique," in *Advances in Micro and Nano Manufacturing and Surface Engineering*, Springer, 2019, pp. 339–347.

[38] S. Kumar, P. Dileep, K. Mishra, J. Arab, and P. Dixit, "Numerical and experimental analysis of high-aspect-ratio micro-tool electrode fabrication using controlled electrochemical machining," *J. Appl. Electrochem.*, vol. 50, no. 2, pp. 169–184, 2020, doi: 10.1007/s10800-019-01380-5.

[39] S. Saha, A. Kumar Ball, A. Mukherjee, A. Das, S. Halder, and N. Hanumaiah, "Optimization of electrochemical etching process for manufacturing of micro electrodes for micro-EDM application," *Proc. Inst. Mech. Eng. Part B J. Eng. Manuf.*, p. 0954405420958961, 2020.

[40] D. Brent, T. A. Saunders, F. Garcia Moreno, and P. Tyagi, "Taguchi Design of Experiment for the Optimization of Electrochemical Polishing of Metal Additive Manufacturing Components," in *ASME International Mechanical Engineering Congress and Exposition*, no. 50527, 2016, p. V002T02A014.

[41] ASTM-E1558, "Standard Guide for Electrolytic Polishing of Metallographic Specimens," *100 Barr Harb. Drive, West Conshohocken United States*, 2009, doi: 10.1520/E1558-09R14.

[42] P. Tyagi *et al.*, "Reducing the roughness of internal surface of an additive manufacturing produced 316 steel component by chempolishing and electropolishing," *Addit. Manuf.*, vol. 25, pp. 32–38, Jan. 2019, doi: 10.1016/j.addma.2018.11.001.

[43] X. Zhao, S. G. Corcoran, and M. J. Kelley, "Sulfuric acid-methanol electrolytes as an alternative to sulfuric-hydrofluoric acid mixtures for electropolishing of niobium," *J. Appl. Electrochem.*, vol. 41, no. 6, pp. 633–643, 2011.

[44] S. C. Chen, G. C. Tu, and C. A. Huang, “The electrochemical polishing behavior of porous austenitic stainless steel (AISI 316L) in phosphoric-sulfuric mixed acids,” *Surf. Coatings Technol.*, vol. 200, no. 7, pp. 2065–2071, 2005.

[45] D. Ma, S. Li, and C. Liang, “Electropolishing of high-purity aluminium in perchloric acid and ethanol solutions,” *Corros. Sci.*, vol. 51, no. 4, pp. 713–718, 2009.

[46] P. Tyagi *et al.*, “Roughness Reduction of Additively Manufactured Steel by Electropolishing,” *Int. J. Adv. Manuf. Technol.*, vol. 106, no. 3–4, pp. 1337–1344, Feb. 2020, doi: 10.1007/s00170-019-04720-z.

[47] Z. ur Rahman, K. M. Deen, L. Cano, and W. Haider, “The effects of parametric changes in electropolishing process on surface properties of 316L stainless steel,” *Appl. Surf. Sci.*, vol. 410, pp. 432–444, 2017, doi: 10.1016/j.apsusc.2017.03.081.

[48] D. Landolt, “Fundamental aspects of electropolishing,” *Electrochim. Acta*, vol. 32, no. 1, pp. 1–11, 1987, doi: 10.1016/0013-4686(87)87001-9.

[49] S.-C. Chang, J.-M. Shieh, C.-C. Huang, B.-T. Dai, and M.-S. Feng, “Pattern effects on planarization efficiency of Cu electropolishing,” *Jpn. J. Appl. Phys.*, vol. 41, no. 12R, p. 7332, 2002.

[50] K. Fushimi, M. Stratmann, and A. W. Hassel, “Electropolishing of NiTi shape memory alloys in methanolic H2SO4,” *Electrochim. Acta*, vol. 52, pp. 1290–1295, 2006, doi: 10.1016/j.electacta.2006.07.030.

[51] P. S. Kao and H. Hocheng, “Optimization of electrochemical polishing of stainless steel by grey relational analysis,” in *Journal of Materials Processing Technology*, Sep. 2003, vol. 140, no. 1-3 SPEC., pp. 255–259, doi: 10.1016/S0924-0136(03)00747-7.

[52] M. Haidopoulos, S. Turgeon, C. Sarra-Bournet, G. Laroche, and D. Mantovani, “Development of an optimized electrochemical process for subsequent coating of 316 stainless steel for stent applications,” *J. Mater. Sci. Mater. Med.*, vol. 17, no. 7, pp. 647–657, 2006.

[53] J. Woo, P. & Deug, and W. Lee, “Pulse electrochemical polishing for microrecesses based on a coulostatic analysis,” *Int. J. Adv. Manuf. Technol.*, vol. 40, no. 7, pp. 742--748, 2009, doi: 10.1007/s00170-008-1391-y.

[54] P. Sojitra, A. Raval, and S. Vallabhbhai, “Electropolishing of 316LVM Stainless Steel Cardiovascular Stents: An Investigation of Material Removal, Surface Roughness and Corrosion Behaviour,” *Artif. Organs*, vol. 23, no. 13, pp. 115--121, 2010.

[55] A. Latifi, M. Imani, M. T. Khorasani, and M. D. Joupari, “Electrochemical and chemical methods for improving surface characteristics of 316L stainless steel for

biomedical applications," *Surf. Coatings Technol.*, vol. 221, pp. 1–12, Apr. 2013, doi: 10.1016/J.SURFCOAT.2013.01.020.

[56] S. Habibzadeh, L. Li, D. Shum-Tim, E. C. Davis, and S. Omanovic, "Electrochemical polishing as a 316L stainless steel surface treatment method: Towards the improvement of biocompatibility," *Corros. Sci.*, vol. 87, pp. 89–100, Oct. 2014, doi: 10.1016/j.corsci.2014.06.010.

[57] Y. Aksu, M. Erdoğan, G. Demirci, and İ. Karakaya, "Electropolishing of an Fe-Ni-Co Alloy in Acetic Acid-Perchloric Acid Mixture," *ECS Trans.*, vol. 72, no. 22, p. 13, 2016, doi: 10.1149/07222.0013ecst.

[58] P. Lochynski, A. Sikora, and B. Szczygiel, "Surface morphology and passive film composition after pickling and electropolishing," *Surf. Eng.*, vol. 33, no. 5, pp. 395–403, May 2017, doi: 10.1080/02670844.2016.1238189.

[59] Y. Han, J. Mei, Q. Peng, E. H. Han, and W. Ke, "Effect of electropolishing on corrosion of nuclear grade 316L stainless steel in deaerated high temperature water," *Corros. Sci.*, vol. 112, pp. 625–634, Nov. 2016, doi: 10.1016/j.corsci.2016.09.002.

[60] Z. ur Rahman, K. M. Deen, L. Cano, and W. Haider, "The effects of parametric changes in electropolishing process on surface properties of 316L stainless steel," *Appl. Surf. Sci.*, vol. 410, pp. 432–444, Jul. 2017, doi: 10.1016/j.apsusc.2017.03.081.

[61] E. Lyczkowska-Widlak, P. Lochynski, G. Nawrat, and E. Chlebus, "Comparison of electropolished 316L steel samples manufactured by SLM and traditional technology," *Rapid Prototyp. J.*, 2019, doi: 10.1108/RPJ-03-2018-0060.

[62] P. Lochyński, S. Charazińska, E. Łyczkowska-Widłak, and A. Sikora, "Electropolishing of Stainless Steel in Laboratory and Industrial Scale," *Metals (Basel).*, vol. 9, no. 8, p. 854, Aug. 2019, doi: 10.3390/MET9080854.

[63] W. Han and F. Fang, "Two-step electropolishing of 316L stainless steel in a sulfuric acid-free electrolyte," *J. Mater. Process. Technol.*, vol. 279, p. 116558, May 2020, doi: 10.1016/j.jmatprotec.2019.116558.

[64] W. Han and F. Fang, "Investigation of electrochemical properties of electropolishing Co–Cr dental alloy," *J. Appl. Electrochem.*, vol. 50, no. 3, pp. 367–381, Mar. 2020, doi: 10.1007/s10800-019-01390-3.

[65] G. Wang, Z. Liu, J. Niu, W. Huang, and B. Wang, "Effect of electrochemical polishing on surface quality of nickel-titanium shape memory alloy after milling," *J. Mater. Res. Technol.*, vol. 9, no. 1, pp. 253–262, Jan. 2020, doi: 10.1016/j.jmrt.2019.10.053.

[66] W. Han and F. Z. Fang, "Investigation of electropolishing characteristics of tungsten in

eco-friendly sodium hydroxide aqueous solution," *Adv. Manuf.*, vol. 8, no. 3, pp. 265–278, Sep. 2020, doi: 10.1007/s40436-020-00309-y.

[67] K. Muhammad, R. Yi, Z. Zhan, J. Ji, X. Zhang, and H. Deng, "Highly efficient smoothing of Inconel 718 via electrochemical-based isotropic etching polishing," *Precis. Eng.*, vol. 71, no. March, pp. 119–129, 2021, doi: 10.1016/j.precisioneng.2021.03.005.

[68] D. Ahmadkhaniha, H. Möller, and C. Zanella, "Studying the Microstructural Effect of Selective Laser Melting and Electropolishing on the Performance of Maraging Steel," *J. Mater. Eng. Perform.*, vol. 30, no. 9, pp. 6588–6605, Jun. 2021, doi: 10.1007/S11665-021-05927-6.

[69] Y. Zhang, J. Li, and S. Che, "Electropolishing mechanism of Ti-6Al-4V alloy fabricated by selective laser melting," *Int. J. Electrochem. Sci.*, vol. 13, no. 5, pp. 4792–4807, 2018, doi: 10.20964/2018.05.79.

[70] Y. Wang, X. Wei, Z. Li, X. Jing, Z. Gong, and C. Liu, "Surface Performance and Optimization of Nickel Titanium Alloy Electropolishing Parameters," *Int. J. Electrochem. Sci.*, vol. 16, no. 7, pp. 1–19, 2021, doi: 10.20964/2021.07.23.

[71] E. S. Lee, "Machining characteristics of the electropolishing of stainless steel (STS316L)," *Int. J. Adv. Manuf. Technol.*, vol. 16, no. 8, pp. 591–599, 2000, doi: 10.1007/s001700070049.

[72] E. S. Lee and T. H. Shin, "An evaluation of the machinability of nitinol shape memory alloy by electrochemical polishing," *J. Mech. Sci. Technol.*, vol. 25, no. 4, pp. 963–969, 2011, doi: 10.1007/s12206-011-0209-2.

[73] H. Hocheng and P. S. Pa, "Continuous secondary ultrasonic electropolishing of an SKD61 cylindrical part," *Int. J. Adv. Manuf. Technol.*, vol. 21, no. 4, pp. 238–242, 2003, doi: 10.1007/s001700300027.

[74] H. Ramasawmy and L. Blunt, "Investigation of the effect of electrochemical polishing on EDM surfaces," *Int. J. Adv. Manuf. Technol.*, vol. 31, no. 11–12, pp. 1135–1147, Feb. 2007, doi: 10.1007/s00170-005-0302-8.

[75] P. B. Tailor, A. Agrawal, and S. S. Joshi, "Numerical modeling of passive layer formation and stabilization in electrochemical polishing process," *J. Manuf. Process.*, vol. 18, pp. 107–116, Apr. 2015, doi: 10.1016/j.jmapro.2015.02.001.

[76] D. Lappin, A. R. Mohammadi, and K. Takahata, "An experimental study of electrochemical polishing for micro-electro- discharge-machined stainless-steel stents," *J. Mater. Sci. Mater. Med.*, vol. 23, no. 2, pp. 349–356, 2012, doi:

10.1007/s10856-011-4513-2.

[77] P. Tyagi, T. Goulet, D. Brent, K. Klein, and F. Garcia-Moreno, “Scanning Electron Microscopy and Optical Profilometry of Electropolished Additively Manufactured 316 Steel Components,” in *ASME International Mechanical Engineering Congress and Exposition*, no. 52019, 2018, p. V002T02A019.

[78] S. Das, M. Klotz, and F. Klocke, “EDM simulation: finite element-based calculation of deformation, microstructure and residual stresses,” *J. Mater. Process. Technol.*, vol. 142, no. 2, pp. 434–451, Nov. 2003, doi: 10.1016/S0924-0136(03)00624-1.

[79] J. Boban and A. Ahmed, “Improving the surface integrity and mechanical properties of additive manufactured stainless steel components by wire electrical discharge polishing,” *J. Mater. Process. Technol.*, vol. 291, p. 117013, 2021, doi: 10.1016/j.jmatprotec.2020.117013.

[80] G. Wang and F. Han, “A comparative study on the surface integrity of single-step and multi-step sequential machining in electric discharge machining,” *Int. J. Adv. Manuf. Technol.*, vol. 114, no. 5–6, pp. 1803–1817, May 2021, doi: 10.1007/S00170-021-06947-1/FIGURES/18.

[81] J. GUO *et al.*, “Investigation on surface integrity of electron beam melted Ti-6Al-4 V by precision grinding and electropolishing,” *Chinese J. Aeronaut.*, vol. 34, no. 12, pp. 28–38, Dec. 2021, doi: 10.1016/J.CJA.2020.08.014.

[82] J. Srinath *et al.*, “Characterization of the electrical discharge machined M300 maraging steel flexures using nanoindentation,” *Mater. Sci. Forum*, vol. 830–831, pp. 395–398, 2015.

[83] T. Hryniewicz, R. Rokicki, and K. Rokosz, “Co–Cr alloy corrosion behaviour after electropolishing and ‘magnetoelectropolishing’ treatments,” *Mater. Lett.*, vol. 62, no. 17–18, pp. 3073–3076, Jun. 2008, doi: 10.1016/J.MATLET.2008.01.130.

[84] A. A. Kityk, V. Pavlik, M. Boča, D. Pangallo, M. Kapustova, and Y. Halahovets, “Electrochemical Surface Treatment to Enhance Corrosion Resistance and Bioresistance of Medical-Grade Stainless Steels,” *J. Mater. Eng. Perform.*, vol. 29, no. 9, pp. 5985–5994, Sep. 2020, doi: 10.1007/s11665-020-05095-z.

[85] G. Yang, B. Wang, K. Tawfiq, H. Wei, S. Zhou, and G. Chen, “Electropolishing of surfaces: theory and applications,” *Surf. Eng.*, vol. 33, no. 2, pp. 149–166, Feb. 2017, doi: 10.1080/02670844.2016.1198452.

[86] T. Schaller, L. Bohn, J. Mayer, and K. Schubert, “Microstructure grooves with a width of less than 50 μm cut with ground hard metal micro end mills,” *Precis. Eng.*, vol. 23,

no. 4, pp. 229–235, Oct. 1999, doi: 10.1016/S0141-6359(99)00011-2.

[87] S. Kissling, K. Bade, M. Börner, and D. M. Klymyshyn, “Electropolishing as a method for deburring high aspect ratio nickel RF MEMS,” *Microsyst. Technol.*, vol. 16, no. 8–9, pp. 1361–1367, Aug. 2010, doi: 10.1007/S00542-010-1075-Z/FIGURES/9.

[88] A. Zhang, Z. Xu, J. Lu, and Y. Wang, “Improvement of blade platform accuracy in ECM utilizing an auxiliary electrode,” *Mater. Manuf. Process.*, vol. 35, no. 9, pp. 951–960, Jul. 2020, doi: 10.1080/10426914.2020.1752920.

[89] X. Zhang, N. Qu, and X. Chen, “Sandwich-like electrochemical micromachining of micro-dimples,” *Surf. Coatings Technol.*, vol. 302, pp. 438–447, 2016, doi: 10.1016/j.surfcoat.2016.05.088.

[90] S. Kunar and B. Bhattacharyya, “Parametric Investigation of Various Electrolytes During Micro-electrochemical Texturing on Stainless Steel,” in *International Conference on Mechanical Engineering*, 2018, pp. 227–245.

[91] M. Hackert-Oschatzchen, Matthias Kowalick, G. Meichsner, and A. Schubert, “Multiphysics Simulation of the Electrochemical Finishing of Micro Bores,” in *Proceedings of the European COMSOL Conference*, 2012.

[92] M. Hackert-Oschätzchen *et al.*, “2D Axisymmetric Simulation of the Electrochemical Finishing of Micro Bores by Inverse Jet Electrochemical Machining,” in *Proceedings of the European COMSOL Conference*, 2013.

[93] E. J. F. Dickinson, H. Ekström, and E. Fontes, “COMSOL Multiphysics®: Finite element software for electrochemical analysis. A mini-review,” *Electrochem. commun.*, vol. 40, pp. 71–74, 2014, doi: 10.1016/j.elecom.2013.12.020.

[94] M. Hackert-Oschätzchen, M Kowalick, R. Paul, M. Zinecker, D. Kuhn, G. Meichsner, and A. Schubert, “2-D Axisymmetric Simulation of the Electrochemical Machining of Internal Precision Geometries,” in *Proceeding of the European COMSOL Conference*, 2016, pp. 2–8.

[95] J. C. Hung, C. H. Chang, K. C. Chiu, and S. J. Lee, “Simulation-based fabrication of micro-helical grooves in a hydrodynamic thrust bearing by using ECMM,” *Int. J. Adv. Manuf. Technol.*, vol. 64, no. 5–8, pp. 813–820, 2013, doi: 10.1007/s00170-012-4062-y.

[96] B. Liu, H. Zou, H. Luo, and X. Yue, “Investigation on the Electrochemical Micromachining of Micro Through-Hole by Using Micro Helical Electrode,” *Micromachines*, vol. 11, no. 2, p. 118, 2020.

[97] A. K. Das and P. Saha, “Fabrication of cylindrical micro tools by micro

electrochemical form turning operation," *Proc. Inst. Mech. Eng. Part B J. Eng. Manuf.*, vol. 228, no. 1, pp. 74–81, 2014.

[98] V. Rathod, B. Doloi, and B. Bhattacharyya, "Sidewall insulation of microtool for electrochemical micromachining to enhance the machining accuracy," *Mater. Manuf. Process.*, vol. 29, no. 3, pp. 305–313, 2014, doi: 10.1080/10426914.2013.864407.

[99] W. Han and F. Fang, "Eco-friendly NaCl-based electrolyte for electropolishing 316L stainless steel," *J. Manuf. Process.*, vol. 58, no. October, pp. 1257–1269, 2020, doi: 10.1016/j.jmapro.2020.09.036.

[100] K. Wang, Y. Yan, P. Zhou, C. Zhang, R. Kang, and D. Guo, "Preparation of Flat and Smooth Copper Surface by Jet Electrochemical Machining and Electrochemical Polishing," *J. Electrochem. Soc.*, vol. 167, no. 16, p. 163501, Nov. 2020, doi: 10.1149/1945-7111/abcbb2.

[101] D. Piotrowski, O and Madore, C and Landolt, "The mechanism of electropolishing of titanium in methanol-sulfuric acid electrolytes," *J. Electrochem. Soc.*, vol. 145, no. 7, p. 2362, 1998.

[102] T. Zhao, S. Wang, Z. Liu, C. Du, and X. Li, "Effect of cathodic polarisation on stress corrosion cracking behaviour of a Ni(Fe, Al)-maraging steel in artificial seawater," *Corros. Sci.*, vol. 179, p. 109176, Feb. 2021, doi: 10.1016/j.corsci.2020.109176.

[103] A. Barman and M. Das, "Nano-finishing of bio-titanium alloy to generate different surface morphologies by changing magnetorheological polishing fluid compositions," *Precis. Eng.*, vol. 51, pp. 145–152, Jan. 2018.

[104] A. Rudawska and E. Jacniacka, "Evaluating uncertainty of surface free energy measurement by the van Oss-Chaudhury-Good method," *Int. J. Adhes. Adhes.*, vol. 82, pp. 139–145, Apr. 2018, doi: 10.1016/j.ijadhadh.2018.01.006.

[105] Y. Hou, R. Li, J. Liang, P. Su, and P. Ju, "Electropolishing of Al and Al alloys in AlCl3/trimethylamine hydrochloride ionic liquid," *Surf. Coatings Technol.*, vol. 335, pp. 72–79, Feb. 2018, doi: 10.1016/J.SURFCOAT.2017.12.028.

[106] V. Urlea and V. Brailovski, "Electropolishing and electropolishing-related allowances for IN625 alloy components fabricated by laser powder-bed fusion," *Int. J. Adv. Manuf. Technol.*, vol. 92, no. 9–12, pp. 4487–4499, Oct. 2017, doi: 10.1007/s00170-017-0546-0.

[107] T. Tran, B. Brown, S. Nesic, and B. Tribollet, "Investigation of the mechanism for acetic acid corrosion of mild steel," in *Corrosion*, vol. 70, no. 3, 2013, pp. 1–12.

[108] W. Han and F. Fang, "Electropolishing of 316L stainless steel using sulfuric acid-free

electrolyte," *J. Manuf. Sci. Eng.*, vol. 141, no. 10, 2019, doi: 10.1115/1.4044518.

[109] C. Félix-Martínez, J. Ibarra-Medina, D. A. Fernández-Benavides, L. A. Cáceres-Díaz, and J. M. Alvarado-Orozco, "Effect of the parametric optimization and heat-treatment on the 18Ni-300 maraging steel microstructural properties manufactured by directed energy deposition," *Int. J. Adv. Manuf. Technol.*, vol. 115, no. 11–12, pp. 3999–4020, Aug. 2021, doi: 10.1007/S00170-021-07320-Y/FIGURES/18.

[110] A. Kumar and M. Das, "Multiphysics simulation and experimental investigation of microtool fabricated by EMM," *Mater. Manuf. Process.*, vol. 36, no. 13, pp. 1489–1500, 2021, doi: 10.1080/10426914.2021.1905837.

[111] J. Yan, Y. Zhou, R. Gu, X. Zhang, W.-M. Quach, and M. Yan, "A Comprehensive Study of Steel Powders (316L, H13, P20 and 18Ni300) for Their Selective Laser Melting Additive Manufacturing," *Metals (Basel).*, vol. 9, no. 1, p. 86, 2019, doi: 10.3390/met9010086.

[112] A. Pal and C. Das, "A novel use of solid waste extract from tea factory as corrosion inhibitor in acidic media on boiler quality steel," *Ind. Crops Prod.*, vol. 151, p. 112468, Sep. 2020, doi: 10.1016/j.indcrop.2020.112468.

[113] A. Kumar, S. Kumar, and M. Das, "Parametric investigation of electropolishing to enhance the surface characteristics of maraging steel with organic electrolytes," *Int. J. Adv. Manuf. Technol.*, vol. 121, no. 7, pp. 5297–5310, Jul. 2022, doi: 10.1007/S00170-022-09695-Y.

[114] M. E. Fitzpatrick, A. T. Fry, P. Holdway, F. A. Kandil, J. Shackleton, and L. Suominen, *Determination of residual stresses by X-ray diffraction*. 2005.

[115] T. Tamura, "Development of on-the-machine surface modification technology in EDM," in *Procedia CIRP*, 2013, vol. 6, pp. 117–122, doi: 10.1016/j.procir.2013.03.049.

[116] O. Anderoglu, "Residual Stress Measurement Using X-Ray Diffraction," Texas A&M University, 2005.

[117] Z. Ding, B. Li, and S. Y. Liang, "Phase transformation and residual stress of Maraging C250 steel during grinding," *Mater. Lett.*, vol. 154, pp. 37–39, Sep. 2015, doi: 10.1016/J.MATLET.2015.04.040.

[118] A. G. Dos Reis, D. A. P. Reis, A. J. Abdalla, and J. Otubo, "High-temperature creep resistance and effects on the austenite reversion and precipitation of 18 Ni (300) maraging steel," *Mater. Charact.*, vol. 107, pp. 350–357, Sep. 2015, doi: 10.1016/J.MATCHAR.2015.08.002.

[119] B. Li, Z. Ding, J. Xiao, and S. Y. Liang, “Maraging steel 3J33 phase transformation during micro-grinding,” *Mater. Lett.*, vol. 164, pp. 217–220, Feb. 2016, doi: 10.1016/J.MATLET.2015.10.162.

[120] Z. Zhang, Z. Zhang, and H. Zhang, “Effect of residual stress of friction stir welding on the fatigue life of AA 2024-T351 joint,” *Proc. Inst. Mech. Eng. Part B J. Eng. Manuf.*, vol. 229, no. 11, pp. 2021–2034, Jul. 2015, doi: 10.1177/0954405414543489.

[121] K. V. A. Chakravarthi, N. T. B. N. Koundinya, S. V. S. Narayana Murty, and B. Nageswara Rao, “Microstructure, properties and hot workability of M300 grade maraging steel,” *Def. Technol.*, vol. 14, no. 1, pp. 51–58, Feb. 2018, doi: 10.1016/J.DT.2017.09.001.

[122] H. T. Lee and T. Y. Tai, “Relationship between EDM parameters and surface crack formation,” *J. Mater. Process. Technol.*, vol. 142, no. 3, pp. 676–683, 2003, doi: 10.1016/S0924-0136(03)00688-5.

[123] S. Arooj, M. Shah, S. Sadiq, S. H. I. Jaffery, and S. Khushnood, “Effect of Current in the EDM Machining of Aluminum 6061 T6 and its Effect on the Surface Morphology,” *Arab. J. Sci. Eng.*, vol. 39, no. 5, pp. 4187–4199, 2014, doi: 10.1007/s13369-014-1020-z.

[124] P. Pendyala, M. S. Bobji, and G. Madras, “Evolution of surface roughness during electropolishing,” *Tribol. Lett.*, vol. 55, no. 1, pp. 93–101, 2014, doi: 10.1007/s11249-014-0336-x.

[125] G. F. Vander Voort, G. M. Lucas, L. Elena, and P. Manilova, “Metallography and Microstructures of Stainless Steels and Maraging Steels,” *Mater. Park. OH ASM Int. 2004.*, pp. 670--700, 2004, doi: 10.1361/asmhba0003767.

[126] V. Urlea and V. Brailovski, “Electropolishing and electropolishing-related allowances for powder bed selectively laser-melted Ti-6Al-4V alloy components,” *J. Mater. Process. Technol.*, vol. 242, pp. 1–11, Apr. 2017, doi: 10.1016/J.JMATPROTEC.2016.11.014.

[127] V. S. Protsenko, T. E. Butyrina, L. S. Bobrova, S. A. Korniy, and F. I. Danilov, “Enhancing corrosion resistance of nickel surface by electropolishing in a deep eutectic solvent,” *Mater. Lett.*, vol. 270, Jul. 2020, doi: 10.1016/J.MATLET.2020.127719.

[128] Y. Wang *et al.*, “Experimental Investigation on the Effects of Different Electrolytic Polishing Solutions on Nitinol Cardiovascular Stents,” *J. Mater. Eng. Perform.*, vol. 30, no. 6, pp. 4318–4327, 2021, doi: 10.1007/s11665-021-05736-x.

[129] E. Pujiyulianto and Suyitno, “The Effect of Electropolishing Time Variation at Room Temperature and Low Voltage on the Surface Quality of Cardiovascular Stent,” *Adv. Mater. Res.*, vol. 1154, no. June, pp. 91–101, 2019, doi: 10.4028/www.scientific.net/amr.1154.91.

[130] A. Kumar, R. Mahanti, and M. Das, “Investigation of electropolishing performance on surface residual stress and morphology of electrical discharge machined maraging steel,” *Proc IMechE Part C J Mech. Eng. Sci.*, 2022, doi: 10.1177/09544062221140735.

[131] A. Ahmed, B. Dhakar, R. Kaul, R. Palai, A. Roy Choudhury, and S. Chatterjee, “Hardfacing of AISI304 steel: fabrication of oxide-boride-nitride ceramic matrix composite layer by laser-assisted high temperature chemical reaction,” *Trans. Inst. Met. Finish.*, vol. 95, no. 4, pp. 207–216, 2017, doi: 10.1080/00202967.2017.1330247.

[132] A. S. Rajput, A. Singh, S. Kapil, and M. Das, “Investigations on the trochoidal toolpath for processing the biomaterial through magnetorheological fluid assisted finishing process,” *J. Manuf. Process.*, vol. 76, pp. 812–827, 2022.

[133] T. Tiwari, A. Dvivedi, and P. Kumar, “Investigations on the fabrication of a patterned tool by chemical etching,” *Mater. Manuf. Process.*, vol. 36, no. 16, pp. 1840–1852, 2021, doi: 10.1080/10426914.2021.1926491.

List of Publications

Journals

1. Jain, V. K., Balasubramaniam, R., Mote, R. G., Das, M., Sharma, A., **Kumar, A.**, Garg, V., & Kamaliya, B. (2020). Micromachining: an overview (part I). Journal of Micromanufacturing, 3(2), 142-158. https://doi.org/10.1177%2F2516598419895828**.**
2. **Kumar, A.**, & Das, M. (2021). Multiphysics simulation and experimental investigation of microtool fabricated by EMM. Materials and Manufacturing Processes, 36(13), 1489-1500.
3. **Kumar, A.**, Yadav, H. N. S., Kumar, M., & Das, M. (2021). Effect of tool rotation on the fabrication of micro-tool by electrochemical micromachining. Journal of Micromanufacturing, 5(2), 217-223.
4. **Kumar, A.**, Kumar, S., & Das, M. (2022). Parametric investigation of electropolishing to enhance the surface characteristics of maraging steel with organic electrolytes. The International Journal of Advanced Manufacturing Technology, 121(7), 5297-5310.
5. **Kumar, A.**, Mahanti, R., & Das, M. (2022). Investigation of electropolishing performance on surface residual stress and morphology of electrical discharge machined maraging steel. Proceedings of the Institution of Mechanical Engineers, Part C: Journal of Mechanical Engineering Science, 09544062221140735.
6. **Kumar, A.**, Mahanti, R., & Das, M. Investigation on the surface integrity improvement of electro-discharge machined maraging steel surfaces by electrochemical polishing. (Submitted to Journal of Materials Processing Technology).
7. **Kumar, A.**, Mahanti, R., & Das, M. (2022). Electropolishing of thin-cruciform gimbal flexure of gyroscope fabricated by electrical discharge machining. Materials and Manufacturing Processes, 1-13.

Conferences

1. **Kumar, A.**, Kumar, M., Alok, A., & Das, M. "Surface texturing by electrochemical micromachining: A review," 8th International Symposium on Fusion of Science and Technology (ISFT), Faridabad, India, 06th -10th January 2020. (IOP Conf. Ser. Mater. Sci. Eng., https://doi.org/10.1088/1757-899X/804/1/012011).

2. **Kumar, A.**, Yadav, H. N. S., Kumar, M., & Das, M. 'Effect of tool rotation on electrochemical milling of stainless steel 316L', 2nd lnternational Conference on Recent Advancements in Mechanical Engineering, Nit Silchar, India, 07th-09th February 2021.
3. **Kumar, A.**, Kumar, M., Alok, A., Yadav, H. N. S., & Das, M. 'Fabrication of microtool for micromachining: A Review', 3rd International Conference on Computational & Experimental Methods in Mechanical Engineering, G.L. Bajaj, Greater Noida, India, 11th-13th February 2021 (*Materials Today: Proceedings*. https://doi.org/10.1016/j.matpr.2021.03.592).
4. **Kumar, A.**, Singh, A., Yadav, H. N. S., Kumar, M., & Das, M. '3D simulation of machining parameters of electrochemical micromachining for stainless steel (316L)', 2nd International Conference on Aspects of Materials Science and Engineering, Panjab University, Chandigarh, India, 05th-06th March 2021 (*Materials Today: Proceedings*. https://doi.org/10.1016/j.matpr.2021.01.005).
5. **Kumar, A.**, Kumar, S., Kumar, M., & Das, M. 'Effect of polishing time on the surface property of Maraging Steel on Electropolishing', 4th World Congress on Micro and Nano Manufacturing (WCMNM 2021), IIT Bombay, India, 21th-23th September 2021.
6. **Kumar, A.**, Kumar, M., Yadav, H. N. S., & Das, M. 'COMSOL simulation to predict the thickness of material removed from surface during electropolishing', 2nd International Conference on Industrial and Manufacturing Systems (CIMS-2021), Dr. B R Ambedkar National Institute of Technology (NIT), Jalandhar and Punjab Engineering College (PEC), Chandigarh, Chandigarh, India, 11th-13th November 2021.
7. **Kumar, A.**, Kumar, M., Yadav, H. N. S., & Das, M. 'Effect of micro tool-tips in Electrochemical Micromachining', 1st international conference on advances in mechanical engg. and material science (ICAMEMS-22), VIT AP, India, 22th-24th January 2022 (Materials Today: Proceedings, https://doi.org/10.1016/j.matpr.2021.11.329).
8. **Kumar, A.**, & Das, M. 'Investigation of process parameters of electropolishing of maraging steel with organic electrolytes', 12th International conference on precision, micro, meso and nano engineering (COPEN-12), IIT Kanpur, India, 08th-10th December 2022.

Book Chapters

1. Dutta, P., Barman, A., **Kumar, A.**, & Das, M. (2020). Design and fabrication of electrochemical micromachining (ECMM) experimental setup for micro-hole drilling. In Advances in Mechanical Engineering (pp. 561-573). Springer, Singapore.

2. **Kumar, A.**, Yadav, H. N. S., Kumar, M., & Das, M. (2023). Effect of Tool Rotation on Electrochemical Milling of Stainless Steel 316L. In *Recent Advancements in Mechanical Engineering* (pp. 601-612). Springer, Singapore.
3. **Kumar, A.**, Kumar, M., Yadav, H. N. S., & Das, M. (2023). COMSOL Simulation to Predict the Thickness of Material Removed from Surface During Electropolishing. In *Recent Advancements in Mechanical Engineering* (pp. 321-337). Springer, Singapore.

Patent

1. **Abhinav Kumar** and Manas Das, A system for electropolishing of dynamically tuned gyroscope, Indian Patent, Application Number: 202131053833. | **Patent filed.**